Formulation Development for 3D Printing of Immediate Release Cabozantinib Tablets with Personalized Dosage

Dissertation

der Mathematisch-Naturwissenschaftlichen Fakultät

der Eberhard Karls Universität Tübingen

zur Erlangung des Grades eines

Doktors der Naturwissenschaften

(Dr. rer. nat.)

vorgelegt von

Jonas Lenhart

aus Mühlacker

Tübingen

2024

Gedruckt mit Genehmigung der Mathematisch-Naturwissenschaftlichen Fakultät der Eberhard Karls Universität Tübingen.

Tag der mündlichen Qualifikation: 19.12.2024
Dekan: Prof. Dr. Thilo Stehle
1. Berichterstatter/-in: Prof. Dr. Dominique Lunter
2. Berichterstatter/-in: Prof. Dr. Rolf Daniels

I. Acknowledgment

Zunächst möchte ich meiner Betreuerin, Professorin Lunter, meinen tiefsten Dank aussprechen. Ihre fachliche Führung, wertvollen Ratschläge, sowie freie Hand bei offenen Forschungsfragen haben nicht nur die Richtung dieser Arbeit geprägt, sondern mich auch fachlich und persönlich wachsen lassen. Ihre Geduld und ihr Engagement in jeder Phase meiner Promotion waren von unschätzbarem Wert. Ebenso möchte ich dem Zweitgutachter, Professor Daniels, für seine konstruktiven Rückmeldungen unter anderem in Bezug auf rheologische Themen und das detaillierte Gutachten danken, die zur Qualität dieser Arbeit beigetragen haben.

Ein ganz besonderer Dank gilt meiner Familie. Meine Eltern, Andrea und Georg, aber auch meine Schwester Rebecca standen immer hinter mir und ohne ihre Unterstützung wäre dieser Weg nicht möglich gewesen. Auch meiner Verlobten Jale möchte ich von Herzen danken, dass sie immer an meiner Seite war, mich ermutigte und mit unerschütterlichem Verständnis durch die Höhen und Tiefen begleitet hat.

Mein Dank gilt auch den technischen Assistenten, allen voran Klaus, dessen Unterstützung durch Geräteeinlernung, Troubleshooting und Reparatur, Bereitschaft jederzeit Forschungsfragen zu diskutieren und seine Zeit im Praktikum viele der Arbeiten erst möglich gemacht haben. Aber auch Irina, Boguslawa und Jutta, die durch ihre Arbeit in der Wartung der Geräte, in der Lagerhaltung und Bestellung und dem Praktikum für einen reibungslosen Ablauf gesorgt haben. Ihr Engagement und ihre Kompetenz sowie regelmäßige Kuchen haben entscheidend zur Arbeit im Institut beigetragen. Auch den Mitarbeitern der Werkstatt habe ich zu Danken für ihre Hilfe bei der Konzeption und Umsetzung von Bauteilen und Reparaturen, sowie der Chemikalienausgabe.

Ein besonderer Dank geht an alle meine Kollegen und Kolleginnen der letzten 4 Jahre aus dem Arbeitskreis Techno für die inspirierende und kollegiale Zusammenarbeit aber vor allem für die spaßigen Momente. Die gemeinsame Zeit, sowohl im Labor als auch in der Lehre, war prägend; Feedback zu Forschungsfragen, das ein oder andere Feierabendbier, gemeinsame Mittagspausen und Pharmapartys sind nur ein paar der Erinnerungen, die bleiben werden.

Abschließend möchte ich meinen langjährigen Freunden sowie Conaktiven danken für Diskussionen, Unterstützung und Ablenkung, die für die nötige Balance gesorgt haben.

Mein tiefster Dank gilt all jenen, die mich auf diesem Weg begleitet und unterstützt haben. Ohne euch wäre diese Arbeit nicht möglich gewesen.

Table of Contents

II.   Abbreviations

AI	Artificial intelligence
API	Active pharmaceutical ingredient
AUC	Area under the curve
CAB	Cabozantinib
CAD	Computer-aided design
CCS	Croscarmellose sodium
CQA	Critical quality attribute
CRM	Confocal Raman microspectroscopy
DoE	Design-of-Experiment
DSC	Differential scanning calorimetry
EMA	European Medicines Agency
EPO	Eudragit E PO
EtOH	Ethanol
FaSSIF	Fasted state simulated intestinal fluid
FDA	U.S. Food and Drug Administration
FDM	Fused deposition modeling
FeSSIF	Fed state simulated intestinal fluid
FFF	Fused filament fabrication
GMP	Good manufacturing practice
HME	Hot melt extrusion
HPMC	Hydroxypropylmethylcellulose
HPLC	High performance liquid chromatography
ICH	International council for harmonisation of technical requirements for pharmaceuticals for human use
IsopropOH	Isopropyl alcohol

KIR	Kollicoat IR
KVA	Kollidon VA64
LOP	Loperamide
LVR	Linear viscoelastic range
MeOH	Methanol
PAR	Parteck MXP
PEO	Polyethylene oxide
PLA	Polylactic acid
PVA	Polyvinylalcohol
SMILES	Simplified molecular input line entry system
SOR	Sorbitol
SSG	Sodium starch glycolate
STA	Simultaneous thermal analysis
T_g	Glass transition temperature
T_{max}	Time until maximum concentration is reached

III. Zusammenfassung

Der 3D-Druck als additives Fertigungsverfahren hat sich in vielen Bereichen bewährt. Vor allem die Möglichkeit der schnellen Herstellung von Prototypen und die flexiblen Produktionsmöglichkeiten machen diese Technologie attraktiv. Die pharmazeutische Produktion ist aufgrund strenger gesetzlicher Vorgaben nicht sehr flexibel, was den Einsatz neuer Technologien angeht. Seit vielen Jahren wird aber auch an den Möglichkeiten und Herausforderungen der additiven Fertigung für die Herstellung von Arzneimitteln und Medizinprodukten gearbeitet. Die ersten Marktzulassungen liegen bereits vor. Im Bereich des 3D-Drucks gibt es jedoch mehrere unterschiedliche Technologien. Die folgende Arbeit beschäftigt sich mit dem Fused Filament Fabrication (FFF) Verfahren. Bei diesem Verfahren werden Objekte gedruckt, indem man ein Gemisch aus Polymeren und anderen Hilfsstoffen schmilzt, schichtet und dann abkühlen und erstarren lässt. Im Prinzip gibt es zwei Möglichkeiten, das Material in eine Position zu bringen, in der es geschmolzen werden kann. Die erste Methode wird vor allem im Hobbydruck und in der Kleinserienfertigung eingesetzt und besteht in der Herstellung so genannter Filamente durch Schmelzextrusion. Dieses Filament kann man sich als einen Faden mit konstanter Dicke vorstellen, der dann über ein Förderelement durch die beheizte Düse eines 3D-Druckers geschoben wird. Die andere Möglichkeit besteht darin, Pellets oder Pulver des Polymers mit Hilfe einer Schnecke oder eines Kolbens direkt zur Düse zu befördern, um es unter Druck und Scherung zu schmelzen und die für den Druck erforderliche Schmelze zu erzeugen. Dieser Ansatz ist im kommerziellen 3D-Druck relativ neu. In der vorliegenden Arbeit wird eine solche Direktextrusion verwendet. Mögliche Anwendungsgebiete für den 3D-Druck im pharmazeutischen Bereich sind vor allem Präparate, die eine patientennahe Dosierung erfordern, da das Verfahren wesentlich langsamer und teurer ist als das Tablettenpressen und daher für die breite Masse der Medikamente nicht interessant ist.

Ziel dieser Studie war die Entwicklung einer Formulierung für die schnelle Freisetzung des Wirkstoffs Cabozantinib (CAB). Dieser wird in der Krebstherapie eingesetzt und seine Dosierung wird aufgrund seines Nebenwirkungsprofils regelmäßig an den einzelnen Patienten angepasst. Verfügbare verschreibungspflichtige Medikamente bieten nur eine begrenzte Möglichkeit zur individuellen Dosierung, wie sie aus der Herstellung von injizierbaren Krebstherapeutika bekannt ist. Je nach Krebsart sind Dosen von 20-140 mg erwünscht, wobei nur 20 mg-Schritte möglich sind und durch die Kombination verschiedener Stärken mehrere Tabletten eingenommen werden müssen.

Für die Herstellung von 3D-gedruckten Tabletten, die Cabozantinib enthalten, muss zwangsweise in einem der Prozessschritte der Wirkstoff eingearbeitet werden. Beim Filamentdruck kann der Wirkstoff während der Produktion direkt in das Filament eingearbeitet oder nachträglich über ein lösungsmittelbasiertes Verfahren eingebracht werden. Unter Verwendung von Ibuprofen und verschiedenen Lösungsmitteln wurde die zweite der beiden Methoden an handelsüblichem PVA-Filament getestet und als zu nachteilig verworfen.

Der nächste Schritt bestand darin, sich auf die Extrusion und den Direktdruck aus dem Pulver zu konzentrieren. Für die ersten Schritte der Formulierungsentwicklung wurde Loperamid (LOP) als Modellarzneimittel auf der Grundlage der Löslichkeitsparameter von Cabozantinib ausgewählt. Die Einstellung der Dosierung durch Änderung des Füllgrades und die Zugabe weiterer Hilfsstoffe zur Verbesserung der Auflösungsgeschwindigkeit getestet. Die Erkenntnisse aus diesen Versuchen wurden auf die laufende Entwicklung von CAB-haltigen Formulierungen übertragen.

Aufgrund der schlechten Löslichkeit von CAB wurde hier versucht, es in Form einer festen amorphen Dispersion zu verarbeiten. Die Freisetzung und scheinbare Löslichkeit können bei vielen Substanzen auf diese Weise verbessert werden. Zusätzlich zur höheren Löslichkeit musste die Auflösungsgeschwindigkeit verbessert werden, um das Ziel der schnellen Freisetzung zu erreichen. Das Mischen von Sorbitol mit den Polymeren erfolgte aus zwei Gründen. Erstens lässt seine hohe Wasserlöslichkeit eine verbesserte Auflösungsgeschwindigkeit der Mischung erwarten. Zweitens führen die Mischbarkeit mit den Polymeren und die weichmachende Wirkung zu einer niedrigeren Extrusions- und Drucktemperatur, die notwendig ist, um einen thermischen Abbau von CAB zu vermeiden. Zusätzlich zu Sorbitol wurden die Sprengmittel Croscarmellose-Natrium und Natriumstärkeglykolat verwendet, um die Freisetzung zu beschleunigen.

Schließlich wurden Formulierungen mit einer schnellen Freisetzung von CAB entwickelt. Anhand dieser Formulierungen wurde ein Ansatz für die Gestaltung individueller Dosierungen aus einer Pulvermischung mit konstanter Wirkstoffkonzentration entwickelt. Er verwendet die Wirkstoffkonzentration, die gewünschte Dosis und die experimentell ermittelte Dichte der gedruckten Mischung, um die CAD-Parameter (computer-aided design) für eine kapselförmige Tablette zu berechnen. Mit diesem Ansatz konnte der Druck von Dosierungen von 20-140 mg in 10 mg-Schritten in einzelnen Tabletten realisiert werden.

Um weitere Einblicke in das Druckverhalten zu gewinnen, wurde die Schmelzrheologie vieler Formulierungen mit einem oszillatorischen Scherrheologie-Testaufbau mit kleinen Amplituden

getestet, dessen Ergebnisse darauf hindeuten, dass für ein erfolgreiches Drucken eine relativ niedrige Viskosität erforderlich ist. Modernste Methoden wie DSC, STA, XRD und Raman-Mikrospektroskopie wurden zur Charakterisierung der Hilfsstoffe und der fertigen Tabletten eingesetzt.

IV. Summary

3D printing as an additive manufacturing technique has proven valuable in many fields. Primarily, the ability to produce prototypes quickly and the flexible production options make this technology desirable. Due to strict regulatory requirements, pharmaceutical production is not very flexible when using new technologies. However, work has also been ongoing for many years on the possibilities and challenges of additive manufacturing for producing pharmaceuticals and medical devices. The first market approvals have already been achieved. There are, however, several different technologies in the field of 3D printing. The following thesis deals with the fused filament fabrication (FFF) process. In this process, objects are printed by melting a mixture of polymer and other excipients, layering them, and allowing them to cool and solidify. There are two ways to move the material to a position where it can be molten. The first is mainly used in hobby printing and small-scale production and consists of producing so-called filaments employing melt extrusion. This filament can be seen as a thread of constant thickness, which is then pushed through the heated nozzle of a 3D printer by a conveyor element. The other option is to convey pellets or powder of the polymer directly to the nozzle using a screw or piston to melt it under pressure and shear to produce the melt required for printing. This approach is relatively new in commercial 3D printing. In the present work, such direct extrusion is used. Possible fields of application for 3D printing in the pharmaceutical sector are primarily preparations that require close patient-specific dosing since the process is much slower and more expensive than tablet pressing and, therefore, not attractive for the broad mass of drugs.

This study aimed to develop a formulation for the immediate release of the active ingredient cabozantinib (CAB). It is used in cancer therapy, and its dosage is regularly adjusted to the individual patient due to its side effect profile. Available prescription drugs offer only a limited possibility for individual dosing, as is known from the production of injectable cancer therapeutics. Doses of 20-140 mg are desired depending on the type of cancer, while only 20 mg increments are possible, and several tablets must be taken due to the combination of different strengths.

To produce 3D-printed tablets containing cabozantinib, the active ingredient must be incorporated at some point. In the case of filament printing, the active ingredient can be incorporated directly into the filament during production or subsequently introduced using a

solvent-based process. Using ibuprofen and different solvents, the second of the two methods was tested on commercial PVA filament and rejected as too disadvantageous.

The next step was to focus on extrusion and direct printing from the powder. For the first steps of formulation development, loperamide (LOP) was selected as a model drug based on the solubility parameters of cabozantinib. Manipulating the dosage via a change of the infill and adding further excipients to improve the dissolution rate were tested. The findings of these trials were transferred to the ongoing formulation development containing CAB.

The poor solubility of CAB is why an attempt was made here to process it in the form of a solid amorphous dispersion. The release and apparent solubility can be improved for many substances in such a way. Additionally, to achieve higher solubility, the dissolution rate had to be improved to reach the goal of immediate release. Mixing sorbitol with the polymers was done for two reasons. First, its highly water-soluble nature leads to the expectation of an improved dissolution rate for the mixture. Second, miscibility with the polymers and the plasticizing effects lead to a reduced extrusion and printing temperature, which is necessary to avoid thermal degradation of CAB. In addition to sorbitol, the class of disintegrants croscarmellose sodium (CCS) and sodium starch glycolate (SSG) were used to accelerate release.

Finally, formulations were developed with an immediate release of CAB. An approach for designing individual dosages from a powder mixture of constant drug concentration was developed using these formulations. It uses the drug concentration, desired dose, and experimentally determined density of the printed mixture to calculate the computer-aided design (CAD) parameters for a capsule-shaped tablet. With this approach, printing 20-140 mg dosages in 10 mg increments could be realized in individual tablets.

To gain further insight into the printing behavior, the melt rheology of many formulations was tested using a small-amplitude oscillatory shear rheology testing setup. The results indicate the need for relatively low viscosity for successful printing. State-of-the-art methods such as DSC, STA, XRD, and Raman microspectroscopy were used to characterize excipients and the final tablets.

V.   List of Publications

Publication 1

Evaluation of Printability of PVA-Based Tablets from Powder and Assessment of Critical Rheological Parameters

Jonas Lenhart, Florian Pöstges, Karl G. Wagner, Dominique J. Lunter

Pharmaceutics 2024, Vol. 16., Issue 4

https://doi.org/10.3390/pharmaceutics16040553

Publication 2

Dosage by design - 3D printing individualized cabozantinib tablets with immediate release

Jonas Lenhart, Dominique J. Lunter

European Journal of Pharmaceutics and Biopharmaceutics 2024 Vol. 204

https://doi.org/10.1016/j.ejpb.2024.114501

Other Publications

Publication 1

Phase homogeneity in ternary amorphous solid dispersions and its impact on solubility, dissolution and supersaturation – Influence of processing and hydroxypropyl cellulose grade

Florian Pöstges, Jonas Lenhart, Edmont Stoyanov, Dominique J. Lunter, Karl G. Wagner

International Journal of Pharmaceutics: X 2023, Volume 6

https://doi.org/10.1016/j.ijpx.2023.100222

VI.   List of poster presentations

Poster presentation 1

DPhG Annual Meeting, September 2022, Marburg, Germany

Feasibility of 3D printing of solid amorphous dispersions from powder and parameters influencing the release behavior

Jonas Lenhart, Dominique Jasmin Lunter

Poster presentation 2

DPhG Annual Meeting, October 2023, Tuebingen, Germany

Characterization of loperamide-containing PVA-based 3D printed tablets regarding dissolution mechanism, API distribution and melt rheology

Jonas Lenhart, Dominique Jasmin Lunter

Poster presentation 3

14th World Meeting on Pharmaceutics, Biopharmaceutics and Pharmaceutical Technology (PBP), March 2024, Vienna, Austria

3D-printed Loperamide tablets – Characterization of printing properties and evaluation via confocal Raman microspectroscopy

Jonas Lenhart, Dominique Jasmin Lunter

1. Introduction

1.1.   Cabozantinib and personalized dosages

Cabozantinib acts on receptor tyrosine kinases that are found in tumor angiogenesis, invasion, and metastasis by binding to the kinase domain, including the ATP-binding site of MET (hepatocyte growth factor receptor), VEGFR2 (vascular endothelial growth factor receptor 2), and AXL [1]. While VEGFR2 takes part in signaling for tumor angiogenesis [2] and is expressed in endothelial cells, MET is expressed in tumor cells as well and improves cell motility and proliferation [3]. Upregulated MET can be found in many types of cancer, especially in more aggressive types (e.g., papillary renal carcinoma) [4,5].

Currently, there are two formulations commercially available. One is a capsule formulation (Cometriq) containing Cabozantinib[(2S)-2hydroxybutandioate] in dosages of 20 and 80 mg equivalents of the free base. In Europe, it is approved for the therapy of medullary unresectable or locally advanced metastatic medullary thyroid cancer. The second formulation is a tablet (Cabometyx) containing cabozantinib-L-malate in dosages of 20, 40, and 60 mg equivalents of the free base. It is approved for the therapy of advanced renal cell carcinoma either as a monotherapy or as a combination with nivolumab. Bioequivalence studies between these two formulations have been conducted, but bioequivalence cannot be shown [6]. After uptake, high plasma protein binding (>99%) was found in healthy volunteers as well as patients with renal impairment [7]. CAB elimination occurs mainly through hepatobiliary metabolization and elimination of both parent CAB and its metabolites, while only the metabolites of CAB are excreted in the urine [8]. Thus, a need for dosage adjustment may arise due to hepatic impairment. While fatty food sources increase the systemic exposure from capsule formulations by prolonging the median time until the maximum concentration is reached (T_{max}), the change in pH by adding proton-pump-inhibitors seemed to have no impact on the plasma exposure [9].

Drug-drug interactions with a significant effect were found in the inhibition of CYP3A4 and a minimal effect during inhibition of CYP2C9. Both effects lead to an increase in the CAB plasma area under the curve (plasma $AUC_{o\text{-}inf}$). On the other hand, CAB itself showed in-vitro effects as an inhibitor for CYP enzymes, namely CYP2C8 and CYP2C9. However, the activity could not be shown in-vivo by changes in rosiglitazone plasma levels [10]. Rosiglitazone is recommended as a substrate probe for the evaluation of CYP2C8 inhibition [11]

While the absolute bioavailability of CAB has not been demonstrated yet, there are indications of high bioavailability. A comparison between a tablet/capsule formulation and a solution revealed that 74-97% of the drug could be recovered from solid formulations [1]. The rapid increase in plasma concentration (T_{max} 1.49 h) serves as an additional indicator of good bioavailability. Enterohepatic recirculation is possible based on the second increase in plasma concentration [8]. Due to its lipophilic nature, its solubility can be described as practically insoluble in water [12]. This places more emphasis on the formulation since the critical factor affecting the uptake of CAB is the release and subsequent dissolution.

Due to the vital need for dose adjustments for many patients during CAB treatment, 3D printing can help achieve personal dosages that are appropriate for each patient [13-17]. 3D printing can also improve dosing precision, even when an original product is available but must be split to reach desired dosages [18].

1.2.   BCS-Classification and improvement of solubility

Following the low solubility and high permeability of CAB, it can be categorized as a biopharmaceutics classification system (BCS) class II drug [19]. Since the publication of the BCS, the amount of research regarding poorly soluble drugs measured by published papers has steadily increased [20]. For many of these drugs, improving solubility is the critical parameter that needs to be improved to make them therapeutically relevant [21].

While dissolution testing is only a surrogate parameter for in-vivo solubility enhancements, the in-vitro dissolution rate can indicate improved bioavailability. In some cases, changing the dissolution medium used for testing the dosage form to a more biorelevant medium can sufficiently alter the dissolution pattern. Although this only affects the in-vitro data (dissolution) and not the actual in-vivo data (bioavailability), it can serve as a helpful predictor. Correlations between in-vitro and in-vivo data can be evaluated for formulations where dissolution, rather than uptake, is the rate-controlling step [22]. Potential modifications include adding surfactant, utilizing milk for solubilization in the fatty phase, or employing simulated intestinal fluids (FaSSIF or FeSSIF) [23]. Changes in the setup of the dissolution equipment can also assist in improving dissolution results, though the options are more limited.

One approach to improving several properties of drugs, such as solubility or bioavailability [24], but also chemical stability or even organoleptic properties, can be the introduction of specific chemical moieties and the conversion of the drug to a prodrug [25]. Currently marketed substances

formulated as prodrugs are Simvastatin, Dabigatran, and Latanoprostene bunod [26]. Also, the solubility can be increased by converting the free base into a salt with higher solubility [27]. The increase in solubility for haloperidol mesylate salt, for example, is up to seven times higher than that of the free drug and hydrochloric salt [28].

Since the dissolution rate of a substance is directly related to the size of the particle used, it can usually be increased by decreasing the particle size. The reduction in particle size can be achieved via two methods, represented by the particle size itself. First, we have micronization, where particle sizes <10 μm can be found [29]. While different milling techniques prevailed in this application for a long time, supercritical fluid techniques have emerged in many applications [30]. Second, described by an even further size reduction, there are nanoparticles. The sizes described for nanometer particles are set at the lower end at 1 nm, while the upper end of the class varies from 100-1000 nm depending on the source [31]. For particles in the nm region, the dissolution rate and the solubility increase with decreasing size due to thermodynamic effects. These particles can be formed by top-down or bottom-up techniques [32]. Top-down means the size reduction of larger particles by mechanical force, while bottom-up means forming these particles by nucleation and growth of crystals [33]. Another way of producing nanosized particles is to dissolve fat-soluble drugs in a fatty phase, which is mixed with a water phase to form nanoemulsions. This approach is used for parental delivery of drugs, e.g., diazepam in Diazepam Lipuro TM [34].

The apparent solubility can also be improved by forming solid dispersions or solutions. These can be produced by solvent evaporation methods such as spray drying [35], freeze-drying [36], or melting [37]. Solid dispersions can be classified by different properties. First, they can be divided into three generations by their excipients. First-generation dispersions have crystalline carriers such as sugars or organic acids. The second generation comprises amorphous carriers (e.g., PEG/PEO, PVA), and the addition of surfactants or self-emulsifying carriers characterizes the third. Further distinguishments can be made by the number of phases found and the state of the drug dispersed in the carrier phase [38].

Research on employing solid dispersion forming techniques to improve the solubility of poorly soluble drugs has significantly increased in the last 60 years since the first solid dispersion was described [39], emphasizing the importance with a greater number of marketed formulations in the last 40 years [40]. While numerous ways exist to produce different kinds of solid dispersion, they are all susceptible to physical and kinetic instabilities, including crystallization, phase separation, and crystal growth. Choosing a suitable carrier can mitigate the risk. Reduced

mobility, found in carriers with high glass transition temperature (T_g), directly slows down the kinetics of crystallization and crystal growth. Solubility in the solid state and possible supersaturation are driving factors for phase separation and key parameters, alongside mobility [41]. Increased miscibility can lead to potentially improved dissolution behavior and storage stability due to the formation of single-phase systems [42]. The following work utilized hot melt extrusion to produce solid dispersions of the APIs (active pharmaceutical ingredients) LOP and CAB.

1.3.　Hot melt extrusion

The first extrusion device (1795) was a hand-operated combination of a piston and a die to produce seamless lead pipes. However, adaptations happened soon after and were used for soap, macaroni, and building materials. In 1935, the first extruder for thermoplastic material was introduced [43]. But while adapting the extruder for pharmaceutical applications was implemented as early as 1971, it took another 20 years to become a viable alternative [44].

During hot-melt extrusion, the material to be extruded is premixed loosely in a physical mixture and loaded into the hopper of an extruder. The material must be fed into the barrel, which can happen by gravity or a conveying system. Conveying systems are usually equipped with additional screws in front of or above the hopper, providing the option to maintain a controlled feeding rate. Generally, extruders can be flood-fed or starve-fed [45]. Flood feeding involves filling the extruder with as much powder as possible, resulting in higher pressure but a shorter time in the extrusion channel. Alternatively, controlled feeding allows a specific amount to flow into the extruder, increasing the transition time and enhancing mixing performance.

Inside the extruder barrel, depending on the configuration, one or two screws or a single piston push the material towards the heated elements. Zones with different functions can be employed in the screw configuration, such as conveying, mixing, and venting, where volatile compounds can be removed. Extruders using a piston lack these varying functions, as well as most of the mixing power screw extruders offer.

One of the main goals during extrusion is to achieve a mixture of high uniformity. Since excipients can exhibit different melt behaviors, extrusion settings such as temperature, screw speed, and screw design must be carefully selected. Convective mixing through laminar flow can generally be expected in polymers with high viscosity, as turbulent flow or eddy diffusion are usually of no practical significance [46]. The mixing mechanism can be classified based on the stress level a particle experiences. Elastic deformation under finite stress results in the

recovery of the initial dimensions, known as distributive mixing. Processing beyond finite stress conditions causes size reduction of the particles, termed dispersive mixing [47]. These two mechanisms are interconnected; when dispersive mixing occurs, distributive mixing must also be present, but the reverse is not obligatory. The stress required for dispersive mixing is typically unattainable in single-screw extruders.

The last part of the extruder is the die. At this point, the molten and possibly uniform mixture emerges from the barrel. Temperature, rheology of the mixture, and geometry of the die all affect the pressure in the die. It should be minimized to reduce unwanted effects such as increased shear rate and decreased viscosity, which can lead to symptoms of flow instabilities like sharkskin [48].

For pharmaceutical applications, selecting appropriate polymers is essential since many factors, such as active ingredients and use case, are fixed terms [49]. In addition to the parameters already discussed, like T_g and solid-state solubility, the thermal properties of the polymers are crucial for extrusion processes. T_g is closely linked to melt viscosity, which must fall within a suitable range for the extruder to stay within its torque limits. However, as previously mentioned, higher viscosity during mixing results in increased stress and, consequently, better mixing. The thermal stability of polymers must be considered due to the potential chemical or thermal decomposition caused by the heat and shearing stress in extrusion processes [50], leading to the formation of unknown degradation products that are unacceptable in products intended for human consumption.

To extrude a polymer, it needs to have specific mechanical properties. They should mainly be thermoplastic, which means they get softer due to increased temperature. The property that can and must be measured in this regard is the (melt) viscosity, and it has to be within a suitable range to keep the torque level of the extruder inside its limits [51,52]. Since the viscosity of thermoplastic materials is temperature-dependent, the William-Landel-Ferry equation was developed to describe the viscosity of such amorphous polymers above T_g [53,54].

Similar considerations must be made for the API, which must be stable at the given temperatures and shear rates used and sufficiently miscible with the polymer. At temperatures around and below T_g of the mixture, there is no equilibrium solubility, as we can determine it for temperatures well above tg. At this point, we are looking at the solubility of the crystalline drug in a meta-stable state. The equilibrium solubility may only be estimated for temperatures below T_g since the stability includes kinetic behaviors such as phase separation and structural relaxation leading to kinetic stabilization [42]. Predictions of the solubility might be possible in a

micro-scale trial analyzing the apparent T_g of polymer-drug-mixtures after an annealing step in the DSC [55]. The stability of solid dispersions strongly correlates with T_g of the polymer or polymer/API mixture. To ensure physical stability, T_g should be around 50°C above the storage condition [56]. While this approach looks at the mobility of polymers and neglects secondary ways of recrystallization, like the mobility found in API-rich phases or beta-relaxation, it can still be used as a rule of thumb for storage conditions.

Despite the high effort expected from the development and production of stable solid dispersions, there are several marketed formulations (e.g., KALETRA [57]®, NORVIR®, and ONMEL®) produced by the hot melt extrusion technique with mainly oral application [37,58].

1.3.1. Pneumatic vs screw-driven direct extruders

To extrude material, it must be moved from the hopper/inlet of the extruder to the heated zone and through the die. There are several options for moving material through the chamber of an extruder. On the one hand, extruders with one or two feed screws. Generally, single-screw extruders are cheaper and offer less customization, while dual-screw extruders are more expensive and offer more customization options for specific applications. By designing the screw elements in a specific way, they can perform different functions (conveying, kneading, mixing, compacting, pressing, relaxing, or backward conveying). Additionally, temperature control is a crucial element in extruding material successfully. Both single and dual-screw extruders offer at least one, often more, heating zones. Multiple heating zones improve the chance of successful extrusion due to the possibility of setting temperatures depending on the purpose of the specific screw section design.

While screw-driven extruders can have added mixing elements, flowing material with a non-homogeneous distribution of particle sizes tends to unmix based on density and particle size before extrusion in the hopper or during extrusion [59]. A way to overcome this challenge and make single-screw extruders without mixing elements viable can be the preparation of a solid dispersion of the API before extrusion [60]. While the single-screw extruder convinces many users with its low maintenance and lower cost, it is unsuitable for heat-sensitive materials. Twin-screw extruders solve some of the challenges found with feeding and mixing of excipients, but they are much more costly and less suitable for shear-sensitive materials [61].

In contrast to screw-driven extruders, there are pneumatic extruders where pressure is applied via a piston. Pneumatic hot melt extrusion is facilitated by air pressure instead of a screw [62]. Pressure and temperature can be easily controlled, but the adjustment possibilities are limited.

Additionally, a homogeneous mixture must be ensured before feeding it into the extruder since no mixing processes occur other than diffusion. It is a disadvantage that only low-viscosity polymers can be used for pneumatic extruder applications. The low viscosity of the polymer makes filament extrusion impossible, which is why the liquefied material is usually printed directly. Combining filament extrusion and printing from a filament reduces thermal stress and the number of process steps.

1.3.2. Production of filament

There are three key parameters to remember when producing filaments intended for 3D printing. One is processability during the hot melt extrusion process. Crucial parameters for a successful extrusion include the screw speed, the diameter of the die, and the powder feed rate/fill level in the extruder [63,64]. The importance of the impact of temperature and speed on the shearing, viscosity of the mixture, and screw torque has been discussed previously, along with the role of the die.

After extrusion, the next step is to ensure that the extruded filament can be printed. Mechanical properties, especially filament flexibility and tensile strength, can often be found in literature [65]. Testing these attributes can prevent two common issues: breaking in the feeding gear due to brittleness and inability to pass through the nozzle due to softness or inadequate resistance to the feeding gear [66]. An optimal filament should have high breaking stress, stiffness, and a long breaking distance [67,68]. These qualities can be evaluated through tensile testing and 3-point bend tests using a texture analyzer. While these tests are well-recognized, even in ISO standards, there are more direct approaches to assess filament feedability for specific printing configurations, such as compression tests simulating the feeding process during printing [69]. Apart from being strong enough to pass through the feeding gear and extrude the molten material from the nozzle, melt viscosity also influences the printability of a filament, which will be discussed later.

Uniformity in the diameter and API distribution of the filament is the final parameter that decisively determines a successful application in pharmaceutical therapies. The thickness can be adjusted using a specific die. Due to potential swelling behavior, the die's diameter may not perfectly match the filament's diameter, necessitating adjustments in temperature or die based on viscosity and swelling behavior [70]. Modern pharmaceutical production demands extensive in-line quality control. During filament extrusion, laser scanners with automatic feedback to the extrusion equipment can swiftly respond to diameter variations, maintaining them within predetermined values [71]. The consistent filament diameter is crucial for maintaining consistent

printing parameters and is integral to accurately producing dosed tablets. Controlling and optimizing the extrusion process is essential to achieve this goal, along with storing powder and filament under controlled conditions [72].

1.4. General introduction into 3D printing

One of the first sources to describe the principle of 3D printing using fused filament fabrication (FFF), also known as fused deposition modeling (FDM®), is the US patent specification of the Stratasys company for an apparatus and method for creating three-dimensional (3D) objects from 1992 [73]). The company has since expanded its expertise into other areas of 3D printing (polyjet and stereolithography technology), which is not in the scope of the current thesis.

The patent describes a 3D printer that bears great similarities to devices currently available on the market. It explains the movement of the print head or print bed along the x, y, and z axes, utilizing materials with specific properties, and the computer-assisted design and control.

1.4.1. Description of device

The invention above describes a movable dispensing head with a nozzle at the lower end and a base consisting of a plate (printing bed). The plate and the printing head are movable against each other, whereby the plate mainly handles the x-and y-axis, while the printing head realizes the movement in the z-axis. However, this is only a suggestion, as each of the movements could also be achieved by only one of the two components. The material to be printed is ideally thermoplastic and solidifies either at room temperature or at a lower temperature, achieved by cooling. The material should be present as a solid to flexible filament produced by hot-melt extrusion (HME). It should be heated to its melting temperature in the print head and distributed in a liquefied state. Modern filament-based 3D printers are fully described in the details given here. Some differences can be found in how axes are moved or how the filament is pushed through the nozzle (direct extrusion vs. Bowden extrusion). The material is heated above its respective melting point in the print head and converted into a viscous form. The molten material is extruded onto the plate, cools down, and solidifies. The initial movement is only in the x- and y- directions, can take any shape, and cools rapidly. Each subsequent layer can only be applied when the previous one has cooled down sufficiently and can also take on slightly different shapes to form the desired object. Only displacement in the x and y directions usually occurs during the print of one layer. This is followed by movement in the z-direction. For the object to be created, the x and y directions can be varied simultaneously with the z-direction, if necessary, for example, to create a spiral. The resolution in all directions is usually limited by

the nozzle size. As an example, a standard nozzle size would be 0.4 mm, resulting in a layer width of 0.4 mm and a layer height of 0.2 mm for most settings. This layer height ensures sufficient cooling before the next layer is printed. The speed at which the material is conveyed into the printhead must match the speed of the printhead in the x-y plane to ensure a constant output. If no material needs to be dispensed, the movement can be stopped. Proper temperature management, especially at the nozzle, is crucial to ensure the correct amount of material is dispensed; hence, a thermocouple should be installed near a temperature controller.

First-layer adhesion is a critical point for every print due to this area being the only contact point to the print bed and its responsibility to resist forces from the moving printhead. Various options, such as a base for the object or support for the plate, are discussed. The material's adhesiveness and the removability from the plate/support are considered decisive properties. For example, fine mesh sandpaper can be used as it has excellent adhesive properties. To improve this further, it is suggested that a conductive backing that can be slightly heated be used to detach the object. Water-soluble wax is mentioned as a base that could be washed away to release the object. Nowadays, well-known substrates from the hobby and research sector that could be adapted for research purposes are glass plates on which the application of glue or adhesive tape has proved successful [17,74].

In this thesis, the 3D printer "M3dimaker", produced by FabRX and specific for pharmaceutical research, has been used. This printer uses the sample principles of FFF 3D printers described above. Interestingly, it offers three distinct printheads that can be changed quickly on the same printer. One printhead can print from filament, while the others use extrusion techniques to deposit material on the print bed. The direct powder extrusion (DPE) tool can print thermoplastic material with a high melting point. It is a very small-scale single-screw extruder attached to a 3D printer. The semi-solid extrusion (SSE) tool can be used for materials that are viscous with a yield limit at room temperature or slightly above, which can be applied for many biotechnologically requested materials.

1.4.2. Printing process

Using the M3dimaker 3D printer with the DPE tool is essentially the same as most other FFF 3D printers. Software applications for controlling axes and material deposition must be adjusted for the tool head and how material is conveyed. In all other aspects, printing itself consists of four to five steps:

1.4.2.1.   Step 1: Design and g code

The object to be printed must be created as a model file using CAD (computer-assisted design) software. For most pharmaceutical applications, the shapes are based on familiar tablet shapes and are not particularly complex. Patients well accept less common shapes if the background is communicated [75]. The resulting file must be available as a stereolithography file (.stl). This file is generally written in a binary format, specifying the x, y, and z coordinates of the vertices of the triangular elements adapted to approximate the object's surface in the so-called tessellation process [76]. In the next step, the code that 3D printers work with can be created from this file.

1.4.2.2.   Step 2: Slicer

To generate this code (so-called gcode), there are several free or commercial software options (so-called slicers) [77]. Various parameters for the printer can be set. The temperatures for the print head and the print bed are set and can be varied for printing. It may be necessary to heat the print bed to prevent the print from cooling down too quickly, leading to reduced adhesion. The general printing speed is also set and can be varied according to various parameters individually to increase the performance or quality of the print, e.g., infill can generally be printed faster than outer layers. The adhesion of the first layer is crucial for the entire print. The speed and thickness at which the first layer is printed must be optimized. The speed is usually reduced compared to the rest of the print, while the thickness can be increased to achieve good adhesion. The cooling behavior must be strictly controlled, as cooling too much or too fast can lead to the deformation of the model. Cooling the environment is controlled by fans. Their speed can be set depending on the stage of the print.

Since slicers only process the surface of an object, information about the filling of voids and the thickness of walls or surfaces (bottom and top layer) must be specified in the gcode. Infill and wall thickness are decisive for the stability of a printed object. Various patterns are available for filling, primarily from commercial/hobby printing, to generate the most stable structures possible in the shortest possible time or with the least amount of material used. The differences in the patterns are less relevant from a pharmaceutical point of view for now.

After all the information is set, the gcode can be exported. It includes the coordinates of the model inside the printer's specific coordinate system and the amount of material that must be pushed through the nozzle while going to the next point. Settings must be tested systematically to find a robust printing program for the printer and material used. Smaller and more intricate models usually require slower print speeds and more deliberate care with the first layer adhesion

than larger models with a bigger base. Thus, the decision for printing parameters is always a back-and-forth between quality and time-saving interests.

1.4.2.3. Step 3: Preparations for printing

A level print bed with the correct height for the print head at the start must be ensured for the print to be successful. Newer printers can sometimes take care of these points and have appropriate sensors. In this case, the function is set while writing the gcode, and the printer takes care of it before the print job [78]. Otherwise, the user should ensure the positions manually before printing. The material can be fed into the printer after heating the nozzle to the desired temperature. Filament or powder/granules must be pushed through the feeding mechanism to the nozzle to ensure sufficient material flow once the print job starts.

1.4.2.4. Step 4: The print

The zero position of the print head must be verified since all movement is controlled relatively by the movements along the axes. The printhead moves to the first coordinate and starts depositing material. It usually covers the outer layers first and then fills the voids according to the settings. When all coordinates on the first layer are covered, the plate is lowered, or the printhead is raised to deposit the next layer. No intervention should be necessary during the print if all settings are correct. When the whole model has been covered in this way, the printhead moves back to the zero position and lowers the temperature.

1.4.2.5. Step 5: Post-Printing

The model must first be removed from the print bed. If the print bed has been heated, it may be necessary to let it cool down before the model can be detached. Potential but somewhat unusual in the pharmaceutical field (Sandler et al. 2014) is the smoothing of the object. This involves the removal of rough edges or uneven surfaces that result from the layer-by-layer application and can be done by sandblasting or solvent vapor [79].

When not printing continuously, the filament or powder/granules must be removed from the printer and stored under specific conditions to increase shelf life and keep the materials dry [80]. The print head is cleaned (manually or fully automatically, depending on the machine) and can be used for a new print job using, for example, a different material.

1.4.3. Development of research in pharmaceutical applications

Research regarding pharmaceutical applications of hot melt extrusion and 3D printing has increased in the last 20 years [81], especially in FFF printing [82]. The beginning was made using commercial FFF printers with purchased filaments and then loaded with APIs [17,83,84]. While many papers showed the proof of concept, the low API loading and residual solvents proved disadvantageous [85] for real-life use. The next step in the research was to produce a loaded filament with sufficient properties to be used with commercial printers. Polymers used for these instances were cellulose derivatives [86,87], Eudragit products [88], or PVA [59,89]. A variety of release patterns was obtained from immediate to sustained release.

When filament printing was the only way of FFF-based 3D printing of pharmaceuticals, some researchers started to build printers enabling them to print directly from powder or semi-solid formulations [90,91]. Only later in the research, the development of specialized 3D printers for various pharmaceutical applications reached a point where universities and clinics could use them for small-scale development. Looking at the publication dates, the first one was the printer used for this thesis (M3dimaker [92]). Simultaneous development of a 3D printer with a similar concept took place at Triastek in China, leading to the development of the MED™ 3D printer [93]. Soon after, the commercial 3D printer Flexdose®, which enables 2D ink and 3D granules printing in a GMP-compliant device, was revealed [94].

1.4.4. Dual/multiple Extrusion

The development of FFF 3D printers led to the incorporation of more than one printhead. Using two different materials simultaneously enabled the printing of water-soluble support structures around non-water-soluble objects, increasing the possibility of printing objects. In the pharmaceutical sector, this technique can achieve many advantageous properties for tablets, such as multiple APIs and combinations of release kinetics, and improve stability and shelf life.

Two different ways of combining the active ingredients were investigated by Goyanes et al. [95], both based on capsule size four. One option was to combine the two active ingredient-containing filaments in layers with an alternating layer height of approximately 1 mm. The second option was a duo-capsule with a shell-core principle. They showed that combining two APIs is possible, and the design can determine the release pattern. On the other hand [74] had a more practical approach by combining two commonly combined drugs that need different release patterns. They further showed that kinetic control can be obtained by using osmotic tablets that release their API after water permeated [96]. Fast- and slow-releasing filaments made

from HPMC (hydroxypropylmethylcellulose) and PEO (polyethylene oxide) were also used [97] to test the influence of different core-shell tablet designs.

1.5. Customization of 3D-printed tablets

Customization of tablets can be divided into two main reasons. One is the change in the dosage, and the second is the dissolution pattern. A change in the dosage of a tablet produced from a filament or powder/granulate with a fixed API concentration means a change in the volume [98,99]. As explained in the printing section, the software detects outer surfaces and volumes of objects to be printed. This makes the inner volumes an easy target for the change of volume needed for the correct mass. Changing the amount of infill in these volumes can be done directly in the slicing software without changing the model. With the same external dimensions, tablets with different dosages could be produced from the same raw material. Since the dissolution also depends on the surface area available to the medium [100], this seems like a good idea. This holds true for tablets with completely filled inner volumes [17,101,102]. The challenge is that the external dimensions are only the same for different infill amounts as long as no medium gets inside the tablet. From this point, tablets with a lower infill have a much bigger surface area compared to their true volume, leading to faster dissolution times [83,84,103]. If an improvement in dissolution times is sought, this can be beneficial, but if a constant release for a range of dosages should be reached, this can become a problem. A more consistent way of changing the dosage with a much lower impact on the release would be to scale the model with a constant surface area to volume ratio [17,104].

In terms of release, there are many possibilities based on changing the available surface area of the model. As in traditional matrix tablets, pore-forming agents can be incorporated [105], but the manufacturing process also allows gaps/pores to be printed directly in the model [86] [106]. In addition, the shape can be varied to change the surface/volume ratio [104]. This approach is limited by the patient's acceptance and ability to handle and swallow tablets. Coming to more complex dissolution patterns, the onset of the dissolution can be set off by choosing a matching wall thickness [15]. The offset can also be made pH-dependent [107] by using different polymer compositions to match the pH-dependent solubility (e.g., enteric, gastric) [93]. One can imagine the possibilities that could be possible by combining these findings.

1.6. Characterization of powder, extrudate, and printed objects

The ability to correctly characterize the excipients, intermediate products (powder mixtures, extrudates/filaments), and final printed tablets is crucial for explaining the effects on extrusion,

printing settings, and dissolution behavior. The shift from descriptive models to predictive models can be accomplished by measuring and analyzing various variables.

1.6.1. Thermal Analysis

Instruments that can detect temperature-dependent changes in substances are summarized in the category of thermal analysis. Combining many analytical techniques with a controlled temperature change has many applications in the pharmaceutical industry [108]. The research discussed here primarily provides information about thermal stability, water loss, and melting or T_g. Most often, devices can perform dynamic scanning calorimetry (DSC) and simultaneous thermal analysis (STA). The primary capability of DSC is to measure heat flow, which is the amount of energy flowing into or out of the sample. Since transitions such as phase transitions require a change in energy compared to an inert reference, heat flow can be used to detect such transitions. A high heating rate improves the sensitivity of DSC measurements by increasing the heat flow over a shorter timeframe [109]. Helpful properties in this thesis are the presence or absence of melting points and T_g. The melting point indicates the presence of crystalline particles. On the other hand, the glass transition has more implications for (partially) amorphous substances such as polymers and mixtures. During the temperature change, an amorphous substance changes from a supercooled liquid to a rubbery state [110]. While both properties can be measured using DSC, detection limits concerning particle size and phase-separated domains must be discussed. DSC is expected to be able to show phase separations in samples down to 30 nm [111,112]. This means that nanocrystals and API-rich phases below 30 nm might not be detected, giving a false signal for determining a homogeneous solid dispersion. The relation between the stability of solid dispersions and T_g has been discussed. Additionally, for stability, DSC can help detect the polymer-API miscibility. The change in T_g of a polymer in the presence of another substance can indicate the degree of miscibility [113].

1.6.2. X-ray diffraction (XRD)

X-ray´s discovery by Wilhelm Conrad Röntgen in 1895 [114] led to the opening of a new field of applications. Sometime after the discovery, the first experiments regarding the diffraction in crystals were published [115].

X-rays can be described as high-energy electromagnetic waves with a wavelength ranging from 10^{-3} to 10^1 nm [116]. X-rays are generated by heating a tungsten filament in a vacuum (to reduce unintentional impacts with gas molecules). This process causes the tungsten to emit electrons, which are then accelerated by a potential field. As the electrons approach the anode, they

decelerate, resulting in x-rays being emitted with a decrease in energy and a continuous spectrum of wavelengths (bremsstrahlung [117]). When electrons collide with the anode, they can ionize electrons in the inner shell of the anode's atoms. Outer shell electrons compensate for the missing inner shell electrons and release the energy difference as photons. The wavelength of this radiation is specific to the type of atom present in the anode. The resulting X-ray spectrum combines the continuous spectrum from bremsstrahlung with characteristic wavelengths. Since most modern applications utilize only the radiation wavelength with the highest intensity, the remaining spectral components need to be eliminated. This can be achieved using filters or monochromators. Various interactions, such as absorption and scattering effects, can occur when X-rays interact with matter. The elastic scattering process used to create diffraction patterns is known as Raleigh scattering. In elastic scattering, the wave's energy remains constant, maintaining its phase relationship with the original wave while being scattered in all directions, resulting in constructive and destructive superposition. The patterns of constructive and destructive interference of waves depend on the spatial orientation of their origin, specifically the atoms from which they diffract. Within crystal lattices, atoms are arranged at regular intervals, forming planes of atoms [118].

The Braggs equation [119]

$$2 * d_{hkl} * \sin(\Theta)_{hkl} = n\lambda \tag{1}$$

describes the relationship between the lattice spacing (d_{hkl}) and the angle (Θ) depending on the wavelength of the incident x-ray beam (λ). When the conditions for any given multiples (n) of λ are satisfied, diffraction occurs. In pharmaceutical applications, sensitivity to at least 5% of crystalline material can be quantified [120]. While DSC shows higher sensitivity for detecting crystalline structures than XRD, it can only find them at the glass transition or melting temperature. Due to improved solubility at elevated temperatures, the DSC results might not fully apply to the state at room temperature. This disadvantage of DSCs measuring the existence of glass transition or melting temperature at elevated temperatures can be compensated partially by adding XRD measurements [121] since XRD measurements can be done at room temperature.

1.6.3. Confocal Raman Microspectroscopy (CRM)

For the discovery of a light scattering effect, named after its discoverer Sir C.V. Raman [122], Sir Raman was awarded the Nobel Prize in 1930 [123]. In contrast to XRD, the Raman effect relies on the inelastic scattering of an incoming energy source (laser).

Light interactions with the material can result in various phenomena, such as absorption, transmission, and scattering. In absorption, the light's energy is fully absorbed and typically converted into heat. Transmission indicates that light moves through materials with minimal interaction. Scattering, on the other hand, involves variations in energy level and light direction between incoming and emitted light. It can be categorized as elastic or inelastic scattering. Elastic scattering (emitted wavelength is the same as the exciting wavelength) is called Raleigh scattering, which is generally unwanted for CRM and removed via Raleigh filters. The inelastic nature of Raman scattering means that the spectrum depends on the vibrational mode of a specific molecule and not on the wavelength of the excitation source [124]. Inelastic scattering is a rather rare event, considering the occurrence of other optical phenomena. Raman scattering can then again be subdivided into Stokes and anti-Stokes Raman scattering. Stokes Raman scattering appears when the laser photon interacts with a molecule in its ground state, while anti-Stokes Raman scattering only occurs due to the interaction with a molecule in its excited state.

The vibrational mode of a bond can be described as the oscillation movements of an atom around its equilibrium position. They can be divided into stretching and bending or deformation movements. The frequency of a vibration can be described as

$$\omega_{vib} = \sqrt{\frac{f}{m_{red}}} \tag{2}$$

with f representing the force constant (force of interaction) and m_{red} the reduced mass of the vibrating atoms. Plotting the intensity of the detected scattered wave against its wavenumber, which is the reciprocal of the wavelength, leads to an x-axis that changes depending on the excitation wavelength. Thus, the concept of the Raman shift is used, where the intensity is plotted against the shift in wavelength from the excitation wavelength, leading to a universally used x-axis. Vibrations in the high-frequency region ($1500 - 4000 \ \text{cm}^{-1}$) refer to the stretching vibration of single bonds with hydrogen and double bonds containing carbon, oxygen, and nitrogen. Wavelengths below $1500 \ \text{cm}^{-1}$ are called the fingerprint region. In this region, molecules show specific vibrations from the stretching and deformation of single bonds of carbon, nitrogen, and oxygen (C-C, C-N, and C-O) [125]. The spectrum not only depends on the individual bond but also on the molecule's bonding environment, making it a unique pattern. Individual substances and mixtures can be identified and quantified using these spectra.

The choice of the laser wavelength depends on three factors. Raman scattering intensity is proportional to λ^{-4*}, meaning a lower wavelength leads to a much higher signal intensity. The spatial resolution also partially depends on the wavelength [126]. The setup of a focusing lens and a pinhole located confocal to the focus point leads to a device that can reach a spatial resolution of around one μm^3 [127]. The maximum resolution depends on the wavelength and numerical aperture of the objective [128], whereby smaller wavelengths and higher numerical apertures can resolve a smaller distance between two points. The penetration depth of the laser into the sample is also related to the wavelength since larger wavelengths penetrate deeper into the material [129] while offering reduced resolution due to the larger focal point [130]. The choice of the appropriate wavelength is a consideration between the need for depth penetration and higher resolution.

In this work, a laser wavelength of 532 nm was used in a confocal setup to examine the surface of printed tablets. For qualitative analysis of pharmaceutical products, CRM can be used to measure the substances expected to be found. Afterwards, individual spots or areas on the product can be measured. Comparing the spectra to those of the individual substances provides information about the location and phase separation of the API or other excipients. However, since independent positions may not be representative of the entire sample, multiple positions must be measured individually, leading to improved information about the sample at the cost of longer measuring time.

1.6.4. Melt rheology

Melt rheology refers to the information gathered about the rheological properties such as shear rate- or temperature-dependent viscosity. These properties are crucial to the understanding of polymer behavior during extrusion processes. There are three main setups possible for rotational or oscillating rheometers, depending on the type of material and measurement needed. Generally, the setup consists of a stationary and a rotatable part. The stationary part can be a level plate for both the cone-plate and the plate-plate setup. The former uses a cone with a low angle (typically smaller than 4°) to even out the shear rate across the diameter. The latter has a second level plate on top and can be used for a large variety of materials including high-viscosity ones. The third option usually used for low-viscosity materials is the cup-and-bob setup.

The general understanding of a body's shear deformation involves the applied force F to its upper surface area A. It can be viewed as material layers sliding across each other like a deck of cards, resulting in shear stress τ [131].

$$\tau \left[\frac{N}{m^2}\right] = \frac{F}{A} \tag{3}$$

Once deformation is reached, the strain γ can be calculated from

$$\gamma = \frac{\Delta L}{y} \tag{4}$$

where ΔL represents the deformed length and y the height of the deformed body. The uppermost layer shows the highest flow speed, and flow speed drops down to zero in the lowest layer. This speed drop is called shear rate $\dot{\gamma}$ and can be calculated in parallel plate setup as:

$$\dot{\gamma}[s^{-1}] = \frac{v_{max}}{y} \tag{5}$$

with v_{max} the speed at the uppermost layer and y the body's height. The dynamic viscosity can then be calculated as

$$\eta \ [Pa*s] = \frac{\tau}{\dot{\gamma}} \tag{6}$$

The correlation between shear stress and shear rate, which represents the shear rate-dependent viscosity, describes the flow curve. The rheological behavior of polymer melts is complex as they usually exhibit viscous (dissipative) and elastic (storage) characteristics. In the case of long-chain polymers, the elastic portion can be explained by the shape polymer chains exhibit at their minimum-energy state. They are found in an entangled and/or interlooped state. When a directional force is applied, the polymer chains stretch, and after the force is removed, the molecules attempt to relax and return to their unstretched shape [132]. The elastic range can be surpassed with a directional force that is large enough and over a sufficient range and time frame. The chains disentangle and irreversibly orient in the direction of the applied force, resembling the viscous portion. Adding plasticizers to polymers has several effects on thermal and physical properties. The influence on T_g can be detected via DSC. The effect on physical properties, such as viscosity measured by rheological experiments, can be explained by the reduction of spatial restrictions and the increase in chain mobility [133]. Generally, with a reduced T_g at the same temperature, a lower viscosity or the same viscosity at a lower temperature can be expected. This leads to the possibility of increasing the throughput or allows for reduced temperatures during extrusion processes.

A rotational rheometer with a parallel plate setup was used in this thesis. Small amplitude oscillatory shear experiments were conducted after determining the linear viscoelastic range (LVR) for each sample and temperature individually. Some key characteristics of the LVR are explained in the following: Inside the LVR, stress and strain are directly and proportionally linked through the storage (elastic component) and loss modulus (viscous component). Both moduli are constant inside the LVR, indicating that it depends not on the amplitude of stress or strain but the frequency. Also, every deformation that happens inside the LVR is fully reversible. Before the measurements with increasing frequency at a fixed amplitude, the LVR must be tested. This is needed to ensure the linear behavior of the sample and avoid non-reversible and time-dependent behavior.

As a general rule for extrusion processes, the temperature should be selected so that the viscosity at 0.1 rad/sec is 1000-10000 Pa*s (Solanki et al. 2018), but a more precise prognosis can be made after obtaining rheological data.

1.6.5. Texture analyzer

The basic construction of a texture analyzer consists of a sample holder (the shape depends on the test and sample body) and a mobile fixture with a switchable probe that allows vertical movement while measuring load and distance precisely [134]. While many testing setups can be realized by a texture analyzer tensile tests [135], buckling tests [66], 3-point-bending tests [72,136], and indentation tests [74] are used for the testing of filaments for 3D printing.

Low ductility and high stiffness seem to be the primary desired characteristics, as described in the introduction to filament printing. Observing the upper and lower limits for ductility and stiffness in devices used on-site in comparison with stiff or very soft commercial filaments is a good predictor so far (Thakkar et al. 2020).

1.7. Discussion of 3D printing in the pharmaceutical industry

3D printing is a relatively new method for producing pharmaceutical and medical applications. Several techniques are currently under investigation for pharmaceutical applications of 3D printing. With Spritam® (Aprecia Pharmaceuticals, LLC.), the first drug from the 3D printing field using the binder-jetting technique was approved. The following discussion mainly focuses on FFF printing of filaments or powder/granules. There are several advantages to 3D printing that can be exploited for research and development. Rapid prototyping can speed up the development of new drug products by reducing batch size and improving cost efficacy. Due to

the smaller batch sizes, the options for individualization are much more significant. Several sizes and geometries [75], release trends, dosages [17], and drug combinations can be realized with the same setup [137]. Even formulation challenges during the development of a vehicle for a poorly water-soluble but highly promising API can be solved by 3D printing of solid dispersions. Challenging properties of conventionally produced tablets, such as friability and hardness, are usually not an issue [16], and post-processing of the printed object is usually unnecessary.

Pharmaceutical production is a highly regulated field, and 3D printing is not expected to be an exception to this rule. Guidance on the Good Manufacturing Practice (GMP) of 3D printed tablets and other devices must be established. This starts with the quality of raw excipients. While the processability of several polymers was shown for hot melt extrusion processes, temperature and stress-dependent degradation in 3D printing must be fully explored before human trials can be conducted. A major disadvantage of the currently available printers is the variability of operations between different prints. In contrast to a rotary press with fixed process parameters and batch-wise release of the products, filaments or powder/granules must undergo quality assurance as a surrogate for the final product. While generally speaking, ICH 6 guidelines for good clinical practice [138] should be applicable for 3D printed pharmaceuticals as well, one has to keep in mind that they are only set up for routine bulk manufacturing and will need additional guidance for patient-specific production [139]. Additionally, the combination of two or more drugs would be considered a new formulation by the U.S. Food and Drug Administration (FDA), issuing extensive clinical trials. The European Medicines Agency (EMA) acknowledges the need for new regulatory guidelines and changes in the GMP requirement in its strategic reflection paper, foreshadowing the work planned up to 2025 [140]. The draft from 2018 was revised based on results from public consultation [141]. This already led to the foundation of a new expert group in the EMA structures with the task of innovating the regulatory framework of the EMA and exchanging information between the regulators, academia, and industry [142]. Despite emerging interest in the regulation of innovative technologies by regulatory bodies, academia and industry have established the international pharmaceutical 3D printing initiative Pharma3DPI [143] to pursue clinical implementation of 3D printed pharmaceuticals [144]. Although the regulatory framework for pharmaceuticals is not established yet, there is some information regarding additive manufacturing [145] and quality control of medical devices [146,147] that could be a promising approach for the future of pharmaceuticals [148].

Even with an improved regulatory framework, the challenge of missing batch release control is not solved. The need for sufficient validation of the manufacturing process and online and non-destructive analysis methods is not yet met. Extensive research into the critical quality-determining settings and potential corrective or preventive actions related to the specific printing method must occur to set appropriate intervals for in-line and on-line controls. Critical quality attributes (CQAs) and process parameters (CPPs) must be established and monitored [149]. Currently, there is little option for quality control of printed tablets. However, non-destructive analytical methods such as near-infrared spectroscopy [150] and in-line weighing are being considered. For future development and approval, predictive tools such as Design-of-Experiment (DoE), finite element analysis, and emerging AI machine-learning tools can increase the safety and efficacy of manufacturing [151]. Contrary to popular belief, a 3D printer is a high-maintenance device. Many hardware and software-related settings must be checked regularly, and extensive troubleshooting must occur. While European and American members of academia and industry are looking to solve those GMP and approval-related challenges, the Chinese industry seems to be pulling ahead. Triastek has just (29.07.2024) introduced their GMP-conform production center for large-scale continuous manufacturing of 3D-printed pharmaceuticals [152], estimating a maximum annual capacity of 75 million units in the initial continuous production line.

To contribute to the knowledge base on pharmaceutical 3D printing, this thesis leveraged the flexibility of excipient use and dosage design to develop an immediate-release formulation containing CAB for oral administration. State-of-the-art methods such as CRM and XRD were employed for non-destructive analysis, expanding the potential scope of quality control criteria. Melt rheological measurements were conducted to assess material characteristics with potentially predictive value. These measurements can expedite the development of extrudable combinations of excipients while simultaneously reducing the time and material required.

2. Experimental section – Part 1

The first part of the experimental section explains the experiments conducted with ibuprofen before the publication using LOP. Ibuprofen was chosen as a model API for preliminary trials with commercial-grade 3D printing filament to evaluate the feasibility of loading the filament with an API from a solution and printing it afterward.

2.1. Loading by soaking - Ibuprofen

Drug loading of polymers, especially polymer-based filament, can be achieved by extrusion or solvent-based methods such as soaking the filament in an API solution. In preliminary experiments, the loading of filaments made from polylactic acid (PLA) and polyvinyl alcohol (PVA) with ibuprofen was investigated in different organic solvents. Since virtually no ibuprofen was found in the PLA filament, it was discarded for further testing. In the extended setup, the solvents (EtOH and IsopropOH) were supersaturated with ibuprofen to maintain a constant concentration in the medium and heated to 40°C. The PVA filament was submerged in the solution, and for two weeks, daily samples of filament and the solution were evaluated for their concentration and drug content using UV-VIS coupled HPLC. Filament pieces were extracted from the solution and dried. Any residual solvent was removed under vacuum until the mass showed no more change. To determine the correct loading inside the filament, the outer layer where ibuprofen precipitated must be cleaned before drug content evaluation. The method for the HPLC analysis consists of ten minutes of isocratic elution with 55% medium A and 45% medium B (A: acetonitrile; B: water / 0.01% formic acid) at 35°C. The flow rate was set to 1 ml/min with a detection wavelength of 264 nm. Calibration curves were tested from 50 mg/ml to 5 ng/ml with the lowest R^2 of 0.9971. The results of loading PVA filaments in saturated solutions are shown in Figure 1.
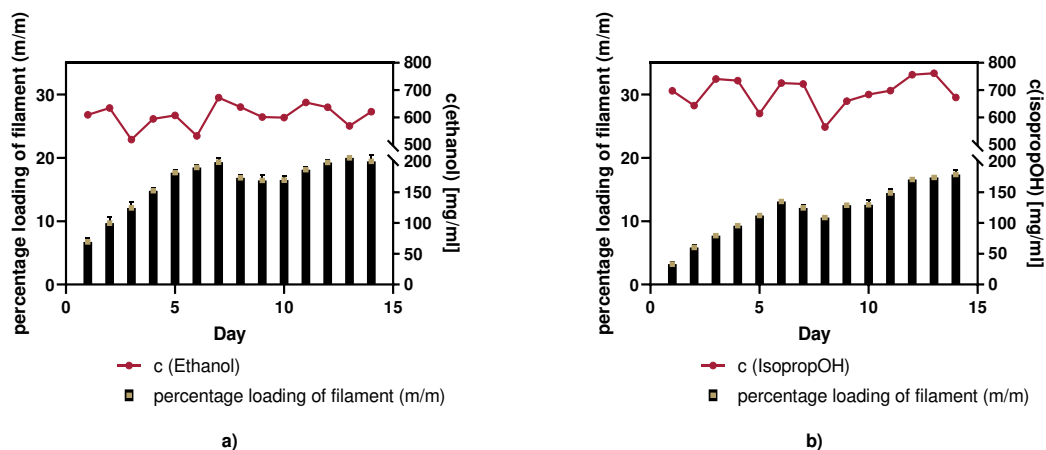
Figure 1 Results of the loading by soaking experiment with ibuprofen (a) ethanol; b) isopropyl alcohol)

From the given results, it can be concluded that ibuprofen has a slightly higher solubility in IsopropOH than in EtOH. Based on the solubility parameters, a higher solubility would be expected in EtOH [153], but there is also a lot of inter-day variability. Also, it could be observed that the swelling behavior of the filament was dependent on the solvent used. Ethanolic solutions led to an increased swelling compared to IsopropOH. While the maximum amount of ibuprofen in the PVA filament depends on the miscibility of both, the kind of solvent does play a role in reaching the maximum loading possible. Thus, even though the concentration in EtOH is slightly lower, the increased swelling properties lead to a faster increase in ibuprofen recovered from the filament. Possibly, after a more extended period, the loading in the IsopropOH would reach the same level as samples in EtOH from day 10 to 14. There is still some slope left. The technique is not very promising, looking at results from previous research [17,84,106,154]. There are several disadvantages to this method. The drug loading that can be expected from loading in a saturated solution is low (usually <5% or even <1%). When comparing the drug load to the amount of drug used for the preparation of the saturated solution, there is a vast imbalance compared to hot melt extrusion. Also, loading filament this way takes considerably longer than extrusion. In the results described above, 14 days were not necessarily enough to reach maximum loading. Still, if the loading time, maximum loading capacity, and material usage were to be solved for individual substances, there would be quite an effort in post-processing. First, the outside of the filament needs to be cleaned, but then organic solvents [155] must also be removed to comply with ICH guidelines [156] and pharmacopeia requirements. These are all relevant reasons why we do not see this technique used in large-scale industrial manufacturing.

2.2. Selection of model API

Ibuprofen was a cheap and harmless API used to explore different methods and devices. However, the correlation to behavior that CAB might show was expected to be low due to their different chemical structures. Since the goal was to find information about miscibility with different polymers and potential crystallization behavior, the solubility parameters were used to predict a similar model API that was cheaper and less harmful than CAB (Thanks to Markus Zimmermann and Marc Engelhard from AK Böckler, University of Tübingen). Based on the solubility parameters calculated for CAB and neratinib, a model API was chosen for further testing. During this screening, the solubility parameters of 39 APIs and 900 other molecules from a database were calculated using their SMILES (Simplified molecular input line entry system) codes. The model API with the highest overlap in all categories checked was used for further experiments. Table 1 shows the results for the best hits found during the screening and their deviation in all the categories compared to neratinib and CAB.

Table 1 Solubility parameters of the best hits for both CAB and neratinib

Name	D_disp	D_polar	D_hydro	Molar_Volume	D_disp_norm	D_polar_norm	D_hydro_norm	Molar_Volume_norm				
Neratinib	19.2	1.79	8.30	435.40	0.87	0.55	0.45	1.02	0.45%	4.06%	3.83%	13.52%
Ibuprofen	17.6	2.63	7.50	202.53	0.80	0.80	0.41	0.47	7.73%	21.52%	8.20%	40.81%
Glibenclamid	18.6	1.93	7.70	376.98	0.85	0.59	0.42	0.88	3.18%	0.04%	7.10%	0.11%
Loperamid	18.9	1.86	8.40	405.27	0.86	0.57	0.46	0.95	1.82%	2.06%	3.28%	6.49%
Cabozantinib	19.3	1.93	9.00	377.45	0.88	0.59	0.49	0.87	0.45%	4.06%	3.83%	13.31%
Ibuprofen	17.6	2.63	7.50	202.53	0.80	0.80	0.41	0.47	7.27%	25.58%	4.37%	53.48%
Verapamil	17.3	1.81	6.00	428.67	0.79	0.55	0.33	0.98	8.64%	0.43%	12.57%	1.55%
Amiodaron	18.9	1.85	5.10	408.35	0.86	0.57	0.28	0.94	1.36%	1.79%	17.49%	6.21%
Glibenclamid	18.6	1.93	7.70	376.98	0.85	0.59	0.42	0.87	2.73%	4.10%	3.28%	13.42%
Loperamid	18.9	1.86	8.40	405.27	0.86	0.57	0.46	0.93	1.36%	2.00%	0.55%	6.92%

Since the best fit, looking at the similarity of both CAB and neratinib was found to be LOP, it was used for further experiments.

2.3. Loading by soaking - Loperamide

Having an API with very different solubility parameters and molar mass than ibuprofen, the loading by soaking strategy was reevaluated. Analogous to previous trials, samples of the PVA filament were stored in saturated solutions made from LOP in different solvents, now adding MeOH as an additional solvent to EtOH and IsopropOH at 40°C. Each day, three samples were removed, cleaned, dried, and dissolved to find their LOP content. Additionally, a sample from the solution was taken to check the concentration. Determination of the LOP content and the concentration of the solution was done according to [157]. Figure 2 shows the results of this experiment.
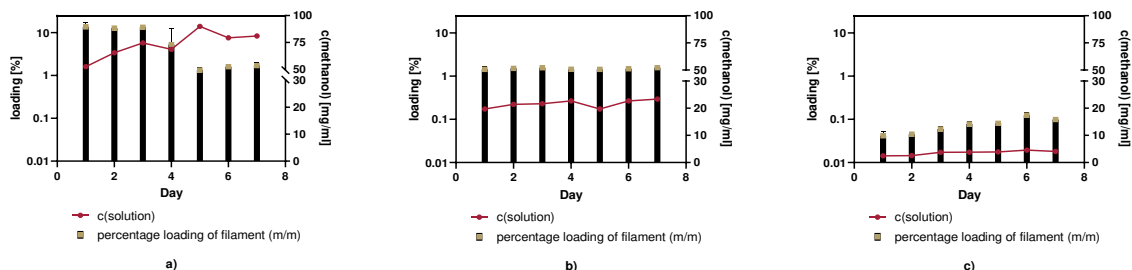
Figure 2 Results of the loading by soaking experiments using LOP

There is an apparent dependency between LOP concentration in the solvent and the maximum loading. MeOH with the highest concentration in the solution leads to the highest concentration in the filament, descending from EtOH to IsopropOH. The time it takes to reach the maximum loading is much faster than the ibuprofen trials but also seems dependent on the kind of solvent. While for MeOH and EtOH, one day seemed enough to reach saturation levels in the filament, it took the IsopropOH samples longer. One reason might again be the swelling potential of the solvents used. It was evident that MeOH led to a massive increase in the swelling of the filament. Thus, the filament pieces could not hold together and broke on their ends. An exemplary picture of the broken filament is shown in Figure 3.

Figure 3 PVA filament stored in ibuprofen-saturated methanolic solution

Since this renders the filament useless independently from the loading, EtOH with the next best solubility and swelling capacity was further evaluated. The results in Figure 2 show that the PVA filament was already at maximum loading after one day. A second experiment with much closer sampling intervals was set up to determine how fast the loading during the soaking phase was. Over seven hours every 30 minutes, with an additional endpoint at 24 hours, samples were drawn and evaluated in the same manner as described previously. Results for the 24 h loading experiment are given in Figure 4.
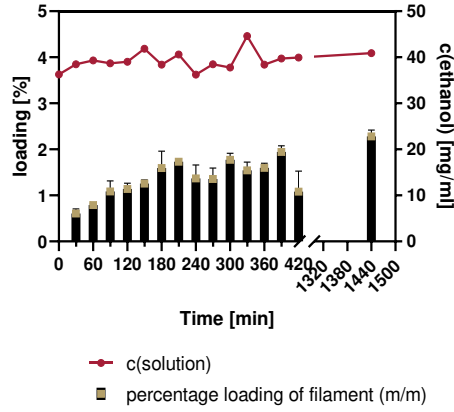
Figure 4 Loading by soaking with PVA in a saturated ethanolic LOP solution throughout 24 h

The 24-hour endpoint was slightly above the expectations from the seven-day trials. More interestingly, the increase of LOP in the filament was visible over the first four hours. From these data points, the steady-state flux and the permeability coefficient can be calculated [85] using values up to 210 min. The surface area of the filament piece is calculated as a cylinder:

$$s[cm^2] = 2\pi r^2 + 2\pi rh \tag{7}$$

with *s* being the surface area of a filament sample with the height *h* and a radius *r*. The samples used had a length of 33.0 ± 0.495 mm and a diameter of 1.75 ± 0.03 mm. This leads to a surface area of 186.24 ± 0.048 mm^2. From the amount of LOP taken up, the steady state flux (J_{ss}) can be calculated:

$$J_{ss}\left[\frac{mg}{cm^2 * h}\right] = \frac{d_M[mg]}{s[cm^2] * d_t[h]} \tag{8}$$

where d_M represents the LOP uptake by the surface s during the time d_t. From the mass difference obtained from weighing the filament pieces prior to and after removal from the solution a J_{ss} value of $3.191 * 10^{-1} \frac{mg}{cm^2 * h}$ was calculated. In the next step the permeability coefficient *P* of LOP into PVA filament can be obtained from:

$$P\left[\frac{cm}{h}\right] = \frac{J_{ss}\left[\frac{mg}{cm^2 * h}\right]}{c_{sat}\left[\frac{mg}{cm^3}\right]} \tag{9}$$

by dividing the steady-state flux by the concentration of the saturated solution c_{sat}. The permeability coefficient *P* of LOP was calculated as $8.121 * 10^{-3} \frac{cm}{h}$. Based on the results from the loading by soaking experiments some miscibility between LOP and PVA could be expected.

- 26 -

These results were underlined by DSC measurements finding no recrystallization when mixing and heating PVA and LOP in comparison to fast recrystallization from pure LOP samples. First indications of miscibility of PVA and LOP were a confidence-inspiring finding leading to the long-term implementation of LOP as the model API.

The next step was printing LOP in Parteck MXP (PVA, Merck KGaA, Germany) using the 3D printer M3dimaker, which enabled direct powder extrusion and tablet printing with LOP. The groundwork for printing procedures and analytical procurement can be seen in the following publication. The printer setup, CAD, and .stl data were developed together with the implementation of XRD and CRM for quality control and melt rheology as a predictive tool for further formulation development.

Article

Evaluation of Printability of PVA-Based Tablets from Powder and Assessment of Critical Rheological Parameters

Jonas Lenhart [1](ID), Florian Pöstges [2](ID), Karl G. Wagner [2](ID) and Dominique J. Lunter [1,*](ID)

1   Department of Pharmaceutical Technology, Eberhard Karls University, 72076 Tuebingen, Germany;
    jonas.lenhart@uni-tuebingen.de
2   Department of Pharmaceutical Technology and Biopharmaceutics, University of Bonn, 53121 Bonn, Germany;
    florian.poestges@uni-bonn.de (F.P.); karl.wagner@uni-bonn.de (K.G.W.)
*   Correspondence: dominique.lunter@uni-tuebingen.de; Tel.: +49-7071-2978790

Abstract: Fused deposition modeling (FDM) is a rather new technology in the production of personalized dosage forms. The melting and printing of polymer–active pharmaceutical ingredient (API)—mixtures can be used to produce oral dosage forms with different dosage as well as release behavior. This process is utilized to increase the bioavailability of pharmaceutically relevant active ingredients that are poorly soluble in physiological medium by transforming them into solid amorphous dispersions (ASD). The release from such ASDs is expected to be faster and higher compared to the raw materials and thus enhance bioavailability. Printing directly from powder while forming ASDs from loperamide in Polyvinylalcohol was realized. Different techniques such as a change in infill and the incorporation of sorbitol as a plastisizer to change release patterns as well as a non-destructive way for the determination of API distribution were shown. By measuring the melt viscosities of the mixtures printed, a rheological model for the printer used is proposed.

Keywords: 3D printing; hot-melt extrusion; personalized dosage; melt-rheology; dissolution; confocal Raman microspectroscopy; FabRX

1. Introduction

Three-dimensional printing as part of additive manufacturing has had huge impacts on different parts of technological advancements. With the beginning of research on the use of 3D printing in medical and pharmaceutical disciplines, the hopes for using the benefits of these techniques have risen. With Spritam® and ZipDose® technology (Aprecia Pharmaceuticals, LLC, Blue Ash, OH, USA), the first 3D printed tablet, using a combination of powder layering and inkjet technology, was approved by the FDA in 2015 [1]. Different extrusion-based technologies such as semi-solid extrusion (SSE) [2,3] and fused deposition modeling (FDM) were considered in the research of medical devices and pharmaceutical products, so much so that recently Triastek (Triastek, Inc., Nanjing, China) has received IND (Investigational New Drug) clearance for their second 3D printed product T20 using melt extrusion deposition (MED™) technology [4]. With the rise of extrusion-ready pharmaceutical-grade excipients, tablets with different release patterns were produced using the FDM-based 3D printing technique. In terms of orally administered dosage forms, immediate release [5], modified release [6,7], bilayer [8], and even intra-gastric floating tablets [9,10] have been developed. The main advantage of 3D printed medicines is seen in the ability to produce customizable and patient-oriented geometries and strengths of tablets as well as in rapid prototyping [11]. While the general acceptability of 3D printing has been shown, concerns were found regarding different shapes. Already established shapes such as capsule or disc-shaped printlets are regarded as acceptable for swallowing, whereas more intricate shapes such as tilted diamonds were harder to "sell" to the testing group [7]. The first approaches of 3D printing used commercially available 3D printers and filaments. The filament was loaded with the API (active pharmaceutical

ingredient) using different techniques such as loading by soaking [12]. The disadvantages found in the control of the loading and general concerns about solvent usage over time rendered this method obsolete. The next step was to extrude the filament needed directly from raw materials and to include the API in the desired concentration [13]. Filament production is challenging since an additional heating step is needed, which can negatively impact thermo-degradable drugs and polymers. Also, production must be strictly controlled to result in a sufficiently uniform filament. To avoid these problems, the extrusion and printing must take place in a single step. The company FabRx (FabRx Ltd., London, UK) developed a 3D printer especially for use in the development of pharmaceutical products. The filament printhead is exchanged for a printhead consisting of a small-scale single-screw extruder with a detachable nozzle which enables so-called direct powder extrusion (DPE) [14]. This opened the door to the printing of many of the excipients already developed for hot-melt extrusion (HME). While printing with filaments requires extensive knowledge of excipients and devices to produce filaments with relevant properties such as tensile strength, these parameters are not relevant when printing directly from the powder. Mechanical properties are key to printability for filament printers. A main prerequisite is longitudinal rigidity, which is shown by a high Young's modulus while allowing no deformation or breakage during mechanical stress in printers feeding elements [15]. Thus, printing temperature can be reduced for the use of thermo-degradable drugs and polymers by incorporating plasticizers.

The aim of our research was to show that biopharmaceutics classification system (BCS) class II [16] drugs can be directly printed from powdered excipients into tablets with different strengths while forming amorphous solid dispersions (ASD). BCS class II compounds show low (water-) solubility and high permeability, so an improvement of the solubility is often searched for. Polyvinylalcohol (PVA) is a well-researched pharmaceutical excipient that shows appropriate thermal behavior (no thermal degradation up to at least 230 °C, appropriate melt viscosity) as well as water solubility [17]. As per the safety data sheet, the melting region is listed as 160–240 °C and the degradation temperature as above 200 °C. The synthetic opioid agonist loperamide (hydrochloride) [18] was used as a thermally stable BCS class II compound. One of the main challenges was to be able to form ASDs while performing the printing at temperatures well below the melting point of loperamide (220–228 °C [19]) since the thermal degradation of PVA starts below the melting temperature of loperamide. Information about the requirements of excipients for extrusion/3D printing using direct powder extrusion is scarce. Thus, a rheological model for PVA showing the minimum melt viscosity needed as well as the temperature and shear rate dependency was investigated.

Melt rheology and information about extrusion processes can be crucial for hot-melt extrusion as well as extrusion-based 3D printing. In previous studies, different approaches have been investigated to generate information regarding certain printers. Temperature as well as the closely related melt viscosity were parameters that were found to be of importance for further development [20,21]. Too low viscosity leads to oozing and dripping from the nozzle, reducing print quality, while too high viscosity leads to improper material flow up to a clogged nozzle or reduced layer adhesion.

Regarding the release behavior, the aim was set to be equivalent to typical formulations with immediate to sustained release.

2. Materials and Methods

2.1. Materials

PVA (Parteck® MXP (Polyvinylalcohol), Merck KGaA, Darmstadt, Germany) was used as a water-soluble pharma-grade excipient available for (HME). Fumed silica (Aerosil® R 972 Pharma, Evonik, Essen, Germany) was added to improve the flowability of the powder mixtures. As model API, loperamide hydrochloride (100% purity, Merck KGaA, Darmstadt, Germany) was selected. As a commonly used plasticizer for PVA, sorbitol

(Parteck SI 400, Merck KGaA, Darmstadt, Germany) was used. All solvents used (Methanol, Acetonitrile, ammonium acetate) were HPLC-grade.

2.2. Methods

2.2.1. Thermal Analysis

Differential Scanning Calorimetry (DSC)

Pure substances were analyzed via DSC (Mettler DSC 820, Mettler-Toledo GmbH, Gießen, Germany) regarding their melting point, glass transition temperature, and possible recrystallization. Printed tablets were measured after 2–4 weeks of storage. Approximately 10–15 mg samples were accurately weighed into sealed aluminum pans with punctured lids. The measurements used a heat-cool-heat cycle to determine the melting point in the first heating and glass transition temperature during the second heating. Information about the miscibility of loperamide (LOP) and Parteck MXP (PAR) was expected to be found during the DSC trials. One of the approaches for the estimation of glass transition temperature is described by the Gordon–Taylor equation, which can be applied to miscible blends.

$$T_{g,\,mix} \approx \frac{[\omega_1 * T_{g,\,1} + K * \omega_2 * T_{g,\,2}]}{\omega_1 + K * \omega_2} \tag{1}$$

with $T_{g,mix}$ and $T_{g,i}$ representing the glass transition temperature of the mixture and the components, ω_i is the mass fraction component I, and K is an adjustable fitting parameter.

It is expected for two miscible substances to show one glass transition temperature instead of two individual glass transition temperatures. The detected temperature should be partially composed of the individual glass transition temperatures [22].

Simultaneous Thermal Analyzer (STA)

Thermal degradation as well as the loss of water taken up from air humidity during printing and storage was tested using a Netzsch STA 409 PG/1/G Luxx (Erich NETZSCH GmbH & Co. Holding KG, Hanau am Main, Germany). All samples were treated the same way, measuring the mass of a sample using Al_2O_3 as a reference during the heating of the samples up to 250 °C. Pure substances and printed tablets were measured at a mass of approximately 22 mg.

2.2.2. XRD-Measurements

Wide angle X-ray (powder) diffraction patterns were obtained in an angular range of 10–50° 2θ with a stepwise size of 0.02° on a Bruker D8 Advance diffractometer (Bruker Corp., Billerica, MA, USA) using monochromatic CuKα radiation (λ = 0.15406 nm). Pure substances were measured in powdered form, while printed tablets were measured intact.

2.2.3. Melt Rheology

To measure the viscosity of the molten mixtures and thus link the rheological properties to the printing process, the shear rate occurring during printing was determined. Two different methods related to different extrusion processes were compared.

The first method is usually used in FDM 3D printers that run on filament. Here, only the shear rate in the nozzle is considered [23].

Volume flow (Q) was determined empirically by accurately weighing printed tablets with 100% infill and measuring their volume (V) using a gas displacement pycnometer (Accupyc 1330, Micromeritics Instrument Corporation, Norcross, GA, USA). The temperature was set to 25 °C while the remaining volume was flushed with Helium. During printing, the time (t) for each individual tablet was recorded. The following equation was employed afterwards:

$$Q = \frac{V\,[\mathrm{mm}^3]}{t\,[\mathrm{s}]} \tag{2}$$

The apparent shear rate at the nozzle wall ($\dot{\gamma}_{wa}$) can be calculated as:

$$\dot{\gamma}_{wa} = \frac{4Q}{\pi r_n^3} \tag{3}$$

with a radius (r) of the equipped nozzle of 0.04 cm.

The second method is applied to extrusion processes and used to calculate shear rates inside single-screw extruders. An approximation of the shear rate $\dot{\gamma}$ in the screw channel can be achieved from the Couette shear rate:

$$\dot{\gamma} = \frac{v_b}{H} = \frac{\pi D N}{H} \tag{4}$$

with v (velocity), H (channel depth = 0.55 mm), D (diameter = 8.0 mm), and N (screw speed) [24].

Melt rheology was conducted using a compact rheometer (Anton Paar Physica MCR 501, Anton Paar GmbH, Ostfildern, Germany) equipped with single-use stainless steel plates with a radius of 10 mm in a plate–plate configuration. The sample specimens used for the melt rheology were produced using the MeltPrep device (MeltPrep GmbH, Graz, Austria) with a 20 mm disc geometry at temperatures of 10 °C above printing temperature, yielding ASDs with a consistent geometric shape [25]. Since the viscosity of non-Newtonian fluids is a product of the temperature and shear rate [26], the samples were measured at a range of temperatures after the determination of the linear viscoelastic region (LVR). The determination of the LVR was conducted for every measured temperature individually by performing amplitude sweeps from 0.01% to 100% deformation (0.0103 to 103 mrad) at 10 rad/s. Frequency sweeps from 100 Hz to 0.1 Hz were performed afterwards at 1% amplitude.

2.2.4. HME of PVA/Sorbitol Mixtures

Apart from PAR/LOP mixtures, also plasticized mixtures were used. Sorbitol (SOR) was used as the plasticizer. The direct powder extrusion of PAR/SOR mixtures was not possible due to the different melting points. To be able to still print this mixture, a single screw extruder (Noztek Pro, Noztek, Shoreham-by-Sea, UK) was used to extrude these two excipients before adding the API and printing the mixture. Afterward, it was milled using an ethanol-cooled mill and sieved while the fraction < 0.400 mm was used in further printing steps.

2.2.5. Preparation of Powder Mixtures

All powder mixtures for printing were produced by sieving (0.400 mm mesh size) and accurately weighing the compounds needed, adding Aerosil (AER) and subsequent mixing in a tumbler mixer (Turbula Type T2C, Willy A. Bachofen AG, Muttenz, Switzerland) for 20 min. Table 1 shows the composition of powder mixtures for printing.

Table 1. Physical mixtures for 3D printing.

Batch		Parteck MXP	Parteck MXP/Sorbitol 15% Extrudate	Loperamide	Aerosil
1	PAR-LOP5%-AER1%	94.0%		5.0%	1.0%
2	PAR_LOP10%_AER1%	89.0%		10.0%	1.0%
3	PAR-SOR15%E_LOP5%_AER1%		93.5%	5.0%	1.5%

2.2.6. 3D Printing Using Direct Powder Extrusion Tool of M3dimaker

A computer-aided design (CAD) tablet-shaped geometry was created using Autodesk® Fusion 360 (Autodesk GmbH, München, Germany). The .stl file (seen in Figure 1) was sliced by Repetier-Host (V2.2.3) (Hot-World GmbH & Co. KG, Willich, Germany). Objects were printed with 2 outer perimeters and 3 bottom and top layers using varying infills to

change the dosage of printed tablets on the M3dimaker 3D printer (FabRx Ltd., London, UK) equipped with the direct powder extrusion (DPE) tool. Print speed and temperature were adjusted according to the properties of the mixtures in a molten state.
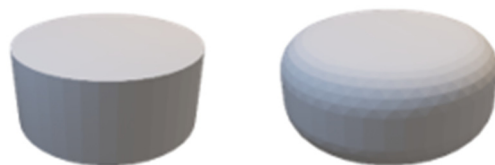
Figure 1. .stl file of tablet-shaped geometry (d = 5 mm; h = 5 mm) (**left**) and .stl file of improved geometry (d = 5 mm; h = 5 mm; edges rounded with r = 2 mm) (**right**).

The reason for choosing the rounded edges for further experiments was that the edges of the printed tablets were sharper than expected and needed to be rounded for more safety in handling.

2.2.7. Confocal Raman Microspectroscopy

Witec's alpha 300R system (WITec GmbH, Ulm, Germany) was employed for the measurements. Pure substances were measured with the 30 mW power of the laser (λ = 532 nm) and the evaluated spectra were used for the true component analysis to show the distribution of loperamide in the tablet.

Printed tablets were measured on the outer surface to find information on potential demixing processes, varying concentrations, and recrystallization on the outer surface.

One printed tablet of each mixture was measured using a 30 mW laser (λ = 532 nm). The surface of the measurement area was evaluated and corrected by the TrueSurface Mk II module. An area of 20×2000 μm with 4×400 pixels was measured using the autofocus function.

For the evaluation of drug content, the true component analysis integrated into the Witec Control 6 software was employed using the previously obtained spectra of individual substances. The software calculates based on individual spectra and the amount of drug found in each pixel measured and reports a colored picture of the distribution and intensity of the signal found.

2.2.8. Drug Content Analysis by HPLC

An evaluation of the drug content was performed on the powdered mixtures as well as on the printed tablets. From the powdered samples, an equivalent of 5 mg of loperamide was accurately weighed and dissolved in 100 mL of the mobile phase used for the subsequent HPLC analysis (purified water/acetonitrile/0.5% ammonium acetate solution 29/36/35 (*v/v*)). Tablets were also dissolved in the mobile phase using stirring and an ultrasonic bath. The drug contents were determined by HPLC-UV/VIS (System 20A, Shimadzu Ltd., Kyoto, Japan) at a wavelength of 254 nm. The method showed a linearity of R^2 = 0.99680 between 0.0023 mg/mL and 0.07 mg/mL with a tested LOQ of 0.00166 mg/mL and an estimated LOD of 0.0005488 mg/mL calculated according to ICH guidelines [27]. All experiments were performed in triplicate.

2.2.9. In Vitro Dissolution

Dissolution testing was adapted from the standard procedures of the FDA [28] used for loperamide capsules using a Pharma Test PT-DT7 (Pharma Test Apparatebau AG, Hainburg, Germany) manual dissolution tester. First, 0.1 M of HCl was used as a dissolution medium (500 or 900 mL, depending on the tablet strength) at 37 °C with 100 RPM paddle speed. Sampling of 1 mL took place every 30 min for 5.5 h and a last sample was drawn after 24 h. The samples were measured using UV-HPLC as described in 2.2.8. For each formulation and infill setting printed, 4 tablets were measured and the mean value including the standard deviation is shown. For each formulation, a linear regression of the correlation

between mass and infill is calculated and the best-fit values are given. Slopes are compared using two-tailed testing with the null hypothesis that the slopes are identical.

3. Results and Discussion

3.1. Results of Thermal Analysis

The thermal properties of the excipients, mainly the melting point and the glass transition temperature (DSC) and degradation (STA), were measured. From the powdered samples, information about the solubility was expected, while printed tablets were controlled for signs of crystallization of the API.

In the following diagrams, the thermograms of the measured samples (pure substances, powder mixtures, and printed tablets) are shown.

3.1.1. Physical Characterization Using DSC

Figures showing the DSC data are contained in the supplementary part Figures S1 and S3, which show the curves of the first heating run where crystalline substances showed their melting point, while amorphous substances showed their glass transition temperature. The glass transition temperature of printed tablets was used as an indicator for the formation of ASDs. Similar Figures S2 and S4 contain the thermograms of the second heating run. The second heating run is used to determine the glass transition temperature of previously crystalline substances and information about the solubility of the API and polymer for powdered mixtures.

Table 2 gives an overview of the measured melting and glass transition temperatures.

Table 2. Comprehensive results of glass transition temperatures found during DSC experiments.

Glass Transition First Heating	Onset [°C]	Endset [°C]	Glass Transition Second Heating	Onset [°C]	Endset [°C]
PAR	49.64	52.99	PAR	61.11	72.76
SOR	crystalline, Mp: 89.75 °C		SOR	−2.60	1.50
AER	N/A		AER	N/A	
LOP	crystalline, Mp: 227.47 °C		LOP	51.04	63.16
Batch 1 powder	47.11	52.35	Batch 1 powder	62.09	73.44
Batch 1 printed	56.44	60.79	Batch 1 printed	58.67	74.56
Batch 2 powder	44.33	48.40	Batch 2 powder	58.43	75.10
Batch 2 printed	56.07	61.85	Batch 2 printed	54.53	71.96
Batch 3 powder	N/A		Batch 3 powder	31.21	54.07
Batch 3 printed	N/A		Batch 3 printed	34.68	53.98

During the first heating, the melting point of sorbitol and loperamide was detected as well as the semicrystalline nature of PVA indicated by a glass transition at 48–55 °C and a melting point of ∼180 °C. During the second heating run, the glass transition temperatures of sorbitol (−2.60–1.50 °C) and loperamide (51.04–63.16 °C) were found.

In the powdered samples, there were no signs of crystalline loperamide or sorbitol found even during the first heating where crystalline loperamide was contained. This indicates a good solubility of loperamide in PAR, at least at elevated temperatures. The missing individual glass transition of loperamide and sorbitol in the second heating indicates a miscible system formed from the API and the polymer and sorbitol, respectively. The change in Tg due to Loperamide may be only very slight, while it shows no second glass transition. It can still be seen that the measurement of powdered samples shows only the Tg of PVA in the first heating, while printed samples as well as the measurements of the second heating show a slightly lower Tg (than PVA in the second heating), which is more pronounced in the sample with a higher drug content. No clear glass transition

temperature could be obtained from the Batch 3 printed samples over multiple runs; thus, no temperature was given.

The mixtures containing 15% sorbitol showed a decreased glass transition temperature (31.21–54.07 °C for the powder and 34.68–53.98 °C for the printlet), indicating that miscible systems were formed from PAR and SOR. In these thermograms, only one glass transition temperature was found. This temperature is composed of the two individual temperatures one would find for non-miscible systems.

Concluding the DSC experiments, sorbitol showed to be a good choice for use as a plasticizer and loperamide showed miscibility with the polymer in the measured concentrations. The results for sorbitol were expected, as its use as a plasticizer has been shown before [29,30].

3.1.2. Results of Thermal Stability Using STA

The powdered samples were accurately weighed, while printed tablets were broken down and then weighed into the crucibles for analysis of thermal stability and potential water loss. The results are shown in Figure 2.
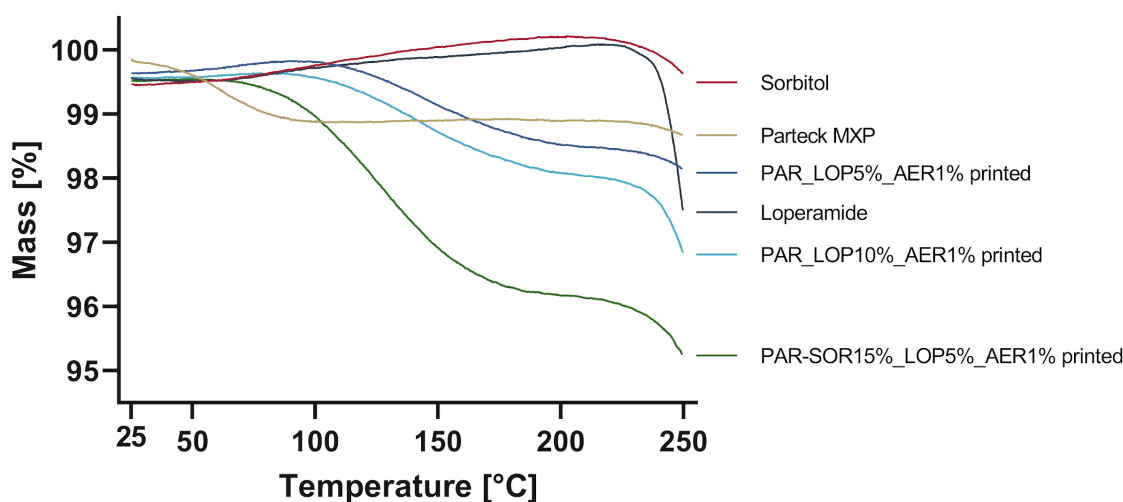
Figure 2. Change in mass during heating up to 250 °C.

Significant mass loss was found for Parteck MXP (1%) as well as for the printed tablets. The mass loss in neat PAR could be attributed to solvent loss, as 1–3% methanol can be expected as per SDS. An increased mass loss was found for the sample containing 15% sorbitol, which might be a result of water uptake from humidity during printing or storage. An increase in sorbitol in PVA-based films has been shown to also increase its capacity to retain water, which is attributed to physically weak but chemically strong bonded water [29,30]. Loperamide and sorbitol were thermally stable up to at least 230 °C, as no degradation could be found.

3.2. Physical State Examination—XRD

The DSC measurements indicated the amorphous state of loperamide in PAR. To further harden this assumption, a second method to gain information about the physical state of the API at room temperature was implemented.

Using XRD, whole printed tablets were measured, and the obtained spectra were compared to the spectra of pure substances. The results are given in Figure 3.

The spectra obtained from loperamide and sorbitol showed distinct peaks at a variety of angles, which was expected from crystalline substances. In the printed tablets, no signs of crystalline loperamide or sorbitol were found. The semicrystalline nature of PAR was found in the pure PAR as well as the printed tablets. This complies with the results from thermal analysis, underpinning the amorphous nature of loperamide in the printed tablets.

Although the amorphous halo is widely regarded as a sign of absent crystalline structures, it can be found in other instances that include disordered nanocrystalline phases as well as glassy or amorphous ones [31].
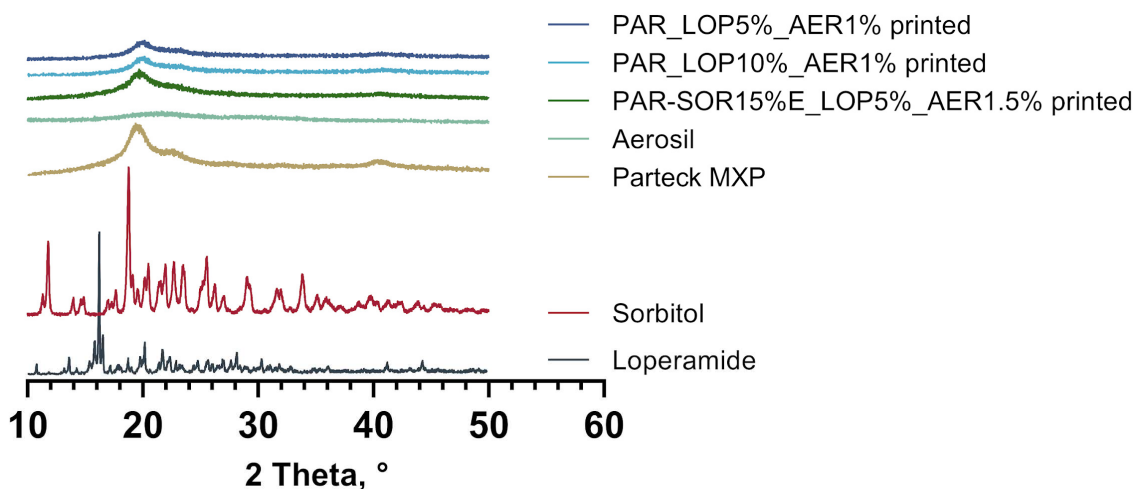

Figure 3. XRD spectra of pure substances and printed tablets.

3.3. 3D Printing

3.3.1. PVA without Plasticizer

Apart from the suitable temperature regarding melt viscosity, there are further parameters of interest for extrusion using a small-scale single-screw extruder. Powder flowability is a key characteristic since the powder must flow into the barrel before it can be melted and pushed through. As the mixtures showed insufficient flowability, adjustments were made by adding 1% of AER to ensure sufficient flow behavior.

The direct printing of Batch 1 (Table 1) was successful using a 200 °C nozzle temperature and 40 °C print bed temperature. Tablets of different strengths were produced by varying the infill in 25% increments (100%, 75%, 50%, 25%, 0%). In the next iteration, the drug load was increased by doubling the API concentration in the powder mixture (Batch 2, Table 1). Printing was successful at 205 °C/40 °C, with tablets printed from 100–0% infill in 25% increments. Figure 4 shows the average mass including the standard deviation of the printed tablets as well as pictures of one tablet from each infill (FLTR: 100–0% Infill). To enhance understanding of the infill procedure, sliced pictures of the tablets can be found in Figure S5.
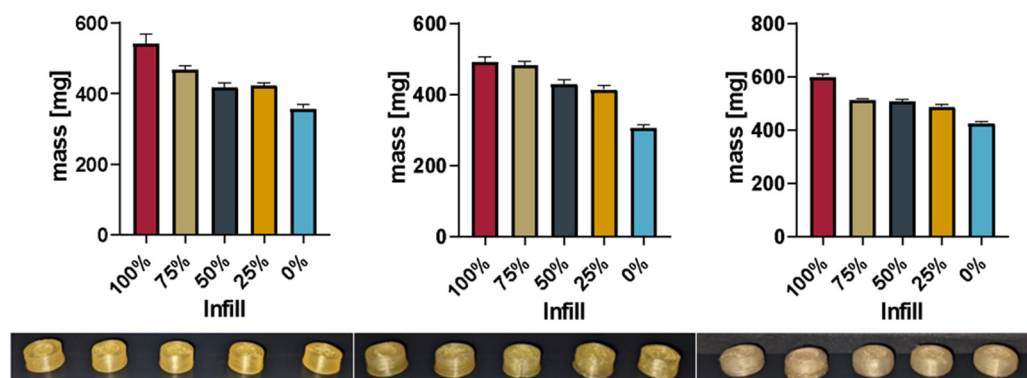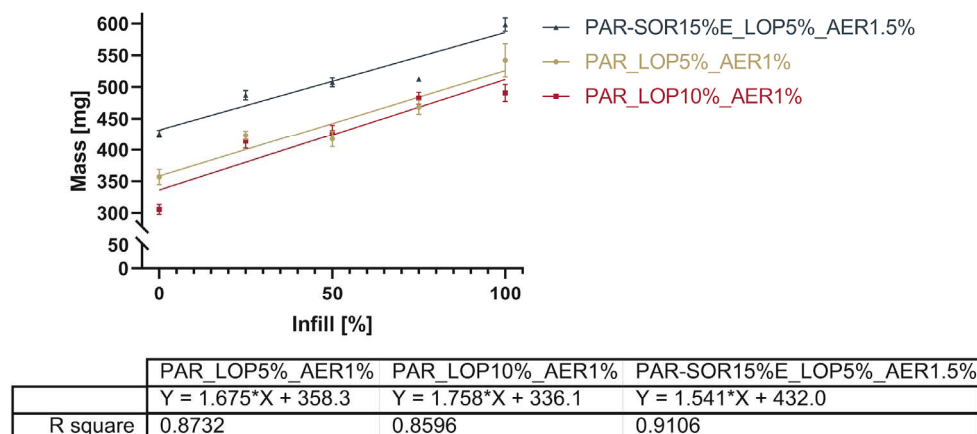

Figure 4. Masses of printed tablets Batch 1–3 (fltr) and printed tablets from corresponding batch (100–0% Infill fltr) in the individual pictures.

3.3.2. PVA with 15% Sorbitol

To decrease the dissolution times and reduce the printing temperature, 15% sorbitol was added to the PAR. Batch 3 (Table 1) was successfully printed using 185 °C/40 °C to print tablets varying in infill, as seen inthe pictures in Figure 4. Figure 4 shows the mass and standard deviation of the printed tablets and exemplary pictures of the tablets from each infill percentage using the updated shape.

Figure 5 gives a comprehensive overview of the mass of all printed tablets.

	PAR_LOP5%_AER1%	PAR_LOP10%_AER1%	PAR-SOR15%E_LOP5%_AER1.5%
	Y = 1.675*X + 358.3	Y = 1.758*X + 336.1	Y = 1.541*X + 432.0
R square	0.8732	0.8596	0.9106

Figure 5. Linearity of the relation between set infill and measured mass.

The total mass of the printed tablets showed a reduction with the reduced infill, as expected. Figure 5 shows the relation between the infill set in the slicing software and the actual mass of the printed tablets.

The linearity of the correlation between the infill and total mass (as shown in Figure 5) is found to be between 0.8596 and 0.9106. A comparison of the slopes by analysis of the covariances showed no significant difference between the slopes ($p = 0.5053$). This indicates that it is possible to dictate the drug load from the infill independent of the powder mixture used. The slicing software determined based on the shape of the object and nozzle size at which position additional material would be deposited. Differences between 25%, 50%, and 75% were not as predictable as the software suggested, e.g., the difference in the mass between the tablets with 25% and 50% infill was way smaller than the correlation seemed to predict. Stepping forward to 3D printing from material evaluation such as melt rheology, one has to keep in mind that being able to extrude material does not necessarily mean that it is the right setup for printing as well. Successful printing, unlike extrusion, does not only depend on material being able to push from the nozzle; sometimes, the adhesion of the print bed as well as the adhesion of different layers need an increase or decrease in temperature for the successful bonding of the layers. Therefore, subtle differences in printing temperatures were found to be necessary.

### 3.4. Measurement of Rheological Properties of the Mixtures in Molten State

The determination of the shear rate was conducted using tablets consisting of PAR-SOR15%E/LOP5%/AER1% printed at 185 °C and 6 mm/s print speed. The print speed represents a consideration between decreasing the time needed to print a tablet and the torque capacity of the motor as well as finding a temperature where material could be printed without oozing from the nozzle.

Individual printing times of 558 ± 2.45 s were measured for a batch of five consecutive printed tablets. During this time, 15.8 screw turns were recorded and an actual volume of the printlet of 0.461 ± 0.005 cm^3 was measured, compared to the theoretical volume of 0.4936 cm^3.

This results in a volume flow Q of $8.26 \times 10 - 4 \pm 7.80 \times 10^{-6}$ cm^3/s, which gives a shear rate in the nozzle of 16.43 ± 0.155 1/s.

For the same tablets, the couette shear rate was calculated using the aforementioned dimensions of the extruder screw used. With an N (screw rotational speed) of $2.83 \times 10^{-2} \pm 1.24 \times 10^{-4}$ 1/s, a Couette shear rate of $1.294 \pm 5.68 \times 10^{-3}$ 1/s was calculated. The calculated shear rates were intended to be used in combination with the rheological data to make a claim about the viscosity of a polymer melt suitable for printing.

In rheologic measurements, the linear viscoelastic range (LVR) was determined via amplitude sweeps. A deformation of 1% was found to be in the LVR for all the samples at the measured temperatures. Afterwards, frequency sweeps from 100 to 0.1 Hz were performed at a temperature around the printing temperature (Figure 6). As expected, the viscosity decreased with the increasing temperature, increasing frequency, and with the addition of the plasticizer sorbitol. Prior research indicates that usually viscosities from 100,000 to 10,000 Pa·s are found during HME processes [32]. Maximum viscosities as seen in Figure 6 needed at the lower calculated shear rate (Couette: 1.294 1/s) were found at ranges from 1500 to 4000 Pa·s, which indicates that a rather low melt viscosity is needed to print successfully with the M3dimaker. The dashed lines represent the viscosity of the mixture at the calculated shear rate and temperature used to print.
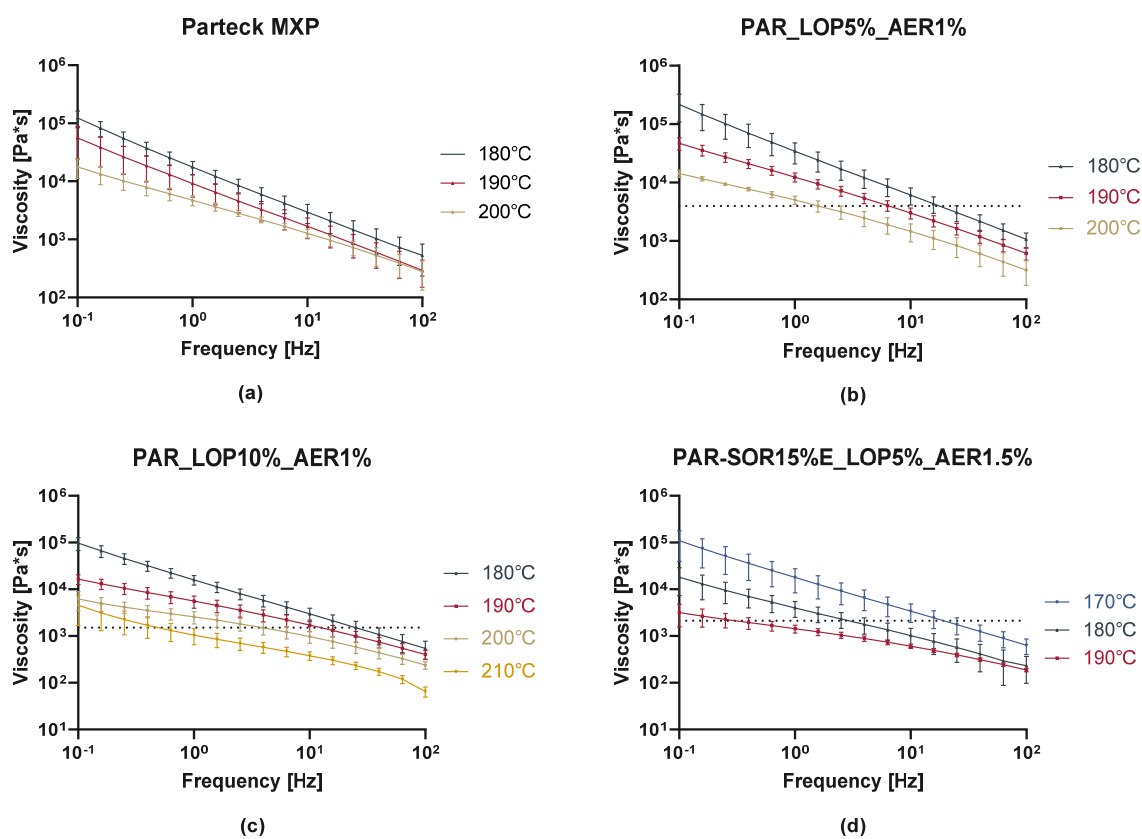

Figure 6. Melt viscosity of neat polymer and printed formulations. (**a**) shows the curves obtained from neat PAR, while (**b**–**d**) show the curves obtained from the three printed batches, respectively.

This correlates well with the fact that compared to lab-scale extruders, this printer comprises a very small screw and a motor of lower torque to keep the weight down and increase the precision of the printing. We propose that the selection of polymer and its expected printing temperature should include frequency sweeps with increasing temperature until a viscosity of a maximum of 5000 Pa·s is measured. Similar experiments to find information about melt viscosity and temperature dependence have been conducted for other APIs and different use cases. They are often found under the name of "small amplitude oscillatory shear" (SAOS) experiments. It was shown that vacuum compression modeling (VCM) is a useful tool for the simulation of extruded samples in order to correctly

predict extrusion parameters. Also, temperature as a crucial parameter for printability was predicted by melt rheology experiments [20,33].

3.5. Confocal Raman Microspectroscopy

The visualization of API content, distribution, and potential recrystallization can be achieved via confocal Raman microspectroscopy (CRM). The overlay of the single spectra of LOP, SOR, and PAR (Figure 7) showed peaks that can be used for the evaluation of contained API in the printed tablets. The peak in the high wavenumber range (3040–3090 1/cm) as well as the peak in the fingerprint region (1575–1615 1/cm) have no significant overlapping with the peaks from other substances and can be used to identify loperamide. The low drug load of 5 and 10%, respectively, lead to a decreased signal intensity of these peaks in the resulting spectra of printed tablets relative to the single spectra obtained from pure substances.
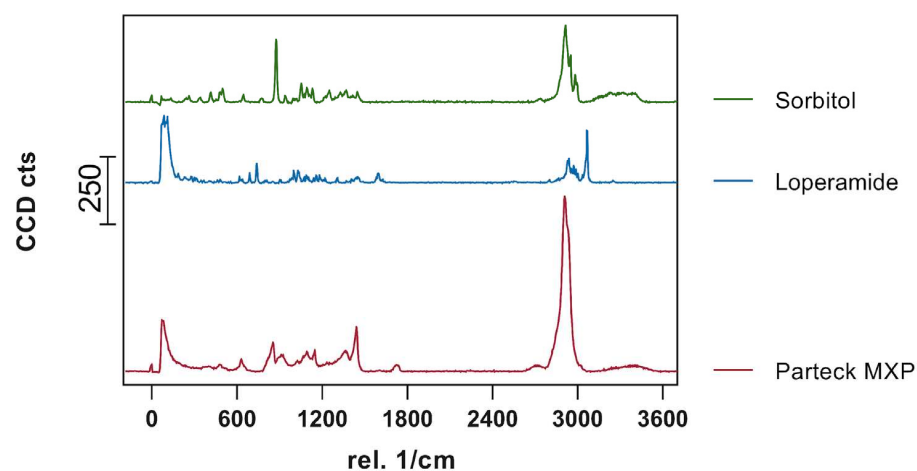

Figure 7. Obtained single spectra (0.5 s; 10 Acc.) red = Parteck MXP, blue = loperamide, green = sorbitol.

Figure 8 shows an example of the measured area on the side of the printed tablet. The true surface module was able to cover most of the differences in the height of the surface area. Fine-tuning to achieve good spectra was completed via auto-focus.
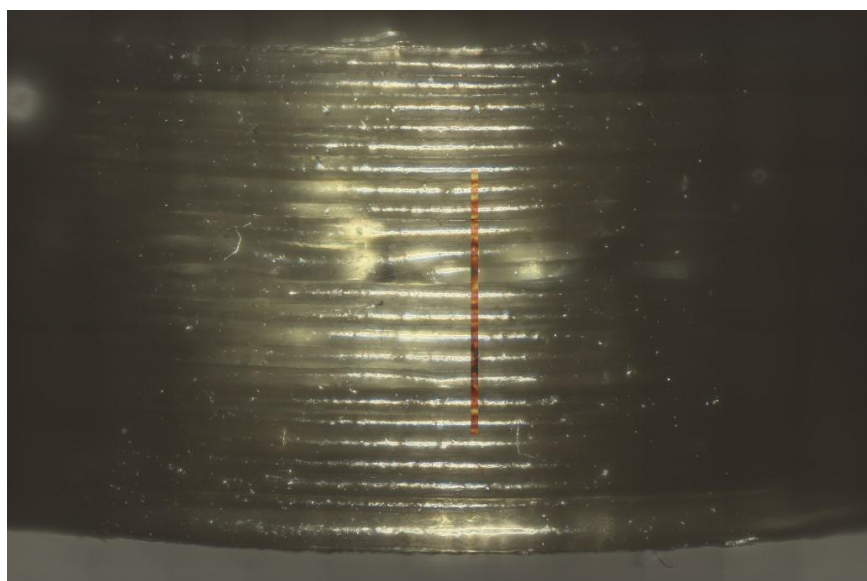
Figure 8. Picture of tablet printed from PAR_LOP5%_AER1% with an overlay of the measured area by true surface model.

Exemplary spectra (Figure 9) were given for the individual colors used in the color coded pictures (Figure 10). Red shows the signal where loperamide was found and spectrum intensity was sufficient. With the loss in signal intensity (as seen in the lighter and blue-colored regions), the signal-to-noise ratio of the loperamide peaks get worse, although loperamide concentration remains constant.
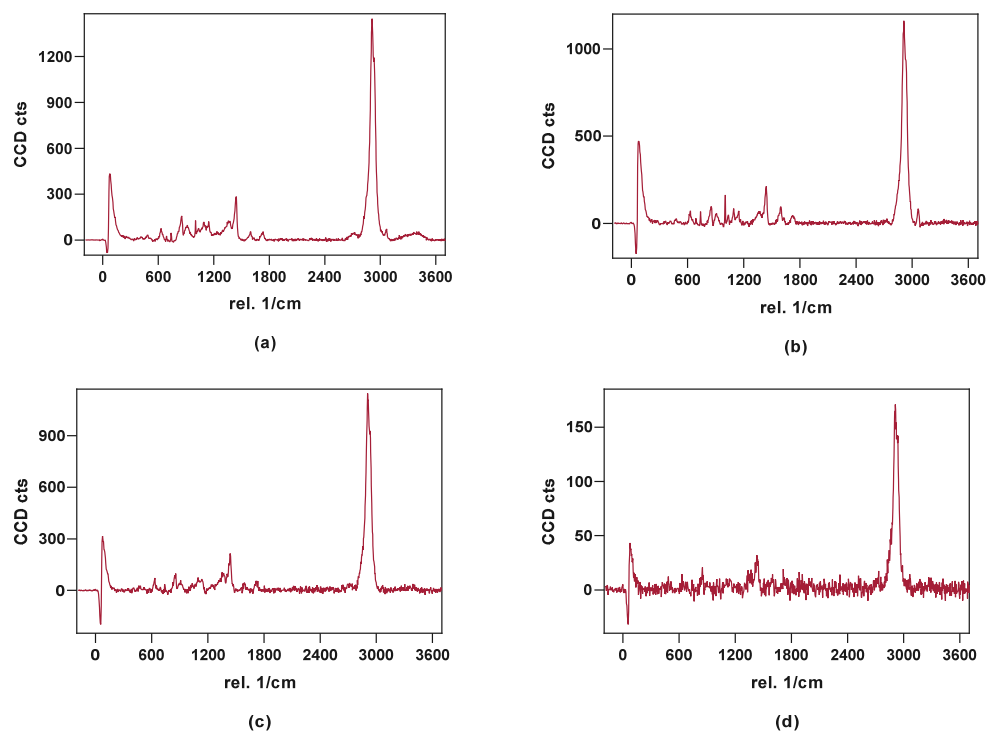
Figure 9. Exemplary spectra obtained from the measured area: (**a**) PAR_LOP5%_AER1%, (**b**) PAR_LOP10%_AER1%, (**c**) PAR-SOR15%E_LOP5%_AER1%, (**d**) failed focus or bad spectrum found in the light and blue areas as seen in Figure 10.

Raman imaging was able to show consistent spectra containing polymer and API over a range of points distributed over roughly 40% of the printing time. No "hotspots" or crystalline API were found during these measurements, which supports findings from the XRPD measurements of a uniform ASD.

3.6. Drug Content

Since the powder mixtures contained 5% (m/m) and 10% of API, respectively, the expected drug content was calculated as 5% and 10%, respectively, of the total mass of the printed tablets. The actual drug content was assessed to make sure the correct amount was referred to as 100% release during in vitro measurements. By dissolving the whole tablet in a suitable medium, the actual drug content was determined. The results of this experiment are given in Table 3.

Table 3. Loperamide content in powdered and printed samples.

	PAR_LOP5%_AER1%		PAR_LOP10%_AER1%		PAR-SOR15%E_LOP5%_AER1%	
	Powdered	Printed	Powdered	Printed	Powdered	Printed
Mean API content	92.63%	95.13%	88.49%	82.99%	95.85%	85.40%
Standard deviation	2.74%	12.88%	1.50%	1.30%	5.65%	0.92%
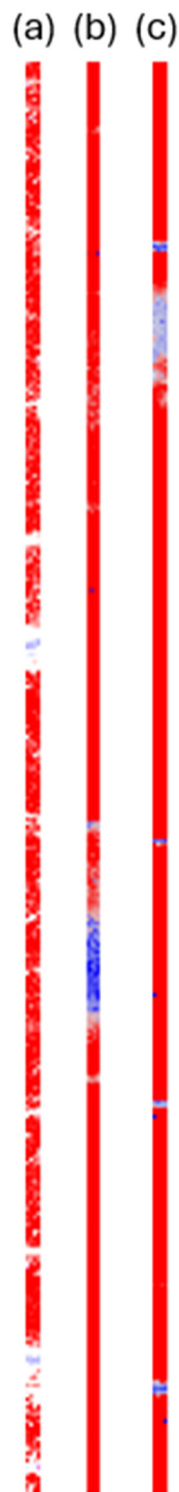
Figure 10. Distribution of loperamide based on the true component analysis is shown for all three printed tablets. (**a**–**c**) showing the distribution of tablets made from Batch 1, 2, and 3 respectively.

The drug content shown in Table 3 deviates from the expected amount. The deviations in content from the expected amount in the powdered samples can be attributed to adhesion to the mixing vessels and spatulas used. The reduction in the measured content of the printed tablets can partially be explained by the water uptake, which increases the determined total mass of the tablet without adding further API. Also, adhesion to the screw in the extruder is a possible explanation. Other reasons could be found in the demixing processes during printing, imperfect powder homogeneity, and adhesion to the glass and

plastics of tubular glasses during mixing. Small batch sizes as well as small sampling sizes increase the errors found. Deviation regarding the drug content has been shown in previous studies as well [20,34–36], which might be reduced by in-line quality control mechanisms.

3.7. In Vitro Dissolution Testing of Printed Tablets

Four tablets were tested at once to show the average ± SD. The total drug content was calculated from the mass of the printed tablet as well as the measured content shown in Table 3. The cumulative released drug was calculated and put into relation to the measured content to give the percentage released. Figure 11 shows the percentage of cumulative drug release from PAR_LOP5%_AER1%, while Figures 12 and 13 show the release of PAR_LOP10%_AER1% and PAR-SOR15%E_LOP5%_AER1%, respectively.

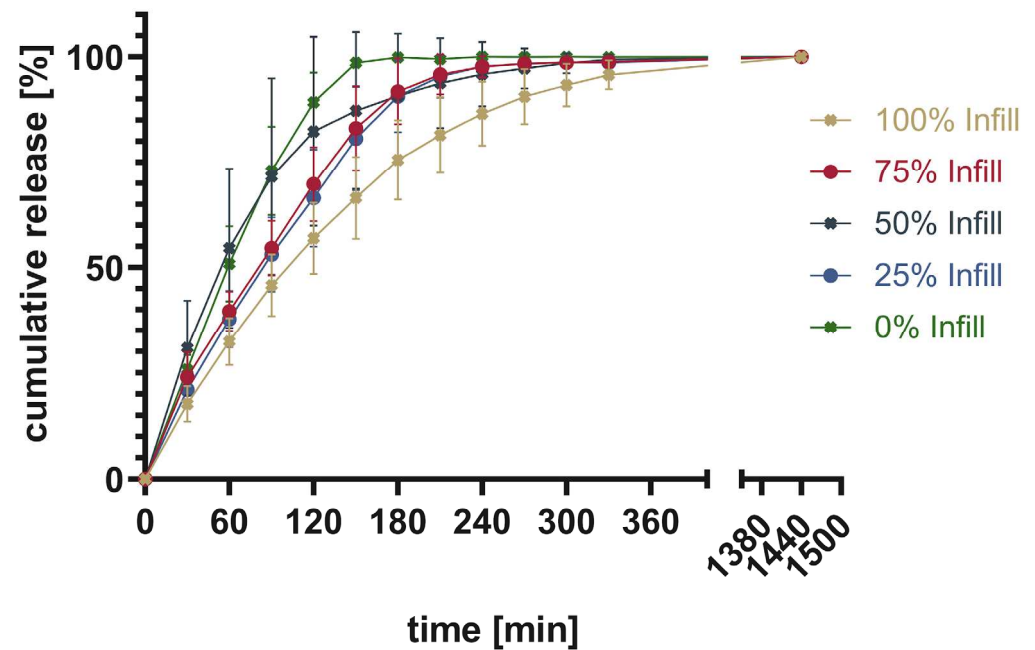**Figure 11.** Cumulative release given in percentage of calculated drug load for PAR_LOP5%_AER1%.
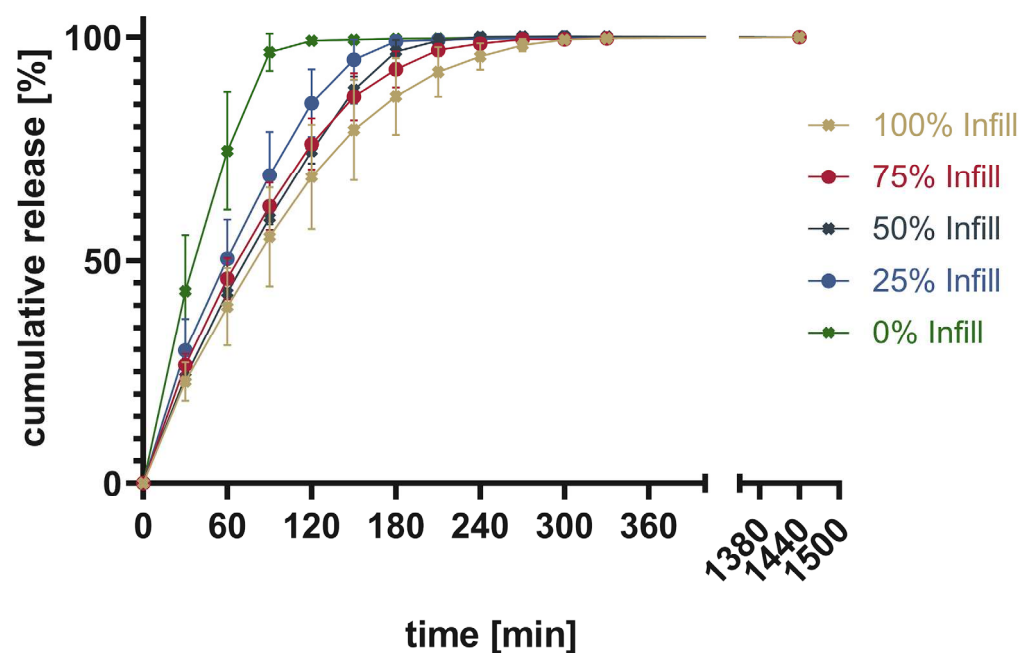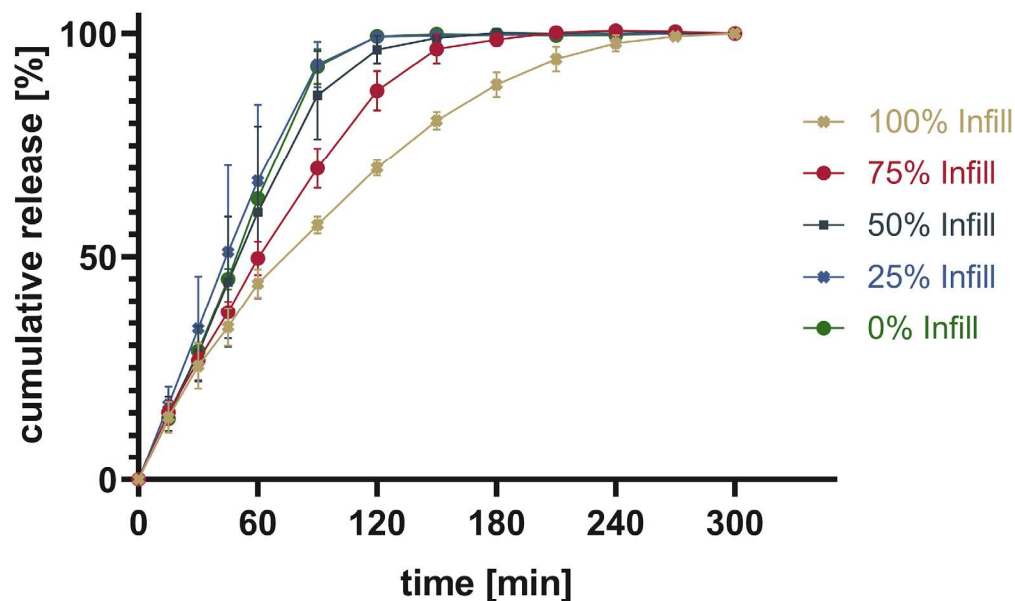

Figure 12. Cumulative release given in percentage of calculated drug load for PAR_LOP10%_AER1%.

Figure 13. Cumulative release given in percentage of calculated drug load for PAR-SOR15%E_LOP5%_AER1%.

The release patterns of loperamide from printed PAR or PAR/SOR mixtures show that the higher the percentage infill of the tablets, the slower the release. This matches the expectations based on existing research [37]. Unexpectedly, overall, a very slow release was found for PAR without a plasticizer. This indicates that the incorporation of a poorly water-soluble drug into PAR resulted in a slower release. The addition of 15% sorbitol improved the dissolution time of the printed tablets independent of the infill. While for 100% infill, there was no difference between Batch 2 and 3, as both dissolved faster than Batch 1. For 75% and 50%, both Batch 1 and 2 showed no real difference in the dissolution time, while Batch 3 showed the fastest dissolution. For 25%, it can be observed that the dissolution time decreases from Batch 1 to Batch 3 with Batch 2 in between. Finally, for 0% infill, both Batch 2 and 3 showed an improved dissolution rate over Batch 1. Increasing the drug load which leads to a reduction in polymer already improved the dissolution rate slightly. Still, the amount of infill showed a larger impact on the dissolution time than the addition of the highly water-soluble plasticizer. This can be explained by the different infill resulting in changes in the area-to-volume ratio. As soon as the outer layers of the tablet are penetrated by media, tablets with lower infill offer a larger area, and thus, the dissolution rate increases. Additionally, there were large standard deviations observed in the earlier sampling points. They can be attributed to the deviation of the dissolution behavior of individual tablets. These results are not surprising as tablets generally and 3D printed tablets especially do not always show very narrow dissolution profiles [38–40]. Thus, usually, only three sampling points are used to assess if the dissolution behavior is sufficient. One is used to secure against dose dumping, one intermediate to show control over the dissolution profile, and a final one to show full release [41]. Individual dissolution curves can be found in the supplementary, divided into each infill percentage (Figure S6).

4. Conclusions

Direct powder extrusion and the 3D printing of tablets was achieved with formulations containing PAR, sorbitol, and loperamide using the M3dimaker 3D printer. In printed tablets, loperamide appeared to form amorphous solid dispersions as characterized by DSC and XRPD. Confocal Raman microspectroscopy showed a homogenous distribution of the API during the print, underlining this hypothesis. Nevertheless, one has to keep in mind the limitations of the methods used. While CRS has a large spatial resolution of 5 μm, DSC is unable to detect phase-separated domains smaller than 30 nm. This makes a

differentiation between amorphous solid dispersion and nanodispersion very tough [42,43]. The use of the two methods (DSC and XRD) is widely acknowledged for being able to resolve mistakes when looking for a solid-state characterization and confirmation of an amorphous state. Such includes increased solubility at elevated temperatures, as mentioned in the DSC results part [44–46]. The resolution of XRD is expected to be found at approx. 1% [47,48]. By employing three complimentary state-of-the-art methods, we can conclude that to the best of our knowledge and to the best of the current methods' capabilities, the drug is present as ASD in the printed tablets.

The printing temperature was sufficiently low to encounter no thermal degradation of API, polymer, or other excipients. By adding the API after extruding the other excipients, one heating step and therefore the potential thermal degradation for the API could be eliminated. Control over the drug content was realized by changing the amount of infill. While this is a proven way to change drug content, one must keep in mind that changes in the area/volume ratio also can impact the release behavior. If the acceleration of the dissolution time is aimed for, the addition of (super)disintegrants could be a promising approach.

From the characterization of the melt properties of the mixtures, a system for the selection of polymers is proposed. Extrudability as well as printability seem to work sufficiently with a melt viscosity below 4000 Pa·s. This value could be used in future trials to reduce material use during preliminary tests. The range of usable polymers and even working temperatures for these polymers could be evaluated by conducting rheological tests.

Supplementary Materials: The following supporting information can be downloaded at: https://www.mdpi.com/article/10.3390/pharmaceutics16040553/s1, Figure S1: First heating neat substances; Figure S2: Second heating: neat substances; Figure S3: First heating: powdered and printed samples; Figure S4: Second heating: powdered and printed samples; Figure S5: Sliced tablets for visualization of infill; Figure S6: Dissolution date of individual tablets (100%: (a), 75%: (b), 50%: (c), 25%: (d), 0%: (e)).

Author Contributions: Conceptualization, J.L. and D.J.L.; methodology, J.L., F.P. and K.G.W.; investigation, J.L. and F.P.; data curation, J.L.; writing—original draft preparation, J.L.; writing—review and editing, F.P., K.G.W. and D.J.L.; supervision, D.J.L. and K.G.W.; project administration, D.J.L. All authors have read and agreed to the published version of the manuscript.

Institutional Review Board Statement: Not applicable.

Informed Consent Statement: Not applicable.

Data Availability Statement: Data is contained within the article or Supplementary Materials.

Conflicts of Interest: The authors declare no conflicts of interest.

References

1. West, T.G.B.; Thomas, J. *3D Printing: A Case of ZipDose®Technology—World's First 3D Printing Platform to Obtain FDA Approval for a Pharmaceutical Product*; Wiley: Hoboken, NJ, USA, 2019. [CrossRef]
2. Li, Q.; Guan, X.; Cui, M.; Zhu, Z.; Chen, K.; Wen, H.; Jia, D.; Hou, J.; Xu, W.; Yang, X.; et al. Preparation and investigation of novel gastro-floating tablets with 3D extrusion-based printing. *Int. J. Pharm.* **2018**, *535*, 325–332. [CrossRef] [PubMed]
3. Khaled, S.A.; Burley, J.C.; Alexander, M.R.; Yang, J.; Roberts, C.J. 3D printing of tablets containing multiple drugs with defined release profiles. *Int. J. Pharm.* **2015**, *494*, 643–650. [CrossRef] [PubMed]
4. Zheng, Y.; Deng, F.; Wang, B.; Wu, Y.; Luo, Q.; Zuo, X.; Liu, X.; Cao, L.; Li, M.; Lu, H.; et al. Melt extrusion deposition (MED) 3D printing technology—A paradigm shift in design and development of modified release drug products. *Int. J. Pharm.* **2021**, *602*, 120639. [CrossRef] [PubMed]

5. Kempin, W. Entwicklung und Charakterisierung 3D-Gedruckter, Wirkstoffhaltiger Darreichungsformen am Beispiel von Tabletten und Implantaten. Ph.D. Thesis, Universität Greifswald, Greifswald, Germany, 2018.

6. Goyanes, A.; Fina, F.; Martorana, A.; Sedough, D.; Gaisford, S.; Basit, A.W. Development of modified release 3D printed tablets (printlets) with pharmaceutical excipients using additive manufacturing. *Int. J. Pharm.* **2017**, *527*, 21–30. [CrossRef] [PubMed]

7. Goyanes, A.; Scarpa, M.; Kamlow, M.; Gaisford, S.; Basit, A.W.; Orlu, M. Patient acceptability of 3D printed medicines. *Int. J. Pharm.* **2017**, *530*, 71–78. [CrossRef] [PubMed]

8. Goyanes, A.; Wang, J.; Buanz, A.; Martinez-Pacheco, R.; Telford, R.; Gaisford, S.; Basit, A.W. 3D Printing of Medicines: Engineering Novel Oral Devices with Unique Design and Drug Release Characteristics. *Mol. Pharm.* **2015**, *12*, 4077–4084. [CrossRef] [PubMed]

9. Chai, X.; Chai, H.; Wang, X.; Yang, J.; Li, J.; Zhao, Y.; Cai, W.; Tao, T.; Xiang, X. Fused Deposition Modeling (FDM) 3D Printed Tablets for Intragastric Floating Delivery of Domperidone. *Sci. Rep.* **2017**, *7*, 2829. [CrossRef]

10. Fu, J.; Yin, H.; Yu, X.; Xie, C.; Jiang, H.; Jin, Y.; Sheng, F. Combination of 3D printing technologies and compressed tablets for preparation of riboflavin floating tablet-in-device (TiD) systems. *Int. J. Pharm.* **2018**, *549*, 370–379. [CrossRef] [PubMed]

11. Prasad, L.K.; Smyth, H. 3D Printing technologies for drug delivery: A review. *Drug Dev. Ind. Pharm.* **2016**, *42*, 1019–1031. [CrossRef]

12. Goyanes, A.; Buanz, A.B.; Basit, A.W.; Gaisford, S. Fused-filament 3D printing (3DP) for fabrication of tablets. *Int. J. Pharm.* **2014**, *476*, 88–92. [CrossRef]

13. Zhang, J.; Feng, X.; Patil, H.; Tiwari, R.V.; Repka, M.A. Coupling 3D printing with hot-melt extrusion to produce controlled-release tablets. *Int. J. Pharm.* **2017**, *519*, 186–197. [CrossRef] [PubMed]

14. Goyanes, A.; Allahham, N.; Trenfield, S.J.; Stoyanov, E.; Gaisford, S.; Basit, A.W. Direct powder extrusion 3D printing: Fabrication of drug products using a novel single-step process. *Int. J. Pharm.* **2019**, *567*, 118471. [CrossRef] [PubMed]

15. Korte, C.; Quodbach, J. Formulation development and process analysis of drug-loaded filaments manufactured via hot-melt extrusion for 3D-printing of medicines. *Pharm. Dev. Technol.* **2018**, *23*, 1117–1127. [CrossRef] [PubMed]

16. Chavda, H.V.; Patel, C.N.; Anand, I.S. Biopharmaceutics classification system. *Syst. Rev. Pharm.* **2010**, *1*, 62. [CrossRef]

17. Wei, C.; Solanki, N.G.; Vasoya, J.M.; Shah, A.V.; Serajuddin, A.T.M. Development of 3D Printed Tablets by Fused Deposition Modeling Using Polyvinyl Alcohol as Polymeric Matrix for Rapid Drug Release. *J. Pharm. Sci.* **2020**, *109*, 1558–1572. [CrossRef] [PubMed]

18. Zaki, N.M.; Artursson, P.; Bergstrom, C.A. A modified physiological BCS for prediction of intestinal absorption in drug discovery. *Mol. Pharm.* **2010**, *7*, 1478–1487. [CrossRef] [PubMed]

19. Pubchem—Loperamide. Available online: https://pubchem.ncbi.nlm.nih.gov/compound/Loperamide (accessed on 30 March 2024).

20. Pflieger, T.; Venkatesh, R.; Dachtler, M.; Eggenreich, K.; Laufer, S.; Lunter, D. Novel Approach to Pharmaceutical 3D-Printing Omitting the Need for Filament-Investigation of Materials, Process, and Product Characteristics. *Pharmaceutics* **2022**, *14*, 2488. [CrossRef]

21. Shadambikar, G.; Kipping, T.; Di-Gallo, N.; Elia, A.G.; Knuttel, A.N.; Treffer, D.; Repka, M.A. Vacuum Compression Molding as a Screening Tool to Investigate Carrier Suitability for Hot-Melt Extrusion Formulations. *Pharmaceutics* **2020**, *12*, 1019. [CrossRef]

22. Bochmann, E.S.; Neumann, D.; Gryczke, A.; Wagner, K.G. Micro-scale prediction method for API-solubility in polymeric matrices and process model for forming amorphous solid dispersion by hot-melt extrusion. *Eur. J. Pharm. Biopharm.* **2016**, *107*, 40–48. [CrossRef]

23. Boetker, J.; Water, J.J.; Aho, J.; Arnfast, L.; Bohr, A.; Rantanen, J. Modifying release characteristics from 3D printed drug-eluting products. *Eur. J. Pharm. Sci.* **2016**, *90*, 47–52. [CrossRef]

24. Rauwendaal, C. *Polymer Extrusion*; Carl Hanser Verlag GmbH Co KG.: Munich, Germany, 2014.

25. Treffer, D.; Troiss, A.; Khinast, J. A novel tool to standardize rheology testing of molten polymers for pharmaceutical applications. *Int. J. Pharm.* **2015**, *495*, 474–481. [CrossRef] [PubMed]

26. Jaluria, Y. Heat and Mass Transfer in the Extrusion of Non-Newtonian Materials. In *Transport Phenomena in Materials Processing*; Advances in Heat Transfer; The State University of New Jersey: New Brunswick, NJ, USA, 1996; pp. 145–230.

27. European Medicines Agency (USA) Q 2 (R1) Validation of Analytical Procedures: Text and Methodology. Available online: https://www.ema.europa.eu/en/ich-q2r2-validation-analytical-procedures-scientific-guideline (accessed on 30 March 2024).

28. Food and Drug Administration, USA. *Dissolution Testing and Acceptance Criteria for Immediate-Release Solid Oral Dosage Form Drug Products Containing High Solubility Drug Substances—Guidance for Industry*; Food and Drug Administration: Silver Spring, MD, USA, 2018.

29. Tian, H.; Liu, D.; Yao, Y.; Ma, S.; Zhang, X.; Xiang, A. Effect of Sorbitol Plasticizer on the Structure and Properties of Melt Processed Polyvinyl Alcohol Films. *J. Food Sci.* **2017**, *82*, 2926–2932. [CrossRef] [PubMed]

30. Mohsin, M.; Hossin, A.; Haik, Y. Thermomechanical properties of poly(vinyl alcohol) plasticized with varying ratios of sorbitol. *Mater. Sci. Eng. A* **2011**, *528*, 925–930. [CrossRef]

31. Bates, S.; Zografi, G.; Engers, D.; Morris, K.; Crowley, K.; Newman, A. Analysis of amorphous and nanocrystalline solids from their X-ray diffraction patterns. *Pharm. Res.* **2006**, *23*, 2333–2349. [CrossRef] [PubMed]

32. LaFountaine, J.S.; McGinity, J.W.; Williams, R.O., 3rd. Challenges and Strategies in Thermal Processing of Amorphous Solid Dispersions: A Review. *AAPS PharmSciTech* **2016**, *17*, 43–55. [CrossRef] [PubMed]

33. Kayser, K.; Monschke, M.; Wagner, K.G. ASD Formation Prior to Material Characterization as Key Parameter for Accurate Measurements and Subsequent Process Simulation for Hot-Melt Extrusion. *AAPS PharmSciTech* **2022**, *23*, 176. [CrossRef] [PubMed]
34. Okwuosa, T.C.; Stefaniak, D.; Arafat, B.; Isreb, A.; Wan, K.W.; Alhnan, M.A. A Lower Temperature FDM 3D Printing for the Manufacture of Patient-Specific Immediate Release Tablets. *Pharm. Res.* **2016**, *33*, 2704–2712. [CrossRef] [PubMed]
35. Gioumouxouzis, C.I.; Baklavaridis, A.; Katsamenis, O.L.; Markopoulou, C.K.; Bouropoulos, N.; Tzetzis, D.; Fatouros, D.G. A 3D printed bilayer oral solid dosage form combining metformin for prolonged and glimepiride for immediate drug delivery. *Eur. J. Pharm. Sci.* **2018**, *120*, 40–52. [CrossRef]
36. Matijasic, G.; Gretic, M.; Kezeric, K.; Petanjek, J.; Vukelic, E. Preparation of Filaments and the 3D Printing of Dronedarone HCl Tablets for Treating Cardiac Arrhythmias. *AAPS PharmSciTech* **2019**, *20*, 310. [CrossRef]
37. Goyanes, A.; Buanz, A.B.; Hatton, G.B.; Gaisford, S.; Basit, A.W. 3D printing of modified-release aminosalicylate (4-ASA and 5-ASA) tablets. *Eur. J. Pharm. Biopharm.* **2015**, *89*, 157–162. [CrossRef]
38. Alzahrani, A.; Narala, S.; Adel Ali Youssef, A.; Nyavanandi, D.; Bandari, S.; Mandati, P.; Almotairy, A.; Almutairi, M.; Repka, M. Fabrication of a shell-core fixed-dose combination tablet using fused deposition modeling 3D printing. *Eur. J. Pharm. Biopharm.* **2022**, *177*, 211–223. [CrossRef] [PubMed]
39. Kempin, W.; Domsta, V.; Grathoff, G.; Brecht, I.; Semmling, B.; Tillmann, S.; Weitschies, W.; Seidlitz, A. Immediate Release 3D-Printed Tablets Produced Via Fused Deposition Modeling of a Thermo-Sensitive Drug. *Pharm. Res.* **2018**, *35*, 124. [CrossRef] [PubMed]
40. Dores, F.; Kuźmińska, M.; Soares, C.; Bohus, M.; Shervington, L.A.; Habashy, R.; Pereira, B.C.; Peak, M.; Isreb, A.; Alhnan, M.A. Temperature and solvent facilitated extrusion based 3D printing for pharmaceuticals. *Eur. J. Pharm. Sci.* **2020**, *152*, 105430. [CrossRef] [PubMed]
41. Long, M.; Chen, Y. Developing Solid Oral Dosage Forms. In *Dissolution Testing of Solid Products*; Academic Press: Cambridge, MA, USA, 2009. [CrossRef]
42. Duan, P.; Lamm, M.S.; Yang, F.; Xu, W.; Skomski, D.; Su, Y.; Schmidt-Rohr, K. Quantifying Molecular Mixing and Heterogeneity in Pharmaceutical Dispersions at Sub-100 nm Resolution by Spin Diffusion NMR. *Mol. Pharm.* **2020**, *17*, 3567–3580. [CrossRef] [PubMed]
43. Krause, S.; Iskandar, M. Phase Separation in Styrene-Alpha-Methyl Styrene Block Copolymers. *Abstr. Pap. Am. Chem. Soc.* **1977**, *173*, 130.
44. Dedroog, S.; Pas, T.; Vergauwen, B.; Huygens, C.; Van den Mooter, G. Solid-state analysis of amorphous solid dispersions: Why DSC and XRPD may not be regarded as stand-alone techniques. *J. Pharm. Biomed. Anal.* **2020**, *178*, 112937. [CrossRef] [PubMed]
45. Baird, J.A.; Taylor, L.S. Evaluation of amorphous solid dispersion properties using thermal analysis techniques. *Adv. Drug Deliv. Rev.* **2012**, *64*, 396–421. [CrossRef] [PubMed]
46. Bikiaris, D.; Papageorgiou, G.Z.; Stergiou, A.; Pavlidou, E.; Karavas, E.; Kanaze, F.; Georgarakis, M. Physicochemical studies on solid dispersions of poorly water-soluble drugs. *Thermochim. Acta* **2005**, *439*, 58–67. [CrossRef]
47. Fawcett, T.G.; Gates-Rector, S.; Gindhart, A.M.; Rost, M.; Kabekkodu, S.N.; Blanton, J.R.; Blanton, T.N. A practical guide to pharmaceutical analyses using X-ray powder diffraction. *Powder Diffr.* **2019**, *34*, 164–183. [CrossRef]
48. Randall, C.S.R.; William, L.; Pierre, R. XRD: XRD in pharmaceutical analysis: A versatile tool for problem-solving. *Am. Pharm. Rev.* **2010**, *13*, 52.
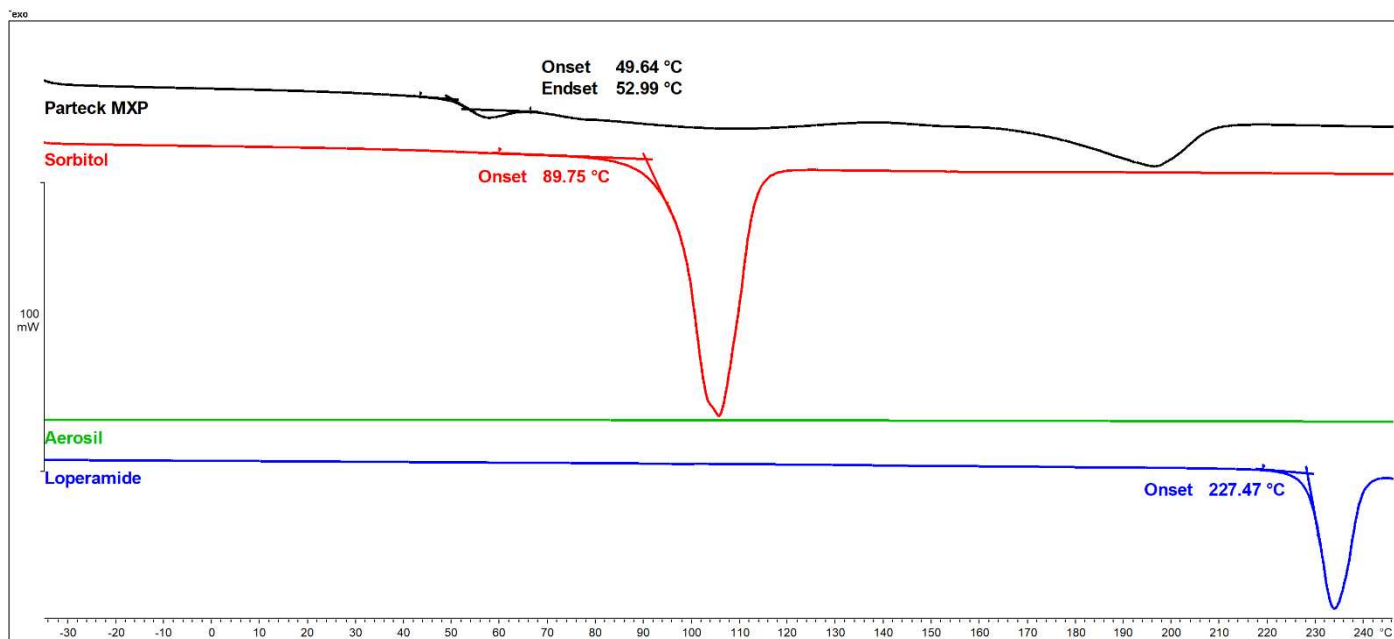
Supplementary

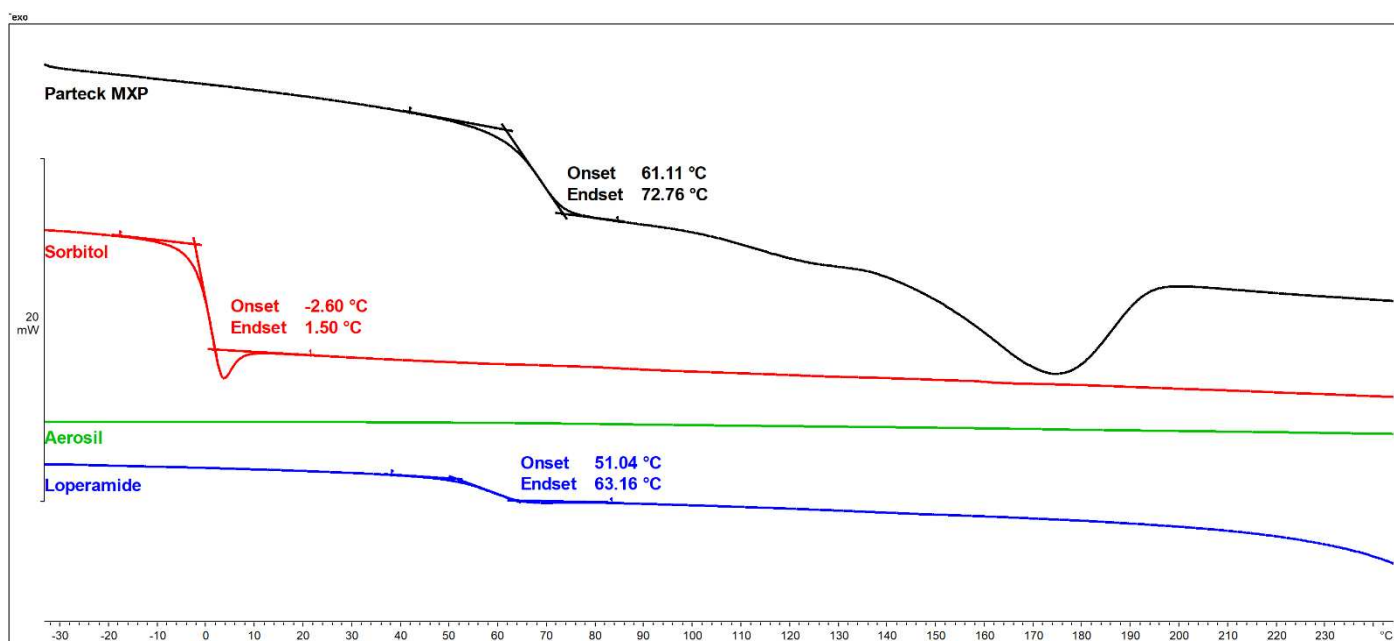**Figure S1.** First heating: neat substances

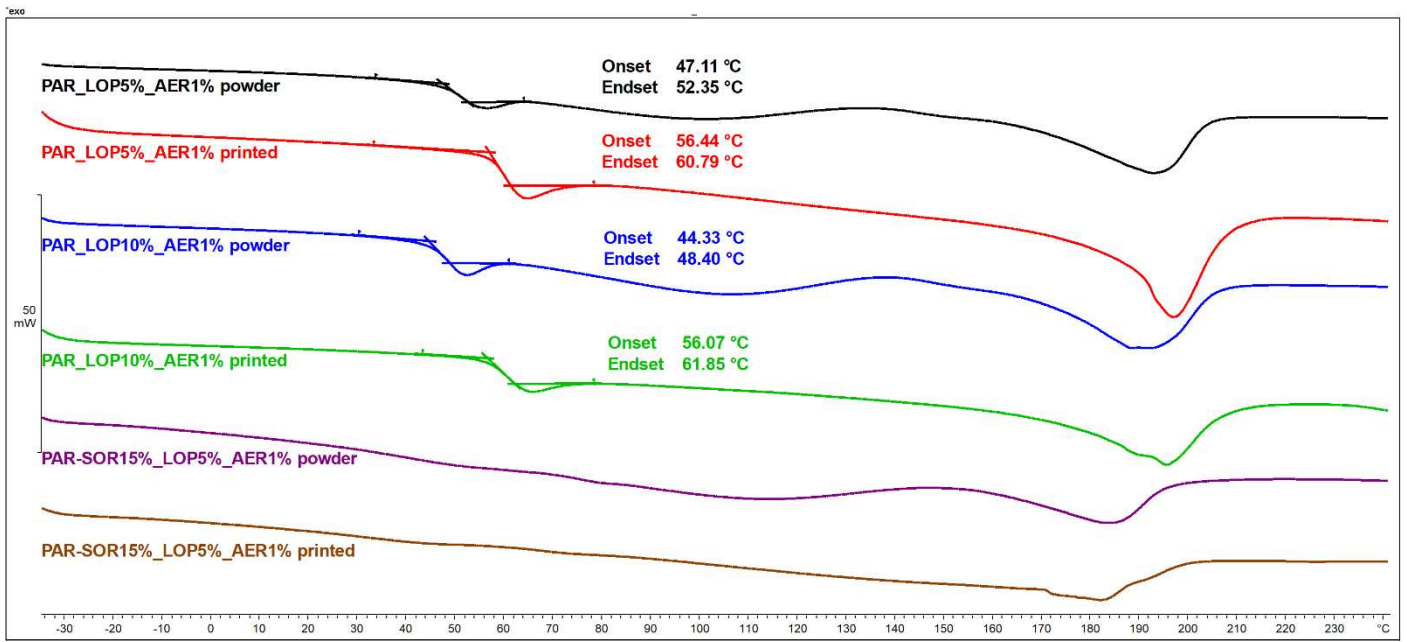**Figure S2.** Second heating: neat substances

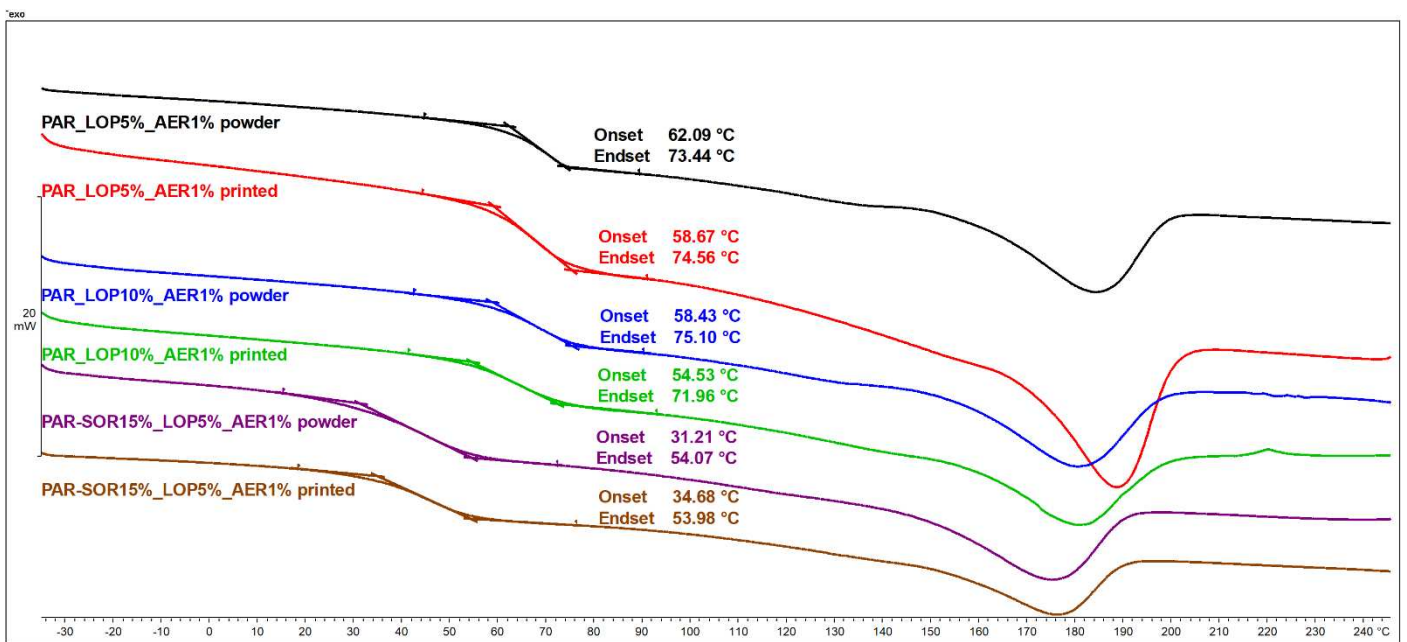**Figure S3.** First heating: powdered and printed samples

Figure S4. Second heating: powdered and printed samples
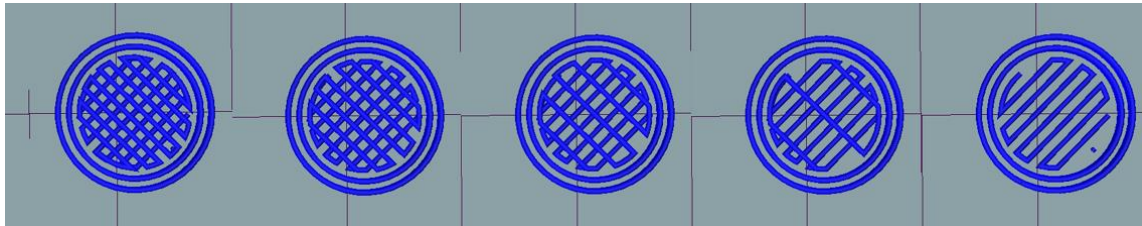
Figure S5. Sliced tablets for visualization of infill

The picture of the sliced tablets shows the layers 2-4 for each individual infill (100% - 0% fltr.) As shown above, the solid layer is constant for each infill and no additional infill is placed for 0% tablets. The addition of 3 top solid layers closes the hollow tablet sufficiently.
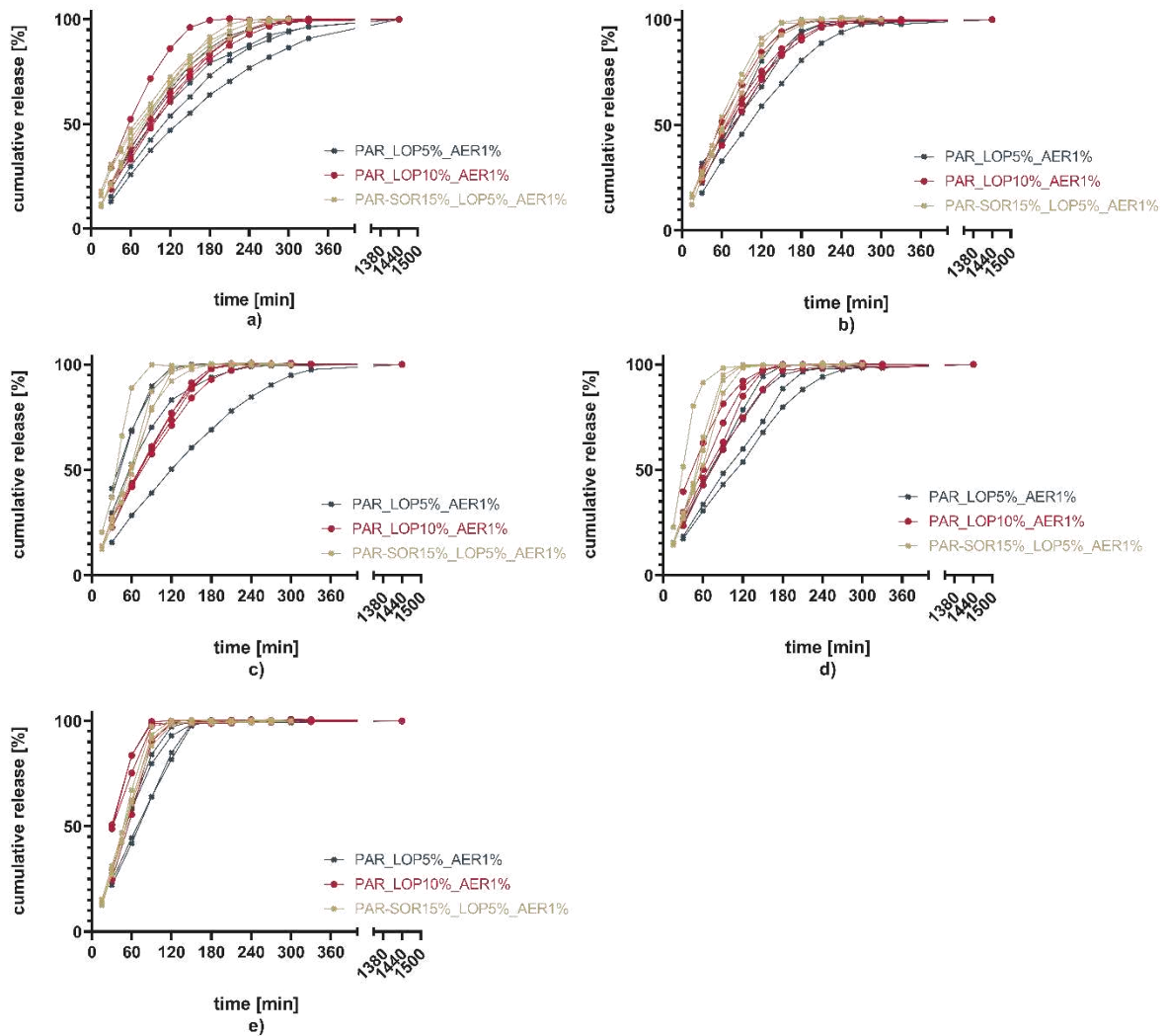

Figure S6. Dissolution data of individual tablets (100%: a), 75%: b), 50%: c), 25%: d), 0%: e))

4. Experimental section – Part 2

Using LOP as a model API to evaluate the methods needed for printing and characterizing tablets laid the foundation for using CAB. However, some mechanistic data were left out of the publication, which is needed to understand the release mechanism from the printed tablets.

4.1.   Evaluation of dissolution mode

Additional information about the release mechanism for LOP from the PAR matrix was sought to improve the dissolution pattern. Typical release mechanisms consist of one or partially both modes of action, diffusion through a swollen layer, and matrix erosion [104,158]. Using an experimental setup, the release from the tablet was determined, and the total mass loss was obtained by removing tablets periodically from the dissolution bath. To gain this information, seven tablets were simultaneously measured in the dissolution apparatus under the conditions described in the publication shown above (2.2.8. Drug Content Analysis by HPLC). At 30 min, 60 min, 120 min, 180 min, and 240 min, the remainder of the tablet was removed from the vessel. Samples of the medium were only drawn from vessels containing tablets or at the point of the removal of the tablet. The removed tablets were thoroughly dried and weighed to calculate the mass difference. The LOP concentration in the dissolution bath was determined via UV-VIS coupled HPLC as described. The overlayed data of the change in mass and LOP content in the solution is shown in Figure 5.
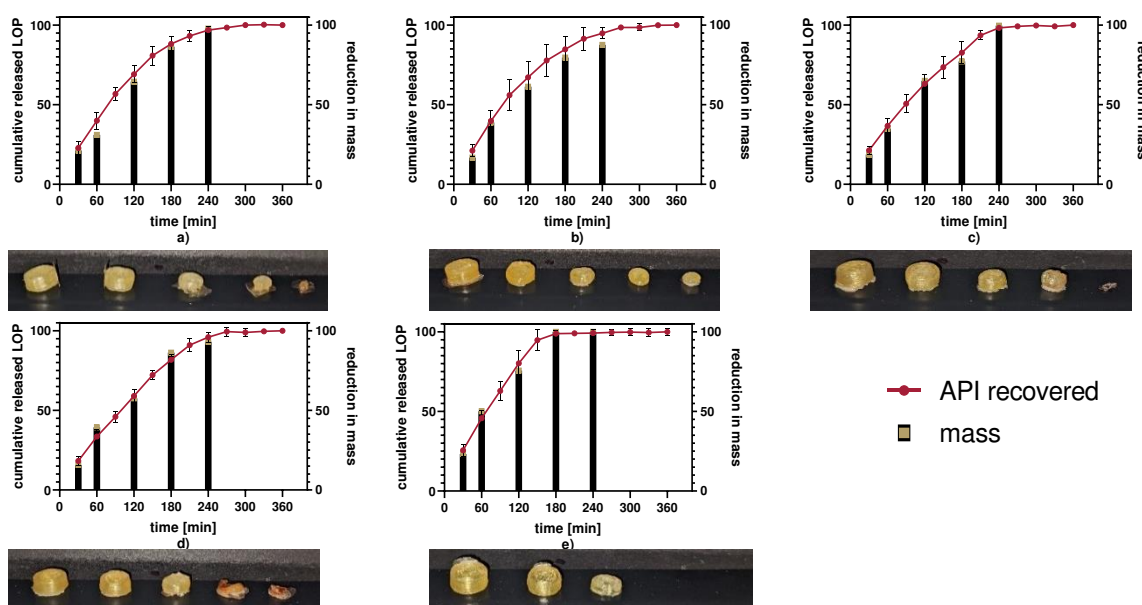

Figure 5 Experimental evaluation of the dissolution mechanism for LOP from PAR-based 3D printed tablets (a) - e) 100%-0% infill in 25% increments); below the graph, pictures of the remainder of the tablets are shown

From the given data, it can be concluded that the primary release mechanism is erosion since the percentage of released drug matches the percentage reduction in total weight. This unsurprising result underlines previous findings from a different setting [83].

With this experience in mind, the transfer to CAB was undertaken. However, formulation development aimed to incorporate CAB into 3D-printed tablets and provide tablets with immediate release. Since the dissolution rate of the printed LOP tablets was still too slow, further formulation development was necessary.

4.2.   Improvement of the Dissolution rate

As described in 1.5, several ways exist to increase the dissolution rate. Changing the formulation by adding excipients or altering their percentage has already been shown. The addition of sorbitol, acting as a plasticizer for PAR, was established to have a positive impact on the dissolution rate during trials with LOP. A similar slow dissolution rate was expected when the formulation was transferred from LOP to CAB since both APIs have similar solubility parameters. The dissolution rate was equally slow as seen with LOP in the formulation with 15% sorbitol. The mixture containing 15% SOR was printed with CAB instead of LOP to confirm this assumption. In addition, testing the increase of SOR to 30% was carried out to determine if further improvement of the dissolution rate is possible without additional excipients. Alongside the SOR change, the polymer PAR was replaced with Kollicoat IR (KIR) to assess its suitability as a substitute. The results of these three experiments are depicted in Figure 6. Dissolution apparatus setup and analytics were conducted as described in [159].
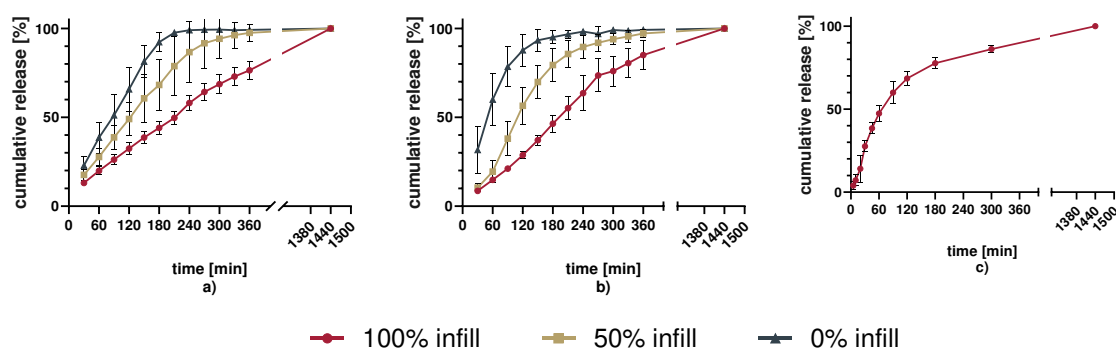

Figure 6 Dissolution data for CAB-containing tablets after the change from LOP (a) PAR-SOR15%E_CAB5%_AER1%; b) PAR-SOR30%E_CAB5%_AER1%; c) KIR-SOR30%E_CAB5%_AER1%)

From the dissolution data, it was concluded that increasing sorbitol amounts would lead to faster dissolution times (comparing a) to b)). It was concluded that under otherwise constant

conditions, the exchange of PAR for KIR improves the dissolution rate (comparing b) to c)). Both interventions will be observed during further formulation development.

Without changing the formulation, changes in the dissolution profile can be achieved by increasing the surface area to volume ratio [104]. To keep changes as minimal as possible, the previously developed tablet design was enhanced by adding pores. The printer's accuracy and resolution impose limitations on the amount and size of pores. Equidistant distribution of pores in sizes 0.4 to 2.4 mm were tested, but only 2.0 and 2.4 mm were successful, with 2.4 mm demonstrating sufficient resolution of the pores. Figure 7 illustrates the iterations tested until the final design of 2.4 mm pores was established.

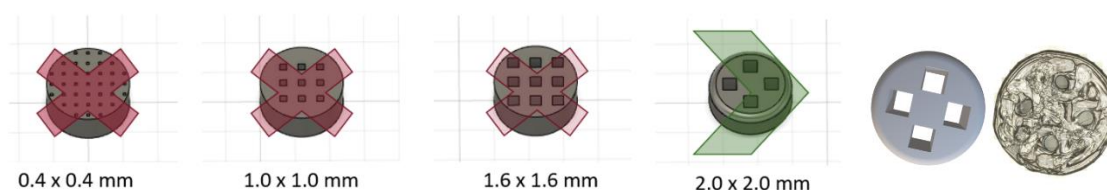0.4 x 0.4 mm   1.0 x 1.0 mm   1.6 x 1.6 mm   2.0 x 2.0 mm

Figure 7 Iterations of CAD designs needed to find a sufficiently printable tablet with internal pores; right: stl and microscopic picture of the 2.4 x 2.4 mm pores design

Table 2 shows the change in calculated volume, area, and surface area to volume ratio (A/V) by comparing the basic tablet model and the models with pores.

Table 2 Calculation of surface area to volume ratio for tablet models

	100% infill	pores 2.0 mm	pores 2.4 mm
Surface Area [mm^2]	342.154	503.908	527.359
Volume [mm^3]	493.598	469.908	434.708
A/V	0.693	1.072	1.213

Adding these pores helped increase the surface area while only slightly decreasing the volume compared to the standard model with full infill. This led to an increased ratio of surface area to volume. The filled tablet and the 2.4 mm x 2.4 mm pores-containing tablet were always printed for the following experiments with new formulations.

Other excipients positively impacting the dissolution rate without decreasing extrusion or print temperature were sought in the class of (super-)disintegrants. CCS and SSG were tested in different concentrations [160]. The third option tested is changing the matrix-building polymer to

other faster water-soluble polymers. Polymers expected to dissolve or disintegrate faster than PAR are KIR, Kollidon VA64 (KVA), and Eudragit E PO (EPO). Results for the porous design and changes in the composition of the excipients based on PAR and KIR are shown in the following publication. During the formulation development, it became more apparent that immediate release was an achievable goal. This led to the critical question of how much drug load would be viable and needed. To obtain tablets with desired drug content and sufficient size, the drug load must be optimized. Considering the high dosages expected (140 mg), the drug load directly influences the size of the tablet. A drug load of 10%, as tested during the formulation development, would lead to tablets with an unmanageable size. Increasing the drug load from 10%, over 15%, up to 25% was tested. Printing tablets with 25% CAB was possible but still dismissed since the print quality did not reach the desired goal. This is likely due to these formulations' very low amount of polymer.

Dosage by design – 3D printing individualized cabozantinib tablets with immediate release

Jonas Lenhart, Dominique J. Lunter *

Department of Pharmaceutical Technology, Eberhard Karls University, 72076 Tuebingen, Germany

ARTICLE INFO

ABSTRACT

Production of patient-specific dosage forms is important to improve patient adherence and effectiveness while reducing the prevalence and severity of adverse effects. Due to its possibility of rapid prototyping 3D printing can be used to produce individual dosages while utilizing techniques such as hot melt extrusion to increase the bioavailability of poorly soluble drugs. In this work, Parteck MXP and Kollicoat IR were used as water-soluble polymer bases for formulation development for 3D printing of various dosages incorporating cabozantinib while enabling immediate release. The effect of tablet design and the excipients sorbitol, croscarmellose sodium, and sodium starch glycolate was investigated for this goal. A way to calculate the size of tablets for pre-determined dosages is proposed to enable the printing of individual strengths from one formulation. Rheological data were collected to deepen the understanding of the role of melt viscosity in 3D printing and hot melt extrusion processes. The production of immediate-release cabozantinib tablets containing every therapeutically relevant dosage in a single unit produced by two-step 3D printing was realized.

1. Introduction

With the implementation of 3D printing in many fields of manufacturing worldwide, its applicability has also been extended to the medical and pharmaceutical fields. Currently, only one 3D-printed tablet is available on the market. Spritam® is produced by Aprecia Pharmaceuticals (Aprecia Pharmaceuticals, LLC, Blue Ash, OH, USA) using their ZipDose® [1] technology. However, two more 3D printed products manufactured by Triastek (Triastek, Inc., Nanjing, China) are already on their way and received investigational new drug clearance recently [2]. For melt extrusion, there are numerous devices described ranging from self-built [3] to commercially developed printers [4,5]. Regarding the design and printing of solid oral dosage forms there has been extensive research [6,7], while also a lot of research has gone into solving individual challenges such as printing despite low thermal degradation temperature of the API [8], delay or enhance dissolution rate [9,10], or improve patient adherence by combining different drugs into single tablets [11,12]. Due to the possibility of rapid prototyping 3D printing is a promising way of manufacturing personalized medicines [13].

The term personalized medicine is usually used for a type of medicine that includes information regarding one's genes or protein expression to prevent, diagnose, or treat a disease. It can generally be seen as the approach to find the "right treatment for the right person at the right time"[14]. For many drugs, there is a need to design dosages based on the patient's needs. Characteristics such as gender [15], body weight [16], genetic expression [17], and health status need to be considered when selecting the correct dosage. Furthermore, for some drugs, the therapeutic window is small while at the same time, adverse effects are more pronounced [18]. In such cases, correct dosing is of utmost importance. One example is the anti-cancer drug cabozantinib.

Cabozantinib got approval in Europe for the treatment of adult patients with advanced renal cell carcinoma (60 mg) who are naive to treatment or at intermediate or poor risk in terms of prognosis, unresectable, or locally advanced metastatic medullary thyroid cancer (140 mg). The cabozantinib monotherapy in the US is approved for the treatment of patients with advanced renal cell carcinoma (60 mg), patients with progressive metastatic medullary thyroid cancer (140 mg), and patients with hepatocellular carcinoma who have previously been treated with sorafenib (60 mg) [19]. The mechanism of action of the tyrosine kinase inhibitor cabozantinib is comprised of three main interactions. It targets the vascular endothelial growth factor (VEGF) receptors and the hepatocyte growth factor receptor (MET) both of which can be found in the signaling pathways of angiogenesis regulation, cell

proliferation, and cell migration [20]. Additionally, it targets the receptor tyrosine kinase AXL which has been implicated as a cancer driver due to its effects on cell proliferation and survival [21]. The dysregulation of these 3 pathways is associated with immune suppression as well, which further increases the risk by inhibition of antitumor immunity.

The standard dosage of cabozantinib for the treatment of medullary thyroid cancer is 140 mg (free base) but typically a dose adjustment is needed during treatment due to adverse effects that are comparable to those of other small molecules with targeted inhibition of VEGFR and other tyrosine kinase-mediated pathways such as skin and gastrointestinal toxicities. Thus, 75 % percent of patients require at least one dose reduction. It is thus being discussed that safety could be improved if a lower dose would be found clinically appropriate [14,22]. Similar results were found for the treatment of renal cell carcinoma, where the dosage starts at 60 mg and dose reduction can be found necessary as the adverse effects increase [23,24]. While cabozantinib cannot improve overall survival, the progression-free survival is prolonged. Decreasing the adverse effects during this time is a goal worth chasing. An additional benefit in progression-free survival for some patients with different RET (rearranged during transfection) mutations was indicated by different studies [22,25]. This underlines the importance of personalized medicine in cancer treatment.

Economic studies of cabozantinib suggest that NICÉs (National Institute for Health and Care Excellence) criteria for life-extending therapies given at the end of life are not met for cabozantinib [26]. Being able to produce only the required amounts and dosages directly in clinical settings might be a way to improve cost efficacy. Currently, two formulations are marketed. One formulation containing cabozantinib [(2S)-2-hydroxybutanedioate] is dosed at 80 mg and 20 mg in capsules (Cometriq [27]), the other containing cabozantinib-L-malate in 60, 40, and 20 mg tablets (Cabometyx [28]). It is evident, that the cost of pharmaceutical products goes down once the generic market is opened due to patent expiration [29]. One of the reasons, that can be applied to 3D printing in clinical settings is that the share of the API cost is much bigger for generic production than it is in original manufacturing while the total price of the product is lower [30]. This may be explained as the original manufacturer needs to reimburse their cost during trials and authorization of the product. In addition to the total cost of the tablets, the number of needed tabelts could be reduced, if each patient's need is produced individually leading to the usage of each individual tablet, which might not be the case for some currently available dosages.

Following the widely acknowledged Biopharmaceutics Classification (BCS) System [31], cabozantinib can be classified as Class II, which is characterized by low solubility and high permeability. The malate salt shows better solubility than the free base ($2.24 \times 10^{-7} \frac{mol CAB}{mol water}$ at 25 °C) [32]. Formulation development is especially important for drugs, whose bioavailability is mainly reduced due to solubility. There are several ways known, that can be deployed to improve dissolution behavior. Most of them can be obtained from an understanding of the Noyes-Whitney equation [33] and the further improvement made by Nernst and Brunner [34]. Mainly the effective surface area, the diffusion coefficient, the diffusion layer thickness, the saturation solubility, the amount of dissolved drug, and the volume of dissolution media are important for understanding the dissolution behavior [35]. Ways to improve the dissolution rate of BCS class II and IV drugs can be found in micronization, selfemulsification, cyclodextrin complexation, co-crystallisation, solubilization by a change in pH, salt formation, use of co-solvents, formation of amorphous solid dispersions or liposomal/niosomal formulation [36].

In the following work hot melt extrusion and formation of amorphous solid dispersions were used for the improvement of dissolution rate for cabozantinib from 3D printed tablets. Parteck MXP (PAR) and Kollicoat IR (KIR) were used as water-soluble polymer bases for 3D printing of various dosages incorporating cabozantinib while enabling immediate release. The effect of tablet design and the excipients sorbitol, croscarmellose sodium (CCS), and sodium starch glycolate SSG) was investigated for this goal. A way to calculate the size of tablets for predetermined dosages is proposed to enable the printing of individual strengths from one formulation. Rheological data were collected to deepen the understanding of the role of melt viscosity in 3D printing and hot melt extrusion processes.

2. Materials and methods

2.1. Materials

Watersoluble polymers were used as the matrix for the API to be distributed in. These were PVA (Parteck® MXP (Polyvinylalcohol), Merck KGaA, Germany), and Kollicoat IR ((Macrogol Poly(Vinyl alcohol)Grafted Copolymer), BASF). Other excipients added to change the dissolution behavior were Sorbitol (Parteck SI 400, Merck KGaA, Germany) and the superdisintegrants croscarmellose sodium (Ac-Di-Sol, DuPont) and sodium starch glycolate (Explotab, JRS Pharma). The widespread availability of these excipients and their regulatory as well as processing experience in extrusion-based processes with low concentrations made them an interesting base for significantly changing the release behavior.

To enhance the flowability of powdered mixtures fumed silica ((AER) Aerosil® R 972 Pharma, Evonik, Germany) was used.The API cabozantinib S-malate (CAB) was obtained from the department of pharmaceutical chemistry (University of Tübingen). The purity was reported as >99 %. For the dissolution medium according to FDA [37] Triton X-100 (Merck Millipore) had to be added to 0.01 M hydrochloric acid. HPLC-grade solvents (Acetonitrile (ACN), formic acid) were used for analysis.

2.2. Methods

2.2.1. Preparation of powder mixtures

Physical mixtures of powdered ingredients were produced by accurately weighing and mixing in a tumble mixer for 20 min (Turbula Type T2C, Willy A. Bachofen AG, Switzerland). Particle sizes were only considered for mixtures used in the printing process. Powders used in extrusion came from the manufacturer and had a sufficiently low particle size (<0.2 mm). Powder mixtures for printing were produced in the same way, but all the ingredients were sieved, and for the milled extrudate as well as the API only the fraction between 0.355 mm and 0.200 mm was processed.

2.2.2. HME of modified mixtures

PVA and especially PAR, as well as KIR, have been described in hot melt extrusion-related processes [38–40]. As excipients for processing, stabilization, and dissolution several substances have been described. The use of polyols such as SOR and mannitol and their plasticizing properties were shown [38,41]. Also, another group of substances, namely the (super)disintegrants have been tested in extrusion processes [41–44]. Furthermore, different amounts of SOR, CCS, and SSG were tested regarding their effect on the extrusion, printing, and dissolution behavior of the polymers PAR and KIR [45]. Literature review showed, that polymers used in oral drug delivery are usually utilized in a range of 35–90 % which was also realized in the current work [45]. Physical mixtures of sieved powders (0.355 mm) were extruded using a single screw extruder (Noztek Pro, Noztek, England) at a fixed speed of 40 revolutions per minute (RPM). The compositions and temperatures used are given in Tables 1 and 2.

For the PAR-based extrudates, the increase in SOR decreased the extrusion temperature, which is well expected, since sorbitol acts as a plasticizer for PVA. By adding and increasing the amount of CCS (10−>20 %) this trend was reversed and the extrusion temperature had to be increased even while the SOR content was increased as well

Table 1
Composition of PAR-based formulations (Parteck MXP (PAR), sorbitol (SOR), croscarmellose sodium (CCS), sodium starch glycolate (SSG)).

Mixture Nr.	PAR [%]	SOR [%]	CCS [%]	SSG [%]	Extrusion temperature [°C]
1	50	40	10	–	140
3	50	40	–	10	140
5	50	50	–	–	115
7	40	50	10	–	135
9	20	60	20	–	180

Table 2
Composition of KIR-based formulations (Kollicoat IR (KIR), sorbitol (SOR), croscarmellose sodium (CCS), sodium starch glycolate (SSG)).

Mixture Nr.	KIR [%]	SOR [%]	CCS [%]	SSG [%]	Extrusion temperature [°C]
2	50	40	10	–	170
4	50	40	–	10	170
6	50	50	–	–	180
8	40	50	10	–	175
10	20	60	20	–	195

(50−>60 %).

KIR generally shows a higher temperature needed for successful extrusion, with less of an impact by adding sorbitol. This indicates that SOR does not act as a plasticizer in KIR as it does with PAR.

After extrusion, the extrudates were frozen and milled using precooled milling devices (M8 2461, Primax, Germany) and sieved while the fraction 0.355 mm > x > 0.200 mm was used in further steps.

2.2.3. Design of tablets

Autodesk Fusion 360 (Autodesk GmbH, München) was used to design the tablets and export them as .stl files. Different designs of tablets (Fig. 1) were printed. The standard model for primary testing was a round tablet with curved edges for improved handling (radius 6.0 mm, height 5.0 mm).

A tablet with an improved surface area to volume ratio was also designed and printed. To this end, 4 pores of 2.4 mm x 2.4 mm proved to be printable for the formulations used. Pores were expected to increase the dissolution rate due to the increased surface area [46,47]. The third tablet shown is exemplary for the oblong-shaped tablet used in dosage scaling. Pictures of all the tablets used for different dosages are shown in the supplementary section (Figs. S2 and S3).

For the design of different dosages for both final formulations (PAR-based and KIR-based), a different approach was used. A Python script (including a Dash front end) was written, that calculated the needed volume based on the density of the printed tablet and the dosage (e.g. a 140 mg tablet at 20 % loading and a density of 1.41 g/cm^3 equals a theoretical volume of 0.4965 cm^3). Using the volumes the optimal dimensions (height, length, and width) of a capsule-shaped tablet were calculated in a brute-force attempt, meaning that every possible operation is calculated and the best fit is given in the results. Constraints for the calculation were achieved by setting borders for the allowed length-

to-width (2.1–2.5) and width-to-height (1.6–1.7) ratios as well as allowing the height to change in 0.2 mm increments (based on the printer's layer height) and the length and width in 0.1 mm increments. The script then gave results for the CAD software on the dimensions of the tablet for each dosage in 10 mg increments. Two different calculations were set up. One for the dosages 140–60 mg using a formulation containing 20 % CAB and one for the dosages 50–20 mg containing 10 % CAB. The total size of the tablet, especially for higher dosages, had to be considered concerning the swallowability of the tablets [48,49]. Thus, the calculation minimized the sum of the length, height, and width of the tablet. Fig. S1 shows the designed tablets based on the aforementioned calculations.

2.2.4. 3D Printing using direct powder extrusion tool of M3dimaker

Designs developed using the Fusion 360 were sliced by the Repetier-Host software (Hot-World GmbH & Co. KG, Germany) provided with the 3D printer (M3dimaker, FabRx Ltd., London) which was equipped with the direct powder extrusion tool. While most settings could be kept constant over all mixtures printed, the printing speed and temperature were adjusted to the formulation.

2.2.5. Meltrheology

Specimens with a consistent geometric shape (circular, radius 10 mm) for the rheological experiments were produced using a VCM device (MeltPrep, Graz, Austria) [50]. Temperatures needed to produce the specimen depended on the mixture and can be found in the results part. Different methods have been described to evaluate the rheology of thermoplastic polymers and mixtures thereof for the use of extrusion-based processes and 3D printing [51–54]. In this work, small amplitude oscillatory shear (SAOS) experiments were conducted. To be able to interpret results according to the printer used, the shear rate during printing was determined. There generally are two ways to determine the shear rate during extrusion processes. They concentrate on different parts of the extruder. One of them, which is more often used for the determination of shear rate in FDM 3D printers looks at the shear rate in the nozzle [55]. It is calculated from the volume flow and the dimensions of the nozzle. For the determination of the volume flow (Q) during the printing of tablets, the time (t) it took to print individual tablets was measured and afterward, the volume of these tablets was analyzed using a gas displacement pycnometer (Accupyc 1330, Micromeritics Instrument Corporation, USA). Temperature for these measurements was set to 25 °C and the remaining volume was flushed with Helium. From the calculated volume flow, the shear rate at the nozzle wall ($\dot{\gamma}_{wa}$) was calculated. The other method described is the approximation of the shear rate inside single screw extruders that can be achieved from the Couette shear rate [56]. To this end, the screw speed during printing was determined by counting revolutions and dividing by the printing time. The complete method is described in [40].

The following melt rheology evaluation was conducted on a rheometer (Anton Paar Physica MCR 501, Anton Paar GmbH, Germany) using a stainless-steel plate with a 10 mm radius in a plate-plate setup. In the first step, the linear viscoelastic range (LVR) was determined by employing amplitude sweeps from 0.01 % to 100 % deformation [52]. In the next step, frequency sweeps were performed at different temperatures around printing and extrusion temperatures [57] from 100 Hz to 0.1 Hz at the amplitude found to be inside the LVR.

2.2.6. Thermal analysis

2.2.6.1 Differential scanning calorimetry (DSC). Excipients as well as printed tablets were analyzed using a DSC (Mettler DSC 820, Mettler-Toledo GmbH, Germany), while their melting points, glass transition temperature, and if occurring recrystallization were detected. Samples were accurately weighed into an aluminum crucible and measured from −50 °C up to max. 240 °C depending on the material analyzed. Layers of

Fig. 1. .stl files of tablets printed; fltr: round tablet with rounded edges, round tablet with rounded edges and pores, exemplary oblong shaped tablet used in dosage trials.

the printed tablets were removed and laid flat into the crucible. Two heating cycles were used to find information regarding melting points (first heating), glass transition, and recrystallization (second cycle). Heating and cooling were done with 20 K/min under nitrogen gas flow.

2.2.6.2 Simultaneous thermal analyzer (STA). Loss of mass due to solvent or water evaporation, as well as thermal degradation, were determined using a Netzsch STA 409 PG/1/G Luxx (Erich NETZSCH GmbH & Co. Holding KG, Germany). Samples were accurately weighed into an aluminum crucible and heated from 25 °C up to 250 °C at 10 K/min. Blank reference was measured using Al_2O_3.

2.2.7. XRD-measurements

X-ray diffraction patterns were measured on a Bruker D8 Advance diffractometer (Bruker Corp. USA) in an angular range from 10 to 50° 2θ using monochromatic CuKα radiation (λ = 0.15406 nm). While excipients were measured as powder, printed tablets were analyzed intact.

2.2.8. Confocal Raman microspectroscopy

Confocal Raman microspectroscopy (CRM) was employed to observe the distribution of API in the tablet without destroying it. The alpha 300R system by Witec (WITec GmbH, Ulm, Germany) equipped with the green laser (λ = 532 nm), a 40x objective (Nikon S Plan Flour 40x/0.60 objective), and the TrueSurface MKII module. Pure substances were measured with a laser intensity of 30 mW, while the intensity had to be adjusted for the printed tablets due to the time needed for autofocus and measurement. Large-area scans were performed with the 40x objective. The surface was evaluated and corrected by the TrueSurface MKII module before the large-area scans were performed. The autofocus had to be used to get the best spectra still before each single spectrum could be acquired. An area of 80 x 2000 μm with 16 x 400 pixels was evaluated for the tablets. While the KIR-based tablets were sufficiently stable at 30 mW, the laser intensity for the PAR-based tablets was reduced to 15 mW.

2.2.9. In vitro dissolution

The dissolution method for CAB was adapted from FDA quality assessment [37] using 0.01 M HCl with 0.375 % Triton X-100 (Sigma Aldrich) at 37 °C with 100 RPM paddle speed on a Pharma Test PT-DT7 (Pharma Test Apparatebau AG, Germany) manual dissolution tester. Sampling depended on the expected dissolution time including a decrease in total monitored time for faster dissolving tablets.

2.2.10. Drug concentration analysis by HPLC

The separation of CAB and Triton X-100 was achieved by using ACN and 0.1 % formic acid in an aqueous solution (54 %/46 %) over 13 min under isocratic conditions at a flow rate of 1 ml/min. Using this method a calibration over 3 powers of ten ranging from 0.2 mg/ml to 0.2 ng/ml with a tested limit of quantification of 0. 52 ng/ml and a calculated limit of detection at 0.172 ng/ml according to ICH [58] guidelines was established. The lowest R^2 found was 0.9943.

2.2.11. Statistical analysis and use of AI

Evaluation of the LargeArea Scans performed on the Raman microspectrometer was done using the TrueComponent analysis feature provided by the Control 6 software. It uses multivariate analysis to calculate the distribution of substances in the scans based on the individual substances' spectra.

Additional aid from the generative AI model ChatGPT-4 was used for writing the Python-Script to calculate the tablets' sizes.

3. Results and discussion

3.1. Formulation development

3.1.1. Meltrheology

First, drug-free excipient mixtures were produced by HME. Extruded mixtures were evaluated rheologically for their behavior at different temperatures and shear rates after the determination of their LVR. In previous studies with the same printer setup, the shear rate was determined and a maximum viscosity of around 4000 Pa*s for successful printing was proposed [40]. Although the shear rate was not fully reached in the current study due to the smaller LVR, the printing temperature was estimated based on these previous findings (Table 3). Full results of the rheological experiment can be found in the supplementary (Figs. S10 and S11). All samples showed a temperature-dependent shear thinning behavior. At the same temperature, generally speaking, KIR shows a higher viscosity than PAR. This is in line with findings from extrusion and printing parameters (KIR needing higher extrusion and printing temperatures). The addition of SOR and CCS leads to reduced viscosities and lower processing temperatures compared to the neat polymers. Compared to CCS the addition of SSG leads to a less pronounced reduction of printing temperature.

While actual printing temperatures followed the trend found in the rheological experiments, they were found to be around 20 °C higher than expected. Thus an even lower viscosity was needed for sufficient printing. One has to keep in mind, that extrusion from the printer was successful at lower temperatures, but first-layer and layer-to-layer adhesion required for printing needed lower viscosity and thus higher temperatures. Due to the shear thinning behavior of the samples, the shear rate-dependent viscosity inside the barrel (couette shear rate) is expected to be determining for the rheology of a successful extrusion. On the other hand the higher shear rate found in the nozzle (Table S1) leads to a decreased viscosity which is crucial for the printing part.

Generally speaking the extrusion with CCS was much more stable than the one with SSG, thus it was used for further formulation development.

3.1.2. 3D printing

Extruded mixtures were printed with 10 % CAB to examine the changes in dissolution rate. All tablets were printed with 100 % infill. Printing temperature as well as pictures of whole tablets and the porous

Table 3
Estimated and experimental values of printing temperatures of extruded mixtures (Parteck MXP (PAR), Kollicoat IR (KIR), sorbitol (SOR), croscarmellose sodium (CCS), sodium starch glycolate (SSG)).

Formulation	Meltprep temperature [°C]	Print temperature expected from meltrheology [°C]	Print temperature used [°C]
PAR-SOR40%-CCS10%E	175	<160	170–200/30
PAR-SOR40%-SSG10%E	175	>160	180–190/30
PAR-SOR50%E	160	>150	160/30
PAR-SOR50%-CCS10%E	170	<160	165/30
PAR-SOR60%-CCS20%E	175	<160	185/35
KIR-SOR40%-CCS10%E	185	>170	190/55
KIR-SOR40%-SSG10%E	180	>170	200/50
KIR-SOR50%E	175	>170	190/50
KIR-SOR50%-CCS10%E	180	<180	185/50
KIR-SOR60%-CCS20%E	175	>170	200/45

design of PAR-based formulations are given in Table 4. The nomenclature for the mixtures consists of the material extruded (…E) and the added amount of CAB and AER. The porous design was expected to decrease the dissolution time due to an increase in the surface area.

The temperatures needed for the successful printing of PAR-based mixtures are much closer to each other than expected from the extrusion parameters. Printing temperatures were found to be needed above the extrusion temperature for two reasons. First, the shear forces in the extruder are higher and thus a lower temperature leads to a successful extrusion, and second, a lower viscosity is needed for proper layer adhesion. Still, all of them can be found well below the thermal degradation temperature of CAB. Table 5 shows the temperatures and exemplary pictures of tablets from KIR-based formulations.

KIR-based formulations, analogous to the extrusion temperatures, showed higher temperatures needed for the printing process than PAR-based ones. Especially the higher temperatures of the print bed show, that more energy is needed for sufficient first-layer adhesion and further layer bonding. Even though in the formulations containing only 40 % SOR, the temperature was close to the onset of thermal degradation of CAB no degradation products were detected. The whole HPLC-elution range was crosschecked with an additional wavelength of 220 nm. Both used wavelengths detected no signals besides the CAB main peak. With the increase in excipients, the printing temperature could be decreased well below the thermal degradation temperature of CAB.

3.1.3 In-vitro dissolution testing

Printed tablets were used for dissolution testing to investigate the impact of excipients (polymers, plasticizers, disintegrants) and pores on drug dissolution kinetics. From each formulation and design, 3 tablets were tested for dissolution over 24 h and results are given in Fig. 2. During formulation development only the time to complete dissolution not the total mass of the drug released was of primary concern. Thus, the diagrams show the percentage released.

Each graph shows the comparison between printed tablets made from certain formulations that differ in the presence of pores (with/without) and in the polymer used (PAR or KIR). In each diagram, the impact of an adjustment in one of the constituents on dissolution behavior is shown. In a), the formulations including 40 % SOR and 10 % CCS can be seen while looking at differences between PAR and KIR. b) shows formulations including 10 % SSG in exchange for the 10 % CCS and formulations containing either PAR or KIR. In c) one can observe the

Table 4

PAR-based 3D printed tablets during formulation development (Parteck MXP (PAR), sorbitol (SOR), croscarmellose sodium (CCS), sodium starch glycolate (SSG)).

Mixture	Printing/printbed temperature [°C]	Photo
PAR-SOR40%-CCS10% E_CAB10%_AER0.5%	175/30	
PAR-SOR40%-SSG10% E_CAB10%_AER0.5%	185/40	
PAR-SOR50%E_CAB10%	185/30	
PAR-SOR50%-CCS10% E_CAB10%_AER0.5%	170/35	

Table 5

KIR-based 3D printed tablets during formulation development (Kollicoat IR (KIR), sorbitol (SOR), croscarmellose sodium (CCS), sodium starch glycolate (SSG)).

Mixture	Printing/printbed temperature [°C]	Photo
KIR-SOR40%-CCS10% E_CAB10%_AER0.5%	190–195/50	
KIR-SOR40%-SSG10% E_CAB10%_AER0.5%	190/55,195/50	
KIR-SOR50%E_CAB10% _AER0.5%	185/50	
KIR-SOR50%-CCS10% E_CAB10%_AER0.5%	180/50	

change in dissolution behavior when the superdisintegrants were omitted and a further increase in SOR from 40 % to 50 % was realized. Finally, d) shows the next iteration of a formulation including 50 % SOR and 10 % CCS.

Generally speaking, the dissolution from PAR-based formulations is slower than from KIR-based ones. But with the addition of the pores PAR-based tablets showed a huge increase in dissolution rate, while pores showed only very little effect in KIR-based tablets. This might be due to the already much faster dissolution rate of KIR-based tablets. In the direct comparison of CCS and SSG in formulations containing 40 % SOR, it can be seen, that there is no difference for the KIR-based tablets, while a significantly faster dissolution is obtained for both the solid and porous PAR-based tablets. Still, the effect is smaller than removing the disintegrant and adding another 10 % SOR. As the SOR content cannot be added indefinitely due to its plasticizing characteristics, the combination of increased SOR and the addition of CCS was tested. As mentioned previously, CCS was chosen due to its improved handling during extrusion. It was seen, that KIR-based tabletś and the porous PAR-based tabletś dissolution rate was improved further, closing in on the goal of immediate release.

In summary, the dissolution rate can be increased with increasing amounts of SOR and the addition of superdisintegrants. The influence of the surface area to volume ratio was shown once again with the porous tablet design [42,59]. The influence of the changes was way less prone for KIR-based formulations. This is expected to be the case since the release of CAB from formulations containing higher percentages of KIR was already much faster.

3.2. Final formulations

3.2.1. 3D printing

Due to the improvements in the dissolution rate of tablets containing 10 % CAB shown in 3.1.3, the next step was to find a formulation, that still shows immediate release for CAB concentrations higher than 10 %. This was necessary to be able to provide dosages of up to 140 mg CAB in single tablets small enough to be swallowable. An increase in both SOR and CCS was sought to improve the dissolution rate while keeping the successful extrusion. The final formulationś extrudate contains 60 % SOR and 20 % CCS, with the remaining 20 % being filled with PAR or KIR respectively. This extrudate was then mixed with 10 % or 20 % CAB depending on the dosage required and 0.2 % AER as a flow agent. These
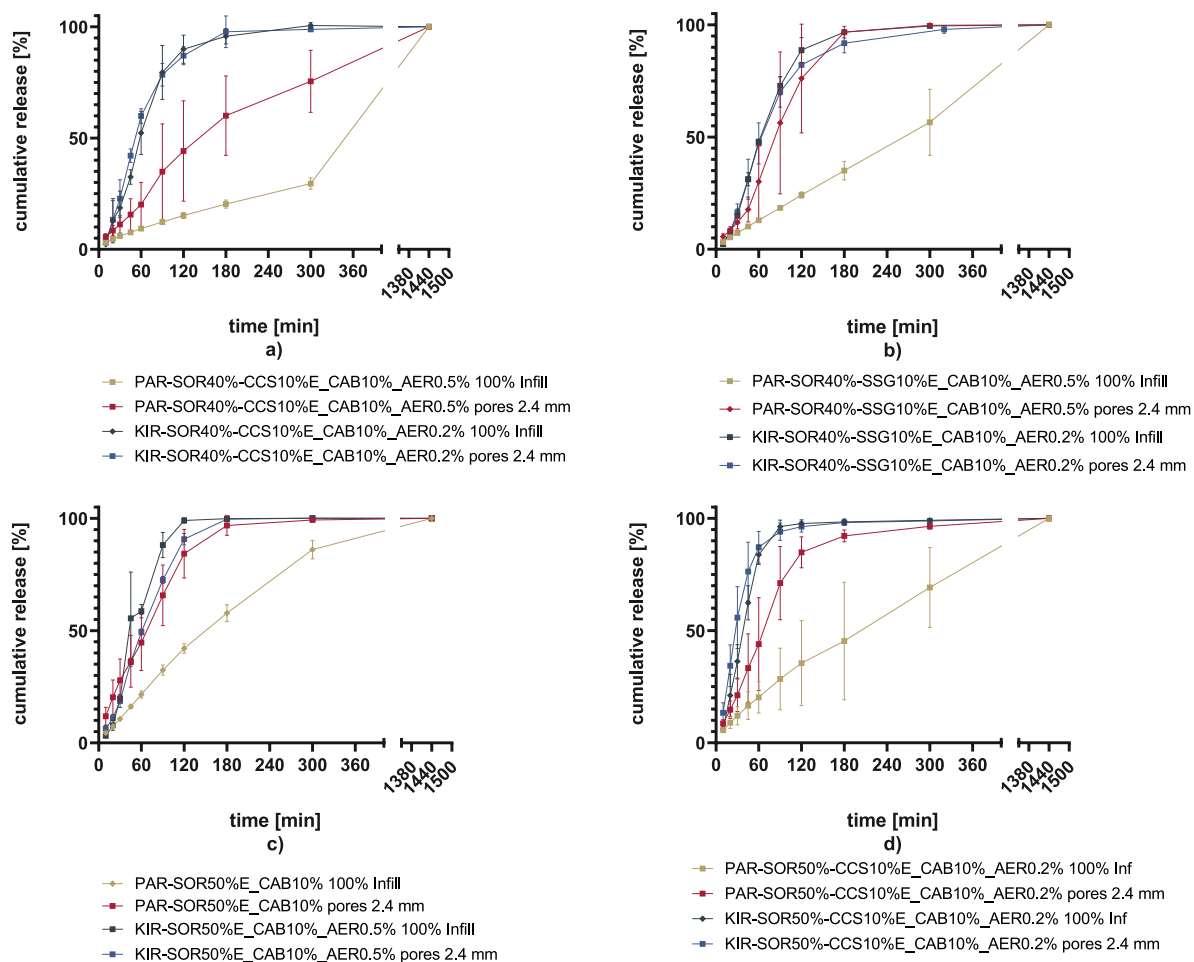
Fig. 2. Dissolution data of tablets during formulation development, n = 3 mean ± SD (Parteck MXP (PAR), Kollicoat IR (KIR), sorbitol (SOR), croscarmellose sodium (CCS), sodium starch glycolate (SSG)).

mixtures were used to print tablets whose size was calculated using the Python script. Tablets design was developed to have the smallest possible size (length height, width) to ensure patient acceptance and allow for swallowability. One set of tablets was designed for the 10 % CAB formulation (used for 20–50 mg) and one set was designed for the 20 % CAB formulation (used for 60–140 mg). Pictures of all the printed tablets can be found in the supplementary material (Figs. S2 and S3), while exemplary pictures of each formulation are shown with the

Table 6
Temperatures needed for printing final formulations and exemplary pictures (Parteck MXP (PAR), Kollicoat IR (KIR), sorbitol (SOR), croscarmellose sodium (CCS)).

Mixture	Printing/printbed temperature [°C]	Photo
PAR-SOR60%-CCS20% E_CAB10%_AER0.2%	180/35	
PAR-SOR60%-CCS20% E_CAB20%_AER0.2%	180/35	
KIR-SOR60%-CCS20% E_CAB10%_AER0.2%	180/30	
KIR-SOR60%-CCS20% E_CAB20%_AER0.2%	180/30	

corresponding printing temperatures in Table 6.

Measurements of the outer shape of each tablet were used to check for deviations in the printing process from the CAD design. While height and length were achieved very well, the tablets lacked some width during printing of the 20 % CAB formulation. Low standard deviations were achieved for the mass of the printed tablets. Results are shown in Fig. S12.

3.2.2. Melt rheology

The apparent shear rate was determined for both final formulations while printing 130 and 140 mg tablets. Due to their longer print time, the error in the determination of printing time and revolutions is expected to be lower. Despite differences in the print speed (PAR with 3.8 mm/s vs KIR with 4.5 mm/s), the determined shear rates for both formulations were found to be close. For the final formulations, the influence of different concentrations of the flow agent AER and the addition of CAB was determined additionally. Results of all rheological experiments can be found in the supplementary section (Figs. S10 and S11). Fig. 3 shows the most important results, being the curves obtained from neat polymers in comparison to the final formulations containing 10 % or 20 % CAB.

Generally speaking, the viscosity of a polymer depends on the molecular weight and the interactions between the polymer strands. While PVA is a linear strand, the degree of saponification and the overall length are decisive for its viscosity. This is why, for the characterization of different PVA types, the viscosity of a solution and degree of hydrolysis are given. PAR used here has a degree of hydrolysis of 87 % and a
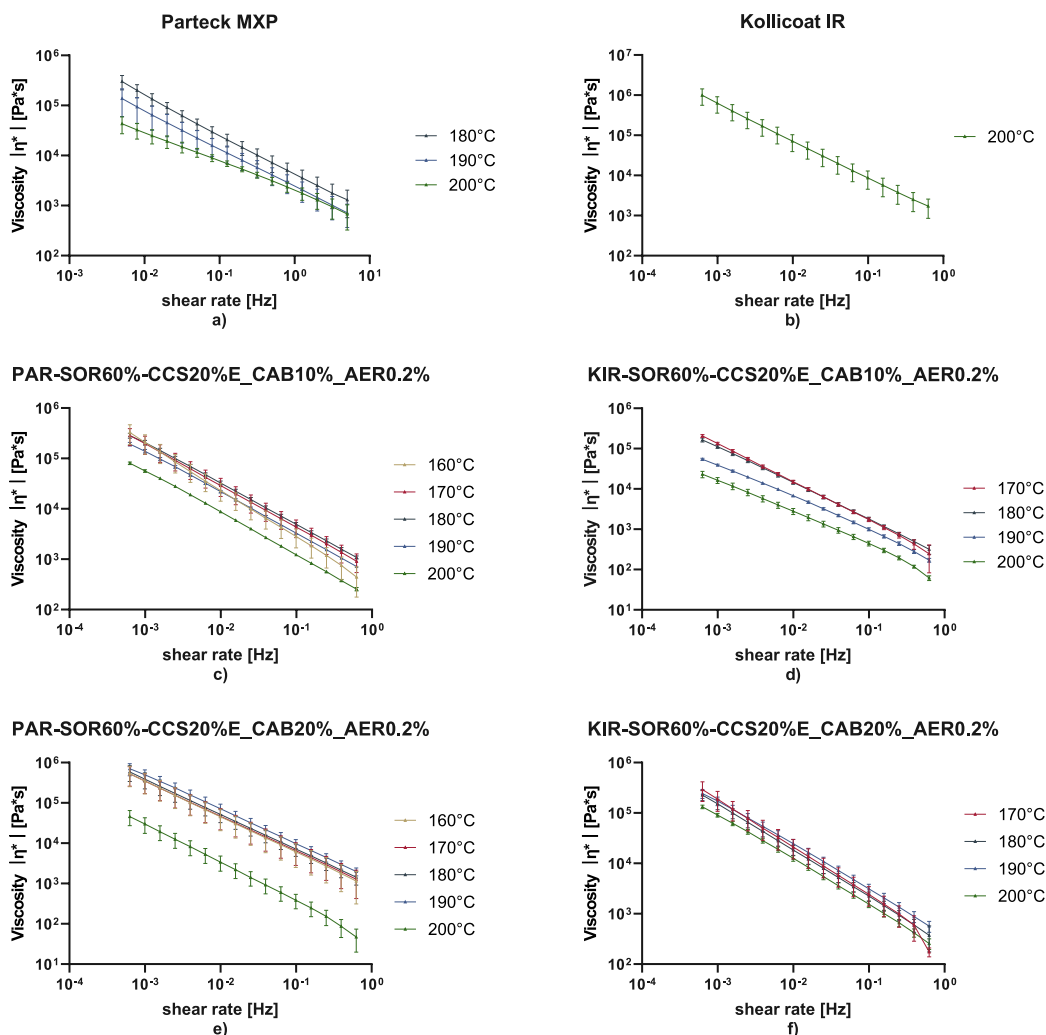
Fig. 3. Melt rheology results of neat polymers and final formulations thereof (n = 4 ± SD) (Parteck MXP (PAR), Kollicoat IR (KIR), sorbitol (SOR), croscarmellose sodium (CCS)).

viscosity of a 4 %-solution of 4.4 mPa*s. The formation of hydrogen bonds from the alcohol groups adds a significant amount to the overall viscosity. Conversely, KIR is a graft-copolymer consisting of polyvinyl and polyethyleneglycol (PEG) groups. From the structure of the polymers, the viscosity of KIR is expected to be lower than that of PAR. This is due to the reduced interactions PEG forms, compared to PVA. Also, the rigidity of the strand is weakened by the PEG groups. Finally, for KIR, the molecular weight of the strand also impacts the final viscosity and leads to the measured data [60].

Neat polymers showed shear thinning as well as a temperature-dependent decrease in melt viscosity. At the same temperature, KIR b) exhibited a higher viscosity than PAR a). This was not the case after the addition of CAB. For PAR-based formulations, 160–190 °C showed no significant difference in the viscosity with overall higher viscosities than before the addition c) and e). KIR-based formulations showed a similar trend. The addition of 10 % CAB led to a decreased temperature dependency d) and with a further increase to 20 % CAB there was no significant difference found between measured viscosities at 170–200 °C f). These findings are expected to be made due to the melting of CAB in this range (melting point depression was observed in the DSC; Table 7 (158°-174°)). To make sure, that the changes can be associated with the addition of CAB and are not an effect of the addition of AER, experiments were conducted with the same formulation but without the CAB. Results showed, that neither the increase in overall viscosity nor the reduction in temperature dependence could be attributed to the addition of AER

Table 7
DSC-results of neat substances.

Formulation	First Heating		Second Heating	
	Onset [°C]	Offset [°C]	Onset [°C]	Offset [°C]
Parteck MXP	49.27	53.59	62.15	72.79
Kollicoat IR			Partially crystalline: M_P: 202.29 °C	
Sorbitol	crystalline, M_P: 95.04 °C		−2.60	1.51
Cabozantinib	crystalline, M_P: 182.92 °C		125.79	143.55
Crosscarmellose Sodium	Peak range: 72.52–185.73 °C		−	−

(Figs. S10 and S11). Literature indicates that, for hot melt extrusion processes viscosities between 100,000 and 10,000 Pa*s can be found [61]. In this work, much lower viscosities were found to be sufficient for 3D printing, where layer adhesion plays a more important role than just pure extrusion. Looking at the higher shear rate found at the nozzle wall (7–9 1/s), even lower viscosities can be expected. We were not able to measure these shear rates with the SAOS experiments, since they are outside of the LVR. For layer adhesion, the behavior of a viscous or visco-elastic liquid can be expected for many thermoplastic polymers used in 3D printing [62]. Thus measurements inside the LVR can not properly display the viscosity at potentially free-flowing conditions.

3.2.3. Results of thermal analysis using DSC

Pure substances as well as powdered mixtures and printed tablets were evaluated for their melting as well as glass transition temperatures. Table 7 shows the results of melting point (M_p) and glass transition temperatures (T_g) of neat substances. In the first heating cycle, the occurrence of a melting peak of CAB was observed. In the second heating cycle, the thermal history of the samples is erased, CAB can dissolve into the mixture and thus was used to determine the T_g of the mixtures. All curves can be found in the supplementary section (Figs. S4 and S9).

PAR and KIR both show properties of semicrystalline substances, as expected. While PAR has a visible T_g, KIR has a much less pronounced glass transition, overlayed with other thermal events. This is in line with findings from the literature, reports on the T_g can be found [63,64]. The melting point of CAB can be found in the literature and is reported as 166–169 °C [64,65]. A slightly higher melting point was found in our studies. CCS shows a huge peak with an onset at 72.52 °C going up to 185.73 °C. This can only be seen during the first heating and looking also at the STA measurements it can be attributed to water loss. Table 8 shows the results of the powdered mixtures and printed tablets.

Melting points of CAB can be found in all the powdered samples, that contain CAB, which shows sufficient sensitivity of the method. In the PAR-based tablets, no melting peak could be observed, while in the KIR-based tablets, there were traces of crystalline CAB found. This indicates a higher solubility of CAB in PAR at least at elevated temperatures. In the curves another thermal event at 60–90 °C can regularly be found. This seems to be the partial melting of recrystallized SOR. The recrystallization of both CAB and SOR does not happen instantly, as can be seen in the second heating cycle. No melting of either CAB or SOR can be found and only one glass transition can be detected there. T_g increases with the addition of CAB. The change in T_g, from the mixtures containing no CAB (5–25 °C) and containing CAB (10–40 °C) is in line with the expectation of miscibility since CAB has higher T_g (125–143 °C). The complex T_g is expected to be found between the T_gs of individual substances [66].

3.2.4. Results of thermal stability using STA

To gather information regarding water uptake during printing or storage and on the thermal stability of substances their mass loss during heating was measured. Fig. 4 shows the results of STA measurements.

STA results show no significant mass loss for KIR and SOR, while PAR shows around 1 % mass loss, which can be explained by solvent loss. As per the Safety Data Sheet, 1–3 % of residual methanol can be expected in PAR. CAB shows thermal stability up to 196 °C (onset temperature found in STA). CCS seems to show some water/solvent loss, which can be correlated to the peak found in the first heating cycle of DSC measurements. Printed mixtures comprising PAR show a mass loss of around 2 % while KIR-based formulations show no mass loss during heating. This mass loss was attributed to water uptake during printing and storage. As the literature shows, from experiments on the water vapor transmission rate it could be expected, that KIR would take up less water than PAR [67].

3.3. Physical state examination − XRD

Additional information about the physical state at room temperature was needed to confirm the data from DSC measurements. Results for pure substances can be found in Fig. 5a), while results for the powder and printed formulations containing 20 % CAB are given in Fig. 5b).

PAR and KIR show well-known patterns of partially crystalline polymers with a broad halo around 20°. CCS and AER show very little to no signal indicating a mostly or completely amorphous state. As expected, CAB and SOR show distinct patterns of crystalline substances in a range from 10 to 35°. In the powder samples, there were clear signs of crystalline CAB, which indicates that this method is suitable for detecting crystalline CAB in a powder mixture at given concentrations. These can be found especially in the double peak at 11-13° and in the peak at 24°. In the printed formulation these signs are less pronounced. In mixtures containing several potentially crystalline substances with varying degrees of crystallinity, it can be difficult to fully interpret results [68]. The aforementioned peaks were clearly visible in the powdered samples. While in the printed formulations a lower degree of crystallinity as well as a different pattern can be observed. This underlines the DSC results, showing that at least partial miscibility can be achieved, while SOR and in the KIR-based samples also some CAB seems to crystallize.

3.4. Confocal Raman microspectroscopy − CRM

In addition to XRD, a second method of non-destructive analysis of printed tablets CRM was employed. Spectra of pure substances are shown in Fig. 6. A distinct pattern of signals can be seen between 1200 and 1800 1/cm. Specific signals were detected at 1249, 1403, and 1606 1/cm, and the whole spectrum was used for the determination of CAB distribution in the tablets.

Fig. 7(a–h) shows the distribution and respective spectra obtained from the printed tablets based on PAR and KIR including 10 % or 20 % CAB. The distribution in the measured area is shown in the left hand of the spectra. An exemplary picture for understanding the area of measurement is given in the supplementary (Fig. S13). For each formulation one good spectrum (red colored in the distribution and one bad spectrum (blue colored in the distribution) is shown. A bad spectrum is characterized by a very low signal intensity and low signal–noise ratio. This is attributed to a failed autofocus on the surface of the tablet.

Spectra obtained from these large-area scans were evaluated using the spectral data of pure substances (Fig. 6) and the true component analysis. Results were color-coded to show the distribution of CAB in the tablets. Mainly high-quality spectra showing distinct CAB patterns were obtained. These are marked red in the color-coded images. In some places, autofocus failed to find the best spectrum possible (blue areas), while in other individual spectra, no CAB was visible (e.g. Fig. 7h)), with the latter occurring only very rarely. Indicated by the high proportion of red areas (good spectra with CAB signal), a mostly uniform distribution of CAB was shown nonetheless. No hotspots or coherent areas with

Table 8
DSC-results of PAR- and KIR-based formulations (Parteck MXP (PAR), Kollicoat IR (KIR), sorbitol (SOR), croscarmellose sodium (CCS)).

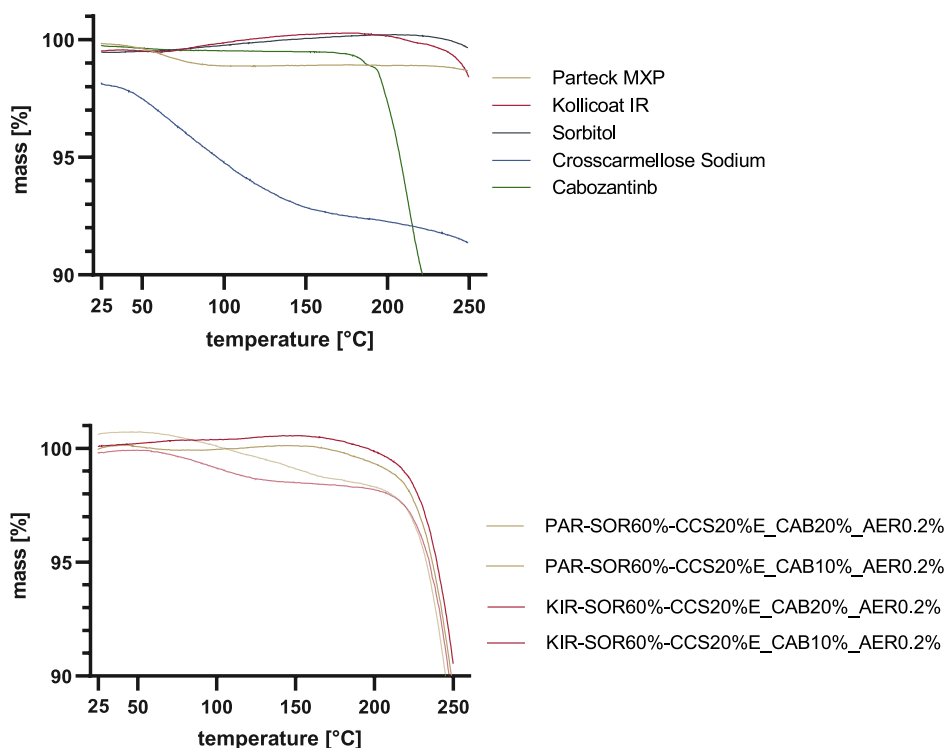|	M_p Cabozantinibfirst Heating [°C]	Glass transition second heating	
		Onset [°C]	Offset [°C]
PAR-SOR60%-CCS20%E powder	–	4.59	25.63
PAR-SOR60%-CCS20%E printed	–	5.89	26.36
PAR-SOR60%-CCS20%E CAB10% powder	166.88	10.49	30.74
PAR-SOR60%-CCS20%E CAB10% printed	–	11.44	30.70
PAR-SOR60%-CCS20%E CAB20% powder	174.05	12.29	33.00
PAR-SOR60%-CCS20%E CAB20% printed	–	14.59	33.32
KIR-SOR60%-CCS20%E powder	–	5.58	21.53
KIR-SOR60%-CCS20%E printed	–	5.56	21.30
KIR-SOR60%-CCS20%E CAB10% powder	158.29	16.96	10.51
KIR-SOR60%-CCS20%E CAB10% printed	170.24	5.38	24.30
KIR-SOR60%-CCS20%E CAB20% powder	174.56		
KIR-SOR60%-CCS20%E CAB20% printed	–	15.74	39.00

Fig. 4. STA-results (n = 3; mean) (Parteck MXP (PAR), Kollicoat IR (KIR), sorbitol (SOR), croscarmellose sodium (CCS)).
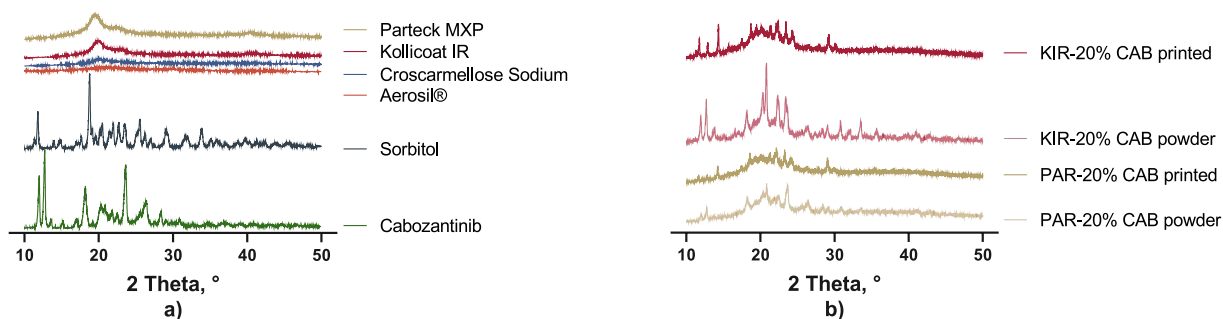

Fig. 5. XRD-results; a) pure substances; b) powdered and printed formulations containing 20% CAB (Parteck MXP (PAR), Kollicoat IR (KIR)).
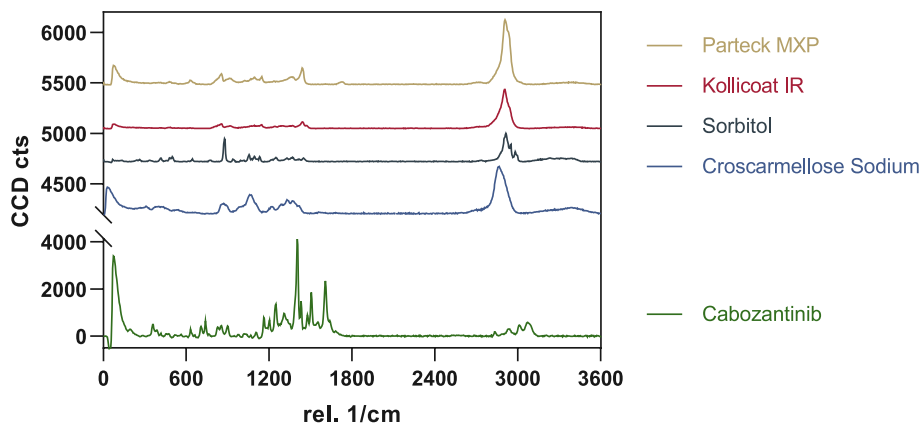

Fig. 6. Pure Raman spectra.

sufficient signal intensity and no CAB signal were found that would lead to the assumption, that CAB would not be dissolved homogeneously within the printed tablet. Crystalline material found in the XRD can thus

be mostly attributed to recrystallized SOR (as seen in DSC results), and the low amounts of recrystallized CAB found in KIR samples are expected to be smaller than the spatial resolution of the Raman device used
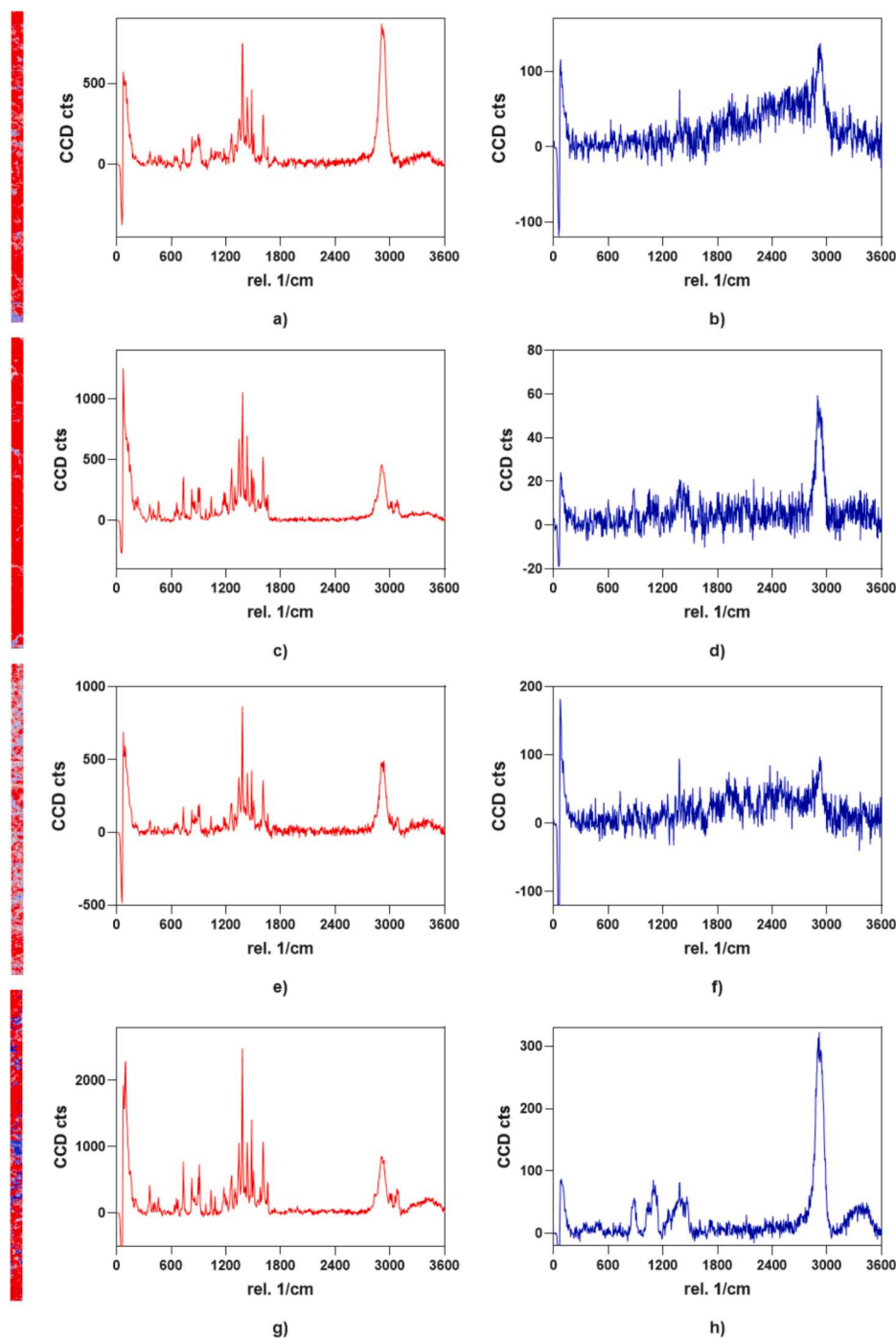
Fig. 7. left column "good spectra"(red), right column "bad spectra"(blue); a)+b) PAR-SOR60%-CCS20%E_CAB10%_AER0.2%; c)+d) KIR-SOR60%-CCS20% E_CAB10%_AER0.2%; e)+f) PAR-SOR60%-CCS20%E_CAB20%_AER0.2%; g)+h) KIR-SOR60%-CCS20%E_CAB20%_AER0.2%; left hand: color-coded distribution based of CAB-signal (Parteck MXP (PAR), Kollicoat IR (KIR), sorbitol (SOR), croscarmellose sodium (CCS))

(5 μm).

3.5 In-vitro dissolution

Non-porous tablets with varying dosages were investigated for their in-vitro release. As mentioned in the introduction clinically relevant dosages are found in between 20 and 140 mg. While commercially available tablets and capsules provide 20 mg steps in between, this work establishes formulations allowing for 10 mg and potentially even smaller stepsizes. Both KIR and PAR were tested by printing the same tablets using 10 % CAB for dosages 20–50 mg and 20 % CAB for 60–140

mg allowing for tablet sizes sufficient for patient handling. Fig. 8 shows the dissolution data of all dosages from both formulations.

PAR-based and KIR-based formulations both showed that distinct dosages can be printed by scaling the designed tablets. Despite the broad range of dosages covered, all of the tablets showed immediate release with usually a 100 % dissolution rate at 45 min as requested by many regulatory authorities [69]. KIR-based tablets showed slightly higher released dosages compared to PAR-based ones. This might be explained by a slightly higher density of the extrudate. The correctness of the obtained dosage can be controlled via the mass of the printed tablets and should be an in-line quality criterion for production in a clinical setting.
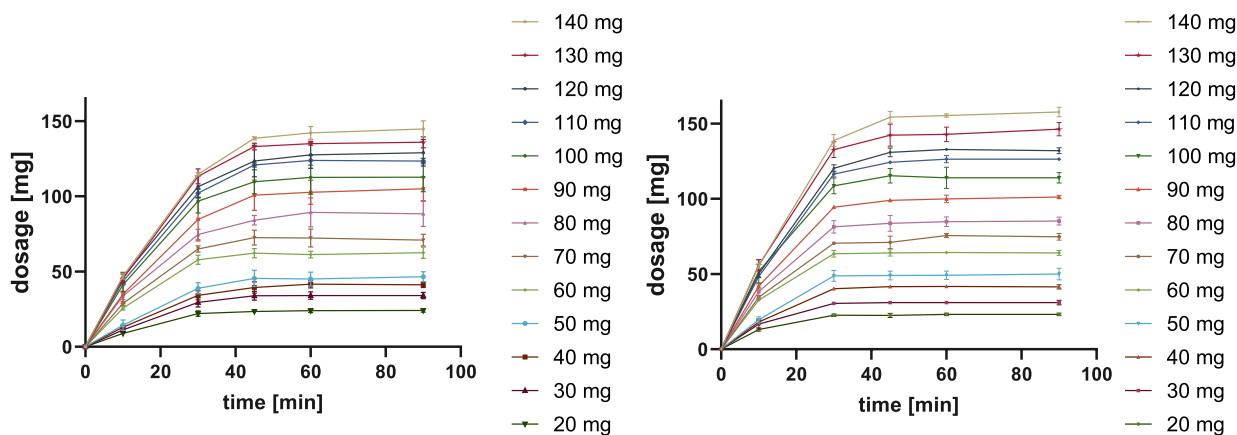
Fig. 8. Dissolution data for final formulations and each dosage (left: PAR-based; right: KIR-based), (n = 3 ± SD).

On the other hand, the standard deviation is smaller for KIR-based formulations, indicating a more uniform printing process.

Interestingly, there is no difference in the release pattern when comparing 10 % and 20 % CAB loading. For a tablet with completely amorphous drug this would not be expected. But as seen in XRD and DSC trials we must conclude that CAB is not fully amorphous in tablets with 20 % loading. We expect that during extruding and heating the mixture CAB got dispersed very evenly in the matrix, as we were able to show with the Raman measurements. During the mixture's cooldown, the matrix's reduced mobility leads to small crystals. The small crystal size results in a large surface area, one of the most important features enabling fast dissolution rates. Also, most of the CAB seems to be in an amorphous state, so only small amounts of crystalline API have to be dissolved.

4. Conclusion

The feasibility of incorporating varying amounts of SOR and superdisintegrants CCS and SSG into the hot-melt-extrusion-ready polymers PAR and KIR was successfully shown. The influence of these excipients on the dissolution rate of solid dosage forms was evaluated. Increasing amounts of highly hydrophilic and wettable substances can improve dissolution times even for badly soluble drugs. From the shown data it can be concluded, that an API such as CAB which is practically insoluble in water [70], can be formulated into immediate-release tablets covering the broad range of dosages which are clinically relevant (20 to 140 mg). Printing tablets of small doses is important for optimal therapy as studys have shown, that printing the desired dosage instead of subdividing tablets improves dosing precision. Thus, incorporation 3D printing in clinical settings can increase the safety of drug administration [71]. Dose individualization was achieved using extrusion and 3D printing techniques. Printing of CAB in a variety of polymer-based matrices was possible below its degradation temperature. The at least partially amorphous nature of the API and no particle sizes larger than 5 μm (spatial resolution of CRM device) were shown by the examination of printed tablets by DSC, XRD, and CRM.

Formulations with very different dissolution profiles were developed along the search for one, that enables immediate release. Formulating tablets with immediate release is an important step for 3D printed tablets from an extrusion process such as DPE, since with the polymers used it is much easier to produce tablets with sustained release [72]. While there are similar examples of dosage personalization in the literature [73], the proposed way of calculating the tablets dimensions is novel. The developed formulations can be used if researchers are looking for starting points for formulations with prolonged release. Depending on the solubility and percentage of API used, changes in SOR and CCS amount might also be needed.

Additionally, data was evaluated to underline the importance of melt rheology for extrusion processes. The rheology of the mixtures as well as of the final formulations showed the influence of different excipients on the temperature dependency of the viscosity, most importantly the melting point of the API. It was shown, that for similar formulations the melt viscosity can be indicative of temperatures required for printing, but there needs to be some common ground of excipients and printer setups to make valid assumptions from these data for the development of ready-to-print formulations.

Looking into the future of 3D printing applications in the pharmaceutical industry and clinic settings it is not evident which of the techniques could come up on top. Each of the methods has its own pros and cons and currently only medical devices are covered by the guidelines for 3D printing issued by the FDA [74,75]. Until there are clear regulatory requirements scientists will have to push the limits of quality standards and understanding of good manufacturing practices to deliver the groundwork for secure implementation of 3D printing of pharmaceuticals.

For approval of the 3D printed tablets, the existence of bioequivalence with the marketed product would need to be shown. Regarding this aspect, there are challenges in showing therapeutic equivalence even if pharmaceutical equivalence is given [76]. This can be shown easily when looking at the comparison data from the tablet and capsule formulation provided by the original manufacturer. The difference in these formulations is the kind of CAB salt being used and the dosage form. Bioequivalence studies were not able to show sufficient bioequivalence at currently used standards even while providing "comparable extents of plasma exposure" [77]. Therefore, the therapeutic equivalence of the 3D printed tablets would be the more useful approach if marketing authorization was sought for. For the time being, the manufacture of individualized 3D printed dosage forms remains in the hands of pharmacists working at hospital pharmacies, preparing formulations upon individual prescriptions by a practitioner. Thus, no market authorization is required. Still, in this setting good manufacturing practice (GMP) conformity of materials and printers is required. To this day access to these and information regarding achieving qualification is limited. Additionally, personnel need to be trained to operate the printers and receive the knowledge currently generated under lab-conditions [72].

Funding

CRediT authorship contribution statement

Jonas Lenhart: Writing – original draft, Methodology, Investigation, Data curation, Conceptualization. **Dominique J. Lunter:** Writing – review & editing, Supervision, Project administration, Conceptualization.

Declaration of Competing Interest

The authors declare that they have no known competing financial interests or personal relationships that could have appeared to influence the work reported in this paper.

Data availability

The data that has been used is confidential.

Acknowledgement

Appendix A. Supplementary data

Supplementary data to this article can be found online at https://doi.org/10.1016/j.ejpb.2024.114501.

References

[1] T.G.B. West, J. Thomas, 3D Printing: A Case of ZipDose® Technology - World's First 3D Printing Platform to Obtain FDA Approval for a Pharmaceutical Product, 2019, doi: 10.1002/9783527813704.ch3.

[2] Y. Zheng, F. Deng, B. Wang, Y. Wu, Q. Luo, X. Zuo, X. Liu, L. Cao, M. Li, H. Lu, et al., Melt extrusion deposition (MED) 3D printing technology - A paradigm shift in design and development of modified release drug products, Int. J. Pharm. 602 (2021) 120639, https://doi.org/10.1016/j.ijpharm.2021.120639.

[3] B.M. Boyle, P.T. Xiong, T.E. Mensch, T.J. Werder, G.M. Miyake, 3D printing using powder melt extrusion, Addit. Manuf. 29 (2019), https://doi.org/10.1016/j.addma.2019.100811.

[4] J. Boniatti, P. Januskaite, L.B.D. Fonseca, A.L. Vicosa, F.C. Amendoeira, C. Tuleu, A.W. Basit, A. Goyanes, M.I. Re, Direct powder extrusion 3D printing of praziquantel to overcome neglected disease formulation challenges in paediatric populations, Pharmaceutics 13 (2021), https://doi.org/10.3390/pharmaceutics13081114.

[5] A. Goyanes, N. Allahham, S.J. Trenfield, E. Stoyanov, S. Gaisford, A.W. Basit, Direct powder extrusion 3D printing: fabrication of drug products using a novel single-step process, Int. J. Pharm. 567 (2019) 118471, https://doi.org/10.1016/j.ijpharm.2019.118471.

[6] A.W.T. Basit, J. Sarah, 3D printing of pharmaceuticals and the role of pharmacy, Pharmaceut. J. (2022), https://doi.org/10.1211/pj.2022.1.135581.

[7] A. Goyanes, M. Scarpa, M. Kamlow, S. Gaisford, A.W. Basit, M. Orlu, Patient acceptability of 3D printed medicines, Int. J. Pharm. 530 (2017) 71–78, https://doi.org/10.1016/j.ijpharm.2017.07.064.

[8] G. Kollamaram, D.M. Croker, G.M. Walker, A. Goyanes, A.W. Basit, S. Gaisford, Low temperature fused deposition modeling (FDM) 3D printing of thermolabile drugs, Int. J. Pharm. 545 (2018) 144–152, https://doi.org/10.1016/j.ijpharm.2018.04.055.

[9] H. Windolf, R. Chamberlain, J. Quodbach, Predicting drug release from 3D printed oral medicines based on the surface area to volume ratio of tablet geometry, Pharmaceutics (2021) 13, https://doi.org/10.3390/pharmaceutics13091453.

[10] M. Sadia, B. Arafat, W. Ahmed, R.T. Forbes, M.A. Alhnan, Channelled tablets: an innovative approach to accelerating drug release from 3D printed tablets, J. Control. Release 269 (2018) 355–363, https://doi.org/10.1016/j.jconrel.2017.11.022.

[11] C.I. Gioumouxouzis, A. Baklavaridis, O.L. Katsamenis, C.K. Markopoulou, N. Bouropoulos, D. Tzetzis, D.G. Fatouros, A 3D printed bilayer oral solid dosage form combining metformin for prolonged and glimepiride for immediate drug delivery, Eur. J. Pharm. Sci. 120 (2018) 40–52, https://doi.org/10.1016/j.ejps.2018.04.020.

[12] S.A. Khaled, J.C. Burley, M.R. Alexander, C.J. Roberts, Desktop 3D printing of controlled release pharmaceutical bilayer tablets, Int. J. Pharm. 461 (2014) 105–111, https://doi.org/10.1016/j.ijpharm.2013.11.021.

[13] A. Goyanes, A.B. Buanz, A.W. Basit, S. Gaisford, Fused-filament 3D printing (3DP) for fabrication of tablets, Int. J. Pharm. 476 (2014) 88–92, https://doi.org/10.1016/j.ijpharm.2014.09.044.

[14] N. Schulz, Personalised Medicine: The right Treatment for the Right Person at the Right Time, 2015.

[15] G.D. Anderson, Gender differences in pharmacological response, Int. Rev. Neurobiol. 83 (2008) 1–10, https://doi.org/10.1016/S0074-7742(08)00001-9.

[16] S.C. McLeay, G.A. Morrish, C.M. Kirkpatrick, B. Green, The relationship between drug clearance and body size: systematic review and meta-analysis of the literature published from 2000 to 2007, Clin. Pharmacokinet. 51 (2012) 319–330, https://doi.org/10.2165/11598930-000000000-00000.

[17] N. Ware, The role of genetics in drug dosing, Pediatr. Nephrol. 27 (2012) 1489–1498, https://doi.org/10.1007/s00467-012-2105-0.

[18] P.Y. Muller, M.N. Milton, The determination and interpretation of the therapeutic index in drug development, Nat. Rev. Drug Discov. 11 (2012) 751–761, https://doi.org/10.1038/nrd3801.

[19] P. Maroto, C. Porta, J. Capdevila, A.B. Apolo, S. Viteri, C. Rodriguez-Antona, L. Martin, D. Castellano, Cabozantinib for the treatment of solid tumors: a systematic review, Ther Adv Med Oncol 14 (2022) 17588359221107112, https://doi.org/10.1177/17588359221107112.

[20] S. Osanto, T. van der Hulle, Cabozantinib in the treatment of advanced renal cell carcinoma in adults following prior vascular endothelial growth factor targeted therapy: clinical trial evidence and experience, Ther. Adv. Urol. 10 (2018) 109–123, https://doi.org/10.1177/1756287217748867.

[21] L. Zhou, X.D. Liu, M. Sun, X. Zhang, P. German, S. Bai, Z. Ding, N. Tannir, C. G. Wood, S.F. Matin, et al., Targeting MET and AXL overcomes resistance to sunitinib therapy in renal cell carcinoma, Oncogene 35 (2016) 2687–2697, https://doi.org/10.1038/onc.2015.343.

[22] CHMP, Cometriq, INN-cabozantinib.

[23] CHMP, Cabometyx, INN-Cabozantinib.

[24] J.H. McElwee, T.S. Gourdin, J. Mikoll, E. Weeda, A.M. Sion, Cabozantinib use in metastatic renal cell carcinoma patients in clinical practice: evaluation of dosing patterns, tolerability, and outcomes compared to clinical trials, J. Oncol. Pharm. Pract. 26 (2020) 861–865, https://doi.org/10.1177/1078155219875509.

[25] S.I. Sherman, E.E.W. Cohen, P. Schoffski, R. Elisei, M. Schlumberger, L.J. Wirth, M. Mangeshkar, D.T. Aftab, D.O. Clary, M.S. Brose, Efficacy of cabozantinib (Cabo) in medullary thyroid cancer (MTC) patients with RAS or RET mutations: results from a phase III study, J. Clin. Oncol. 31 (2013), https://doi.org/10.1200/jco.2013.31.15_suppl.6000.

[26] P. Tappenden, C. Carroll, J. Hamilton, E. Kaltenthaler, R. Wong, J. Wadsley, L. Moss, S. Balasubramanian, Cabozantinib and vandetanib for unresectable locally advanced or metastatic medullary thyroid cancer: a systematic review and economic model, Health Technol. Assess. 23 (2019) 1–144, https://doi.org/10.3310/hta23080.

[27] IpsenPharma, Fachinformation COMETRIQ® 20 mg/80 mg Hartkapseln, 2022.

[28] IpsenPharma, Fachinformation Cabometyx® (20 mg/40 mg/60 mg Filmtabletten), 2022.

[29] P. Dylst, A. Vulto, S. Simoens, Societal value of generic medicines beyond cost-saving through reduced prices, Expert Rev. Pharmacoecon. Outcomes Res. 15 (2015) 701–711, https://doi.org/10.1586/14737167.2015.1017565.

[30] P.E. Girish Malhotra, Comparison of drugs prices: US vs. India; their manufacturing costs and opportunities to improve affordability, Am. Pharmaceut. Rev. (2018).

[31] H.V. Chavda, C.N. Patel, I.S. Anand, Biopharmaceutics classification system, Sys. Rev. Pharm. (2010) 1, https://doi.org/10.4103/0975-8453.59514.

[32] M. Stefinovic, E.P. Schreiner, Cabozantinib Salts and their Use as Anti-Cancer Agents. 10,206,916, 2019.

[33] A.A. Noyes, W.R. Whitney, The rate of solution of solid substances in their own solutions, J. Am. Chem. Soc. 19 (2002) 930–934, https://doi.org/10.1021/ja02086a003.

[34] W. Nernst, Theorie der Reaktionsgeschwindigkeit in heterogenen Systemen, Z. Phys. Chem. 47U (1904) 52–55, https://doi.org/10.1515/zpch-1904-4704.

[35] D. Horter, J.B. Dressman, Influence of physicochemical properties on dissolution of drugs in the gastrointestinal tract, Adv. Drug Deliv. Rev. 46 (2001) 75–87, https://doi.org/10.1016/s0169-409x(00)00130-7.

[36] S. Kumar, D. Bhargava, A. Thakkar, S. Arora, Drug carrier systems for solubility enhancement of BCS class II drugs: a critical review, Crit. Rev. Ther. Drug Carrier Syst. 30 (2013) 217–256, https://doi.org/10.1615/critrevtherdrugcarriersyst.2013005964.

[37] FDA, Drug database; Dissolution methods, Available online: https://www.accessdata.fda.gov/scripts/cder/dissolution/ (accessed on).

[38] H. Tian, D. Liu, Y. Yao, S. Ma, X. Zhang, A. Xiang, Effect of sorbitol plasticizer on the structure and properties of melt processed polyvinyl alcohol films, J. Food Sci. 82 (2017) 2926–2932, https://doi.org/10.1111/1750-3841.13950.

[39] E.A. Fouad, M. El-Badry, S.H. Neau, F.K. Alanazi, I.A. Alsarra, Technology evaluation: Kollicoat IR, Expert Opin. Drug Deliv. 8 (2011) 693–703, https://doi.org/10.1517/17425247.2011.566266.

[40] J. Lenhart, F. Pöstges, K.G. Wagner, D.J. Lunter, Evaluation of printability of PVA-based tablets from powder and assessment of critical rheological parameters, Pharmaceutics (2024) 16, https://doi.org/10.3390/pharmaceutics16040553.

[41] M. Duranovic, M. Madzarevic, B. Ivkovic, S. Ibric, S. Cvijic, The evaluation of the effect of different superdisintegrants on the drug release from FDM 3D printed tablets through different applied strategies: in vitro-in silico assessment, Int. J. Pharm. 610 (2021) 121194, https://doi.org/10.1016/j.ijpharm.2021.121194.

[42] S. Omari, E.A. Ashour, R. Elkanayati, M. Alyahya, M. Almutairi, M.A. Repka, Formulation development of loratadine immediate- release tablets using hot-melt extrusion and 3D printing technology, J. Drug Delivery Sci. Technol. (2022) 74, https://doi.org/10.1016/j.jddst.2022.103505.

[43] R. Chandrasekar, V. Prudhvi Raj, S. Shaik, Formulation development and invitro evaluation of gliclazide pellets using superdisintegrants by extrusion

spheronization technique, Int. J. Pharmaceut. Sci. Nanotechnol. (IJPSN) 16 (6266–6280) (2023), https://doi.org/10.37285/ijpsn.2023.16.1.2.

[44] A. Hussain, F. Mahmood, M.S. Arshad, N. Abbas, N. Qamar, J. Mudassir, S. Farhaj, J.S. Nirwan, M.U. Ghori, Personalised 3D printed fast-dissolving tablets for managing hypertensive crisis: in-vitro/in-vivo studies, Polymers (Basel) (2020) 12, https://doi.org/10.3390/polym12123057.

[45] G.G. Pereira, S. Figueiredo, A.I. Fernandes, J.F. Pinto, Polymer selection for hot-melt extrusion coupled to fused deposition modelling in pharmaceutics, Pharmaceutics (2020) 12, https://doi.org/10.3390/pharmaceutics12090795.

[46] A.G. Crisan, A. Porfire, R. Ambrus, G. Katona, L.M. Rus, A.S. Porav, K. Ilyes, I. Tomuta, Polyvinyl alcohol-based 3D printed tablets: novel insight into the influence of polymer particle size on filament preparation and drug release performance, Pharmaceuticals (Basel) (2021) 14, https://doi.org/10.3390/ph14050418.

[47] N.G. Solanki, M. Tahsin, A.V. Shah, A.T.M. Serajuddin, Formulation of 3D printed tablet for rapid drug release by fused deposition modeling: screening polymers for drug release, drug-polymer miscibility and printability, J. Pharm. Sci. 107 (2018) 390–401, https://doi.org/10.1016/j.xphs.2017.10.021.

[48] K. Kabeya, H. Satoh, S. Hori, Y. Miura, Y. Sawada, Threshold size of medical tablets and capsules: based on information collected by japanese medical wholesaler, Patient Prefer. Adherence 14 (2020) 1251–1258, https://doi.org/10.2147/PPA.S253663.

[49] FDA, Guidance for industry: Size, Shape, and Other Physical Attributes of Generic Tablet and Capsules, 2015.

[50] D. Treffer, A. Troiss, J. Khinast, A novel tool to standardize rheology testing of molten polymers for pharmaceutical applications, Int. J. Pharm. 495 (2015) 474–481, https://doi.org/10.1016/j.ijpharm.2015.09.001.

[51] M. Elbadawi, T. Gustafsson, S. Gaisford, A.W. Basit, 3D printing tablets: predicting printability and drug dissolution from rheological data, Int. J. Pharm. 590 (2020) 119868, https://doi.org/10.1016/j.ijpharm.2020.119868.

[52] J. Aho, J.P. Boetker, S. Baldursdottir, J. Rantanen, Rheology as a tool for evaluation of melt processability of innovative dosage forms, Int. J. Pharm. 494 (2015) 623–642, https://doi.org/10.1016/j.ijpharm.2015.02.009.

[53] D. Dimonie, N. Dragomir, Melt rheology of renewable polymers and of new materials based on them as tool in controlling the 3D/4D printability, Materiale Plastice 57 (2021) 77–87, https://doi.org/10.37358/mp.20.4.5408.

[54] T. Pflieger, R. Venkatesh, M. Dachtler, K. Eggenreich, S. Laufer, D. Lunter, Novel approach to pharmaceutical 3D-printing omitting the need for filament-investigation of materials, process, and product characteristics, Pharmaceutics (2022) 14, https://doi.org/10.3390/pharmaceutics14112488.

[55] J. Boetker, J.J. Water, J. Aho, L. Arnfast, A. Bohr, J. Rantanen, Modifying release characteristics from 3D printed drug-eluting products, Eur. J. Pharm. Sci. 90 (2016) 47–52, https://doi.org/10.1016/j.ejps.2016.03.013.

[56] C. Rauwendaal, Polymer extrusion; Carl Hanser Verlag GmbH Co KG.: Carl Hanser Verlag GmbH Co KG., 2014.

[57] Y. Jaluria, Heat and mass transfer in the extrusion of non-newtonian materials, in: Transport Phenomena in Materials Processing; Advances in Heat Transfer, 1996, pp. 145–230.

[58] E.M. Agency, ICH Topic Q 2 (R1) Validation of Analytical Procedures: Text and Methodology, Available online: https://www.ema.europa.eu/en/ich-q2r2-validation-analytical-procedures-scientific-guideline (accessed on 30 March).

[59] B. Arafat, M. Wojsz, A. Isreb, R.T. Forbes, M. Isreb, W. Ahmed, T. Arafat, M. A. Alhnan, Tablet fragmentation without a disintegrant: a novel design approach for accelerating disintegration and drug release from 3D printed cellulosic tablets, Eur. J. Pharm. Sci. 118 (2018) 191–199, https://doi.org/10.1016/j.ejps.2018.03.019.

[60] J.R. Fried, Polymer Science and Technology, Pearson Education:, 2014.

[61] J.S. LaFountaine, J.W. McGinity, R.O. Williams 3rd., Challenges and strategies in thermal processing of amorphous solid dispersions: a review, AAPS PharmSciTech 17 (2016) 43–55, https://doi.org/10.1208/s12249-015-0393-y.

[62] C. Duty, C. Ajinjeru, V. Kishore, B. Compton, N. Hmeidat, X. Chen, P. Liu, A. A. Hassen, J. Lindahl, V. Kunc, What makes a material printable? A viscoelastic model for extrusion-based 3D printing of polymers, J. Manufact. Process. 35 (2018) 526–537, https://doi.org/10.1016/j.jmapro.2018.08.008.

[63] S. Guns, P. Kayaert, J.A. Martens, J. Van Humbeeck, V. Mathot, T. Pijpers, E. Zhuravlev, C. Schick, G. Van den Mooter, Characterization of the copolymer poly (ethyleneglycol-g-vinylalcohol) as a potential carrier in the formulation of solid dispersions, Eur. J. Pharm. Biopharm. 74 (2010) 239–247, https://doi.org/10.1016/j.ejpb.2009.09.009.

[64] I. Partheniadis, M. Toskas, F.M. Stavras, G. Menexes, I. Nikolakakis, Impact of hot-melt-extrusion on solid-state properties of pharmaceutical polymers and classification using hierarchical cluster analysis, Processes (2020) 8, https://doi.org/10.3390/pr8101208.

[65] chemodex, Cabozantinib S-malate. Available online: https://www.chemodex.com/products/cabozantinib-s-malate/ (accessed on 08.04.2024).

[66] E.S. Bochmann, D. Neumann, A. Gryczke, K.G. Wagner, Micro-scale prediction method for API-solubility in polymeric matrices and process model for forming amorphous solid dispersion by hot-melt extrusion, Eur. J. Pharm. Biopharm. 107 (2016) 40–48, https://doi.org/10.1016/j.ejpb.2016.06.015.

[67] T.A. Chech, K. Kolter, Comparing Different Moisture Protective Instant Release Coatings for Solid Oral Dosage Forms, 2008.

[68] S. Thakral, M.W. Terban, N.K. Thakral, R. Suryanarayanan, Recent advances in the characterization of amorphous pharmaceuticals by X-ray diffractometry, Adv. Drug Deliv. Rev. 100 (2016) 183–193, https://doi.org/10.1016/j.addr.2015.12.013.

[69] D. Fortunato, Dissolution method development for immediate release solid oral dosage forms, Dissolut. Technol. 12 (2005) 12–14, https://doi.org/10.14227/dt120305p12.

[70] F. Shakeel, N. Haq, I.A. Alsarra, Equilibrium solubility determination, Hansen solubility parameters and solution thermodynamics of cabozantinib malate in different monosolvents of pharmaceutical importance, J. Mol. Liq. (2021) 324, https://doi.org/10.1016/j.molliq.2020.115146.

[71] Z. Zheng, J. Lv, W. Yang, X. Pi, W. Lin, W. Zhang, J. Pang, Y. Zeng, Z. Lv, et al., Preparation and application of subdivided tablets using 3D printing for precise hospital dispensing, Eur. J. Pharm. Sci. 149 (2020) 105293, https://doi.org/10.1016/j.ejps.2020.105293.

[72] D.R. Serrano, A. Kara, I. Yuste, F.C. Luciano, B. Ongoren, B.J. Anaya, G. Molina, L. Diez, B.I. Ramirez, I.O. Ramirez, et al., 3D printing technologies in personalized medicine, nanomedicines, and biopharmaceuticals, Pharmaceutics 15 (2023) 1, https://doi.org/10.3390/pharmaceutics15020313.

[73] K. Pietrzak, A. Isreb, M.A. Alhnan, A flexible-dose dispenser for immediate and extended release 3D printed tablets, Eur. J. Pharm. Biopharm. 96 (2015) 380–387, https://doi.org/10.1016/j.ejpb.2015.07.027.

[74] FDA, CDRH. 3D Printing Medical Devices at the Point of Care: Discussion Paper, 2021.

[75] B.G. Beitler, P.F. Abraham, A.R. Glennon, S.M. Tommasini, L.L. Lattanza, J. M. Morris, D.H. Wiznia, Interpretation of regulatory factors for 3D printing at hospitals and medical centers, or at the point of care, 3D Print Med. 8 (2022) 7, https://doi.org/10.1186/s41205-022-00134-y.

[76] R.K. Jalali, D. Rasaily, Generic drug and bioequivalence studies, in: Pharmaceutical Medicine and Translational Clinical Research, Academic Press, 2018, https://doi.org/10.1016/B978-0-12-802103-3.00021-3.

[77] L. Nguyen, N. Benrimoh, Y. Xie, E. Offman, S. Lacy, Pharmacokinetics of cabozantinib tablet and capsule formulations in healthy adults, Anticancer Drugs 27 (2016) 669–678, https://doi.org/10.1097/CAD.0000000000000366.
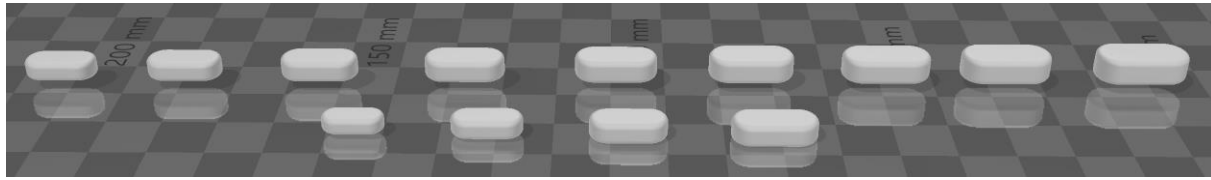
Supplementary

Figure S 1 .stl files of printed tablets from final formulations (upper row: 60-140 mg (fltr), lower row 20-50 mg)
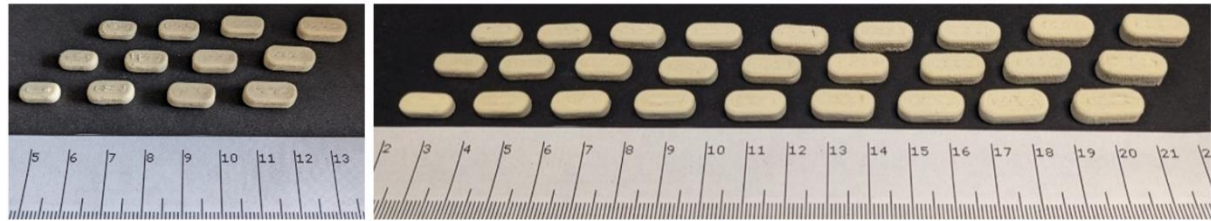
Figure S 2 pictures of printed tablets from PAR-SOR60%-CCS20%E; left 20-50 mg, right 60-140 mg

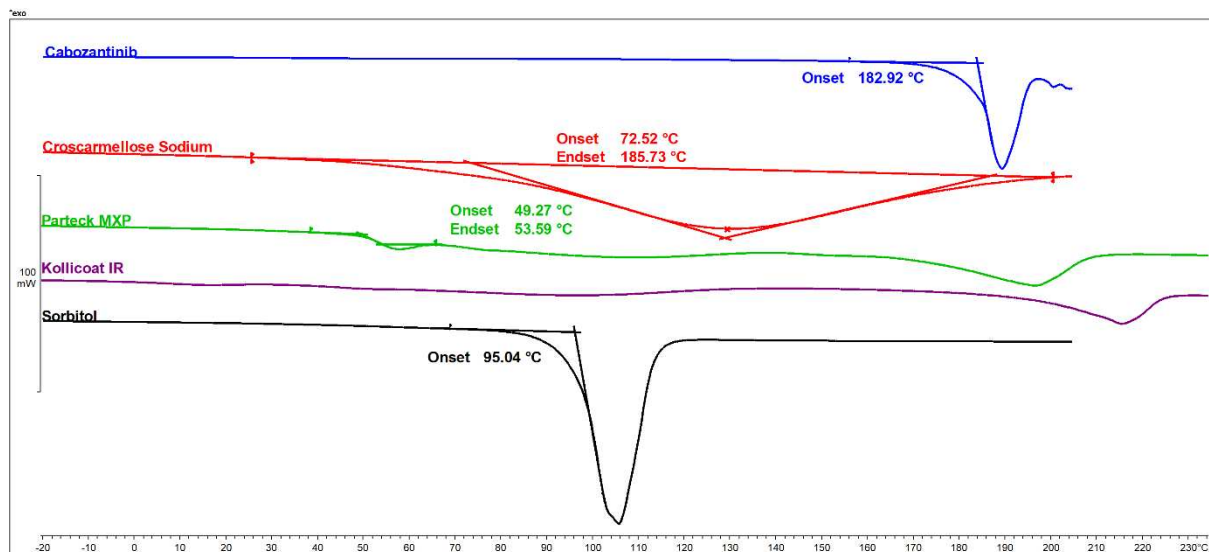Figure S 3 pictures of printed tablets from KIR-SOR60%-CCS20%E; left 20-50 mg, right 60-140 mg

Figure S 4 DSC: first heating of pure substances
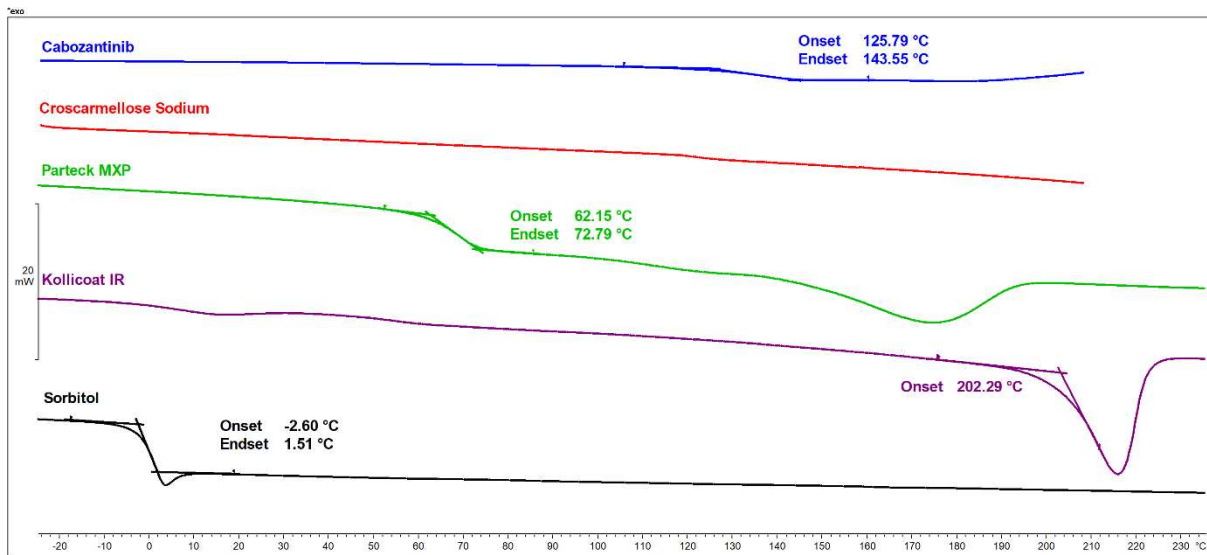
Figure S 5 DSC: second heating of pure substances
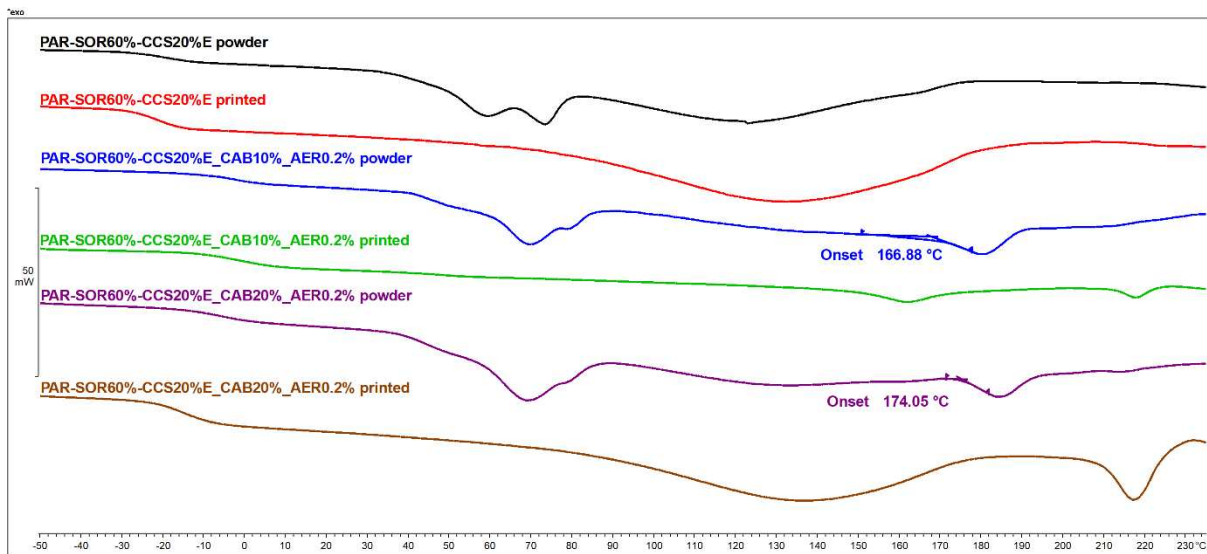
Figure S 6 DSC: fist heating of PAR-based formulations
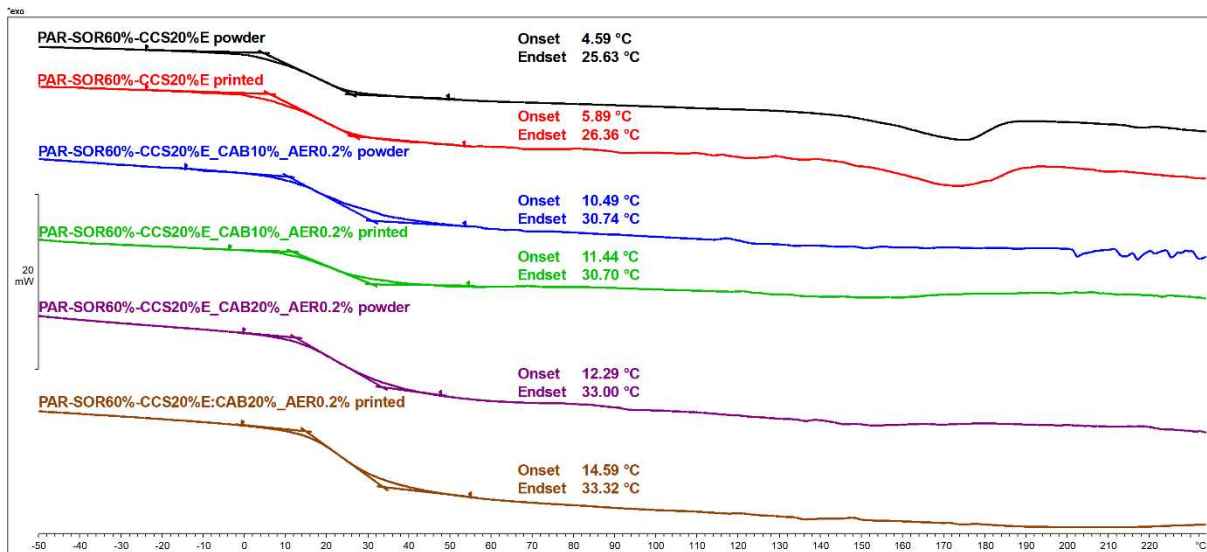
Figure S 7 DSC: second heating of PAR-based formulations
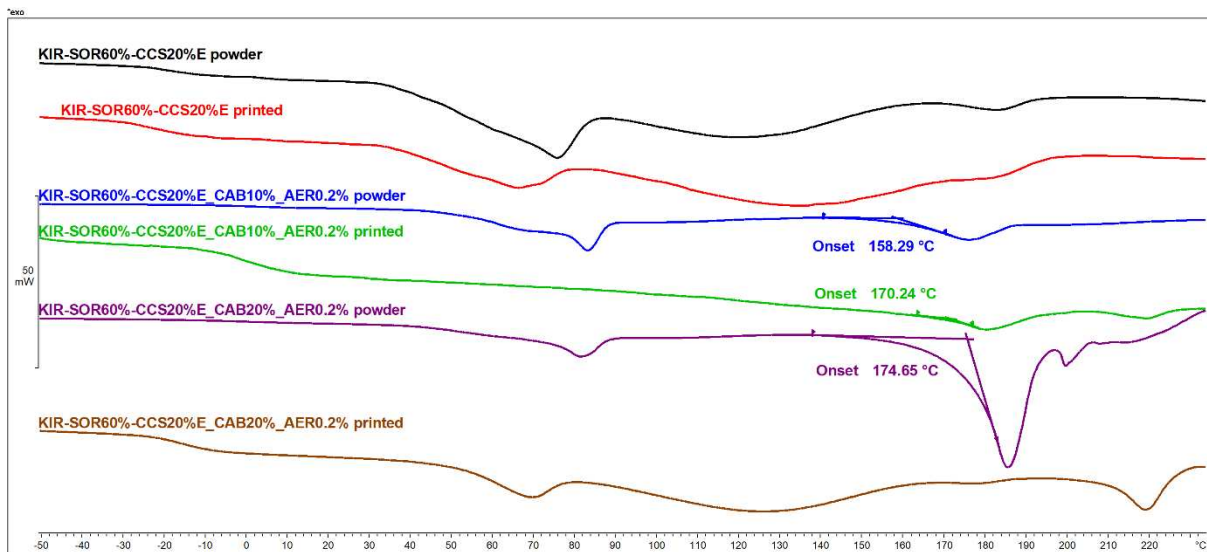
Figure S 8 DSC: first heating of KIR-based formulations

KIR-SOR60%-CCS20%E powder
Onset   5.58 °C
Endset 21.53 °C

KIR-SOR60%-CCS20%E printed
Onset   5.65 °C
Endset 21.30 °C

KIR-SOR60%-CCS20%E_CAB10%_AER0.2% powder
Onset   16.96 °C
Endset 40.51 °C

20 mW

KIR-SOR60%-CCS20%E_CAB10%_AER0.2% printed
Onset   5.38 °C
Endset 24.30 °C

KIR-SOR60%-CCS20%E_CAB20%_AER0.2% powder

KIR-SOR60%-CCS20%E_CAB20%_AER0.2% printed
Onset   15.74 °C
Endset 39.00 °C

Figure S 9 DSC: second heating of KIR-based formulations
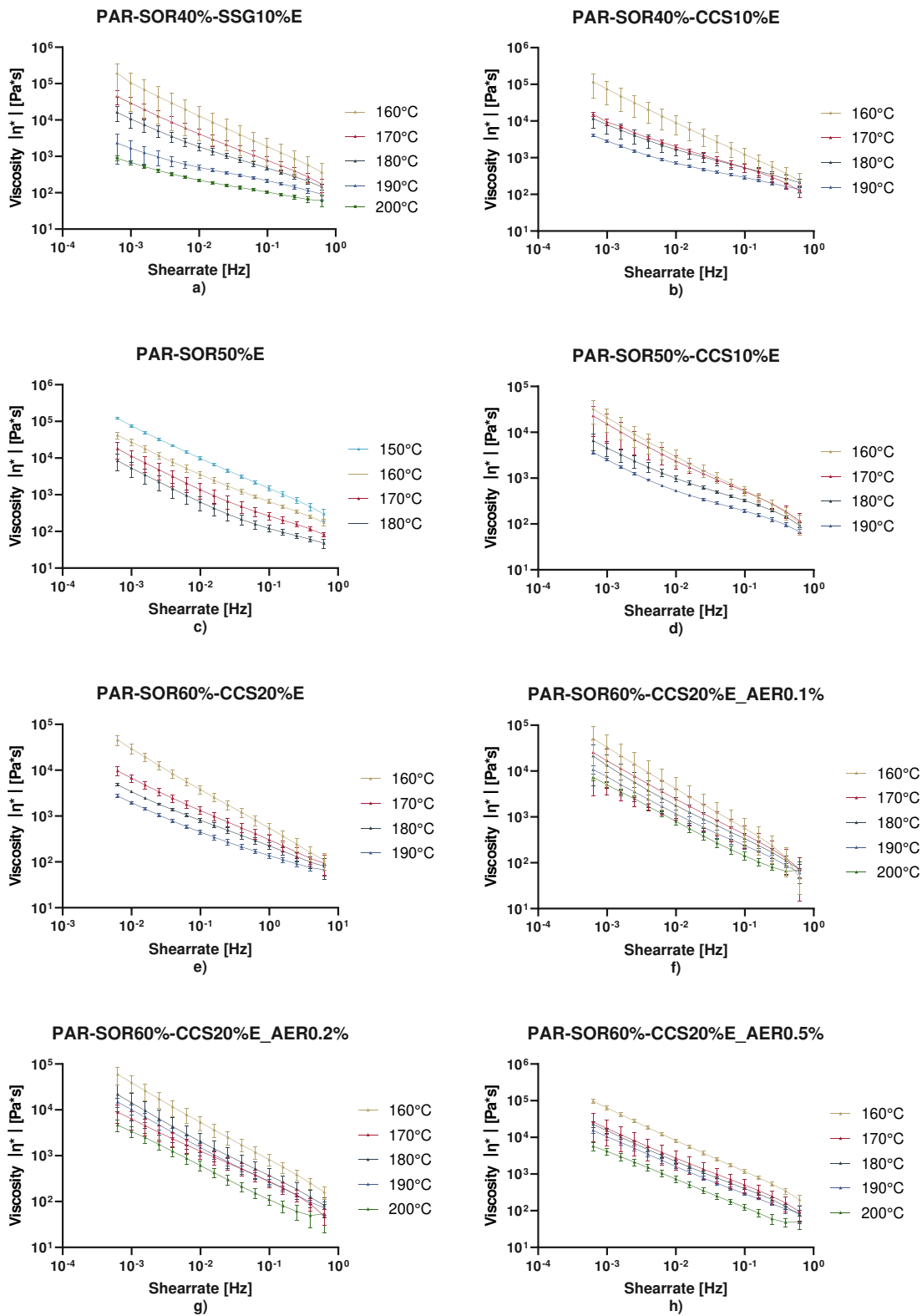
Figure S 10 melt rheology of formulation development and testing of AER influence on PAR-based formulations
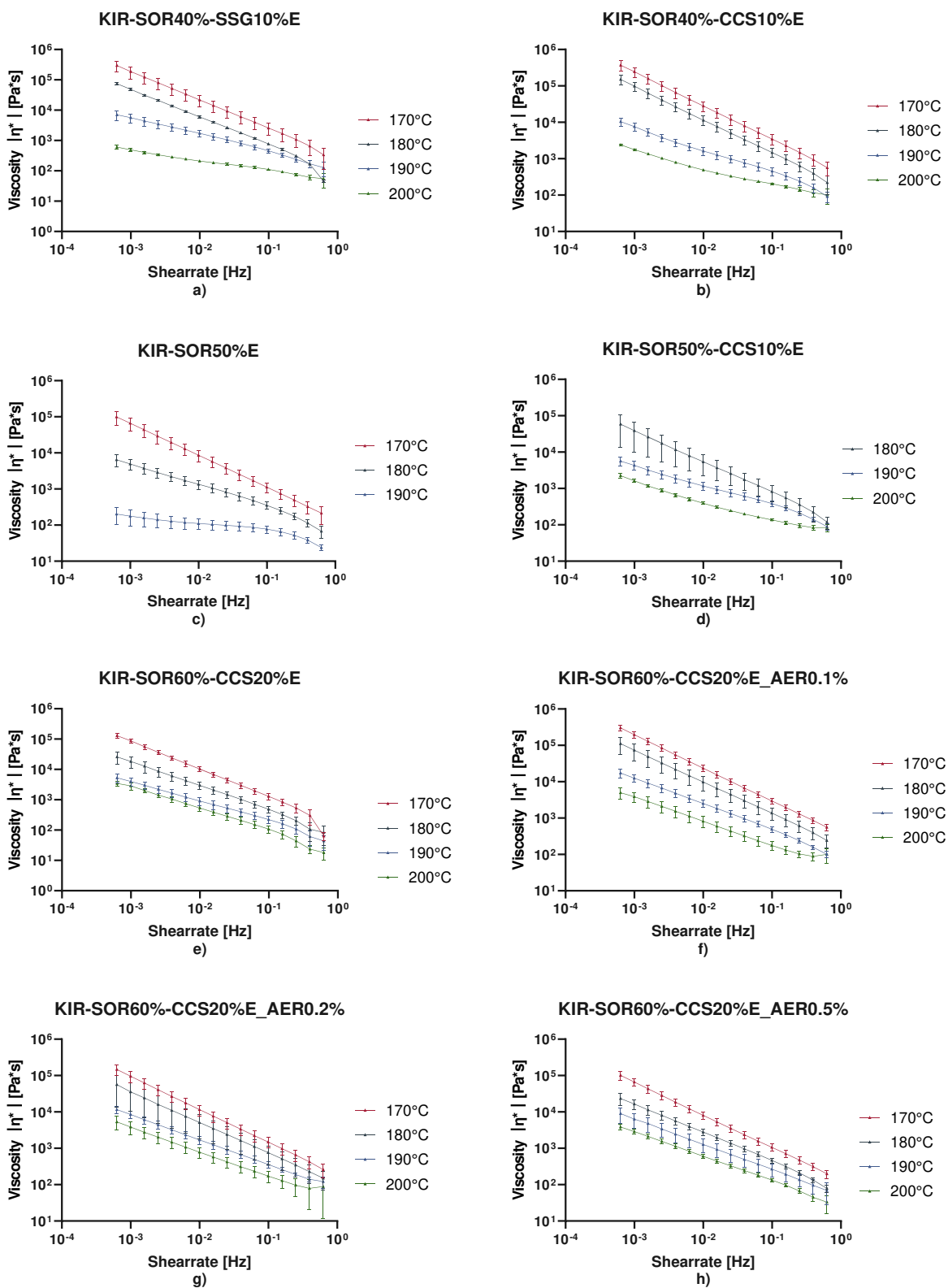
Figure S 11 melt rheology of formulation development and testing of AER influence on KIR-based formulations

Table S 1 Results of calculation of the shear rates for PAR and KIR-based formulations

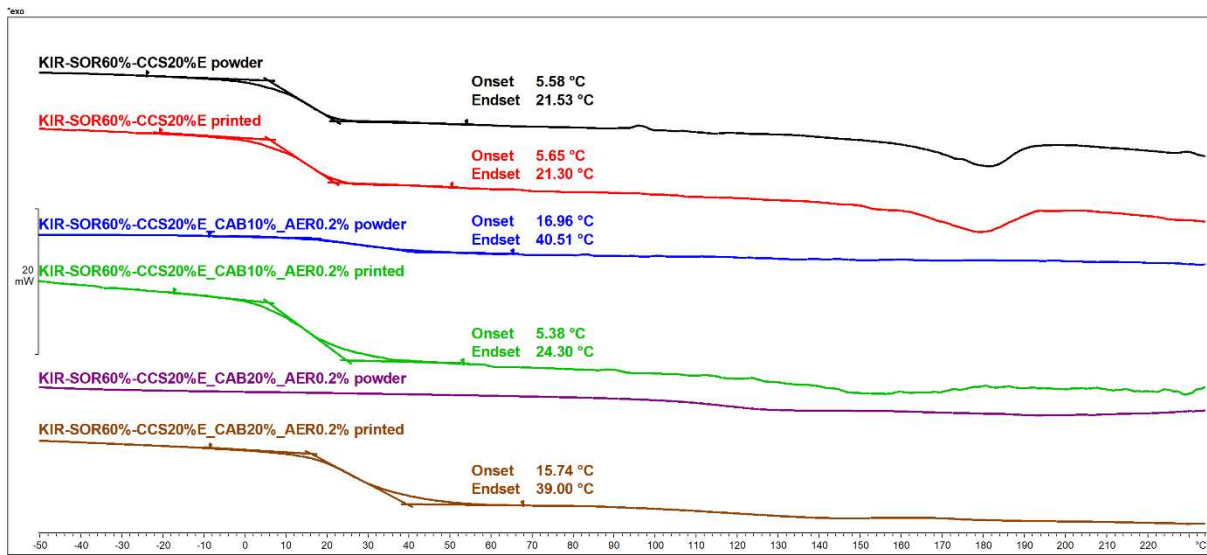|	PAR– print speed: 3.8 mm/s		KIR – print speed: 4.5 mm/s	
Tablet printed	130 mg	130 mg	140 mg	140 mg
Mass [mg]	0.6105	0.6506	0.7334	0.6570
Density measured [g/cm^3]	1.4112	1.4674	1.4290	1.4106
Volume calc [cm^3]	0.4326	0.4434	0.5132	0.4658
Time printed [s]	1211	1069	1182	1339
Revolutions	21.25	20.75	23	23.5
Volume flow [cm^3/s]	$3.57*10^{-4}$	$4.15*10^{-4}$	$4.34*10^{-4}$	$3.48*10^{-4}$
Shear rate in the nozzle [1/s]	7.11	8.25	8.64	6.92
Couette Shear rate [1/s]	0.802	0.887	0.889	0.802
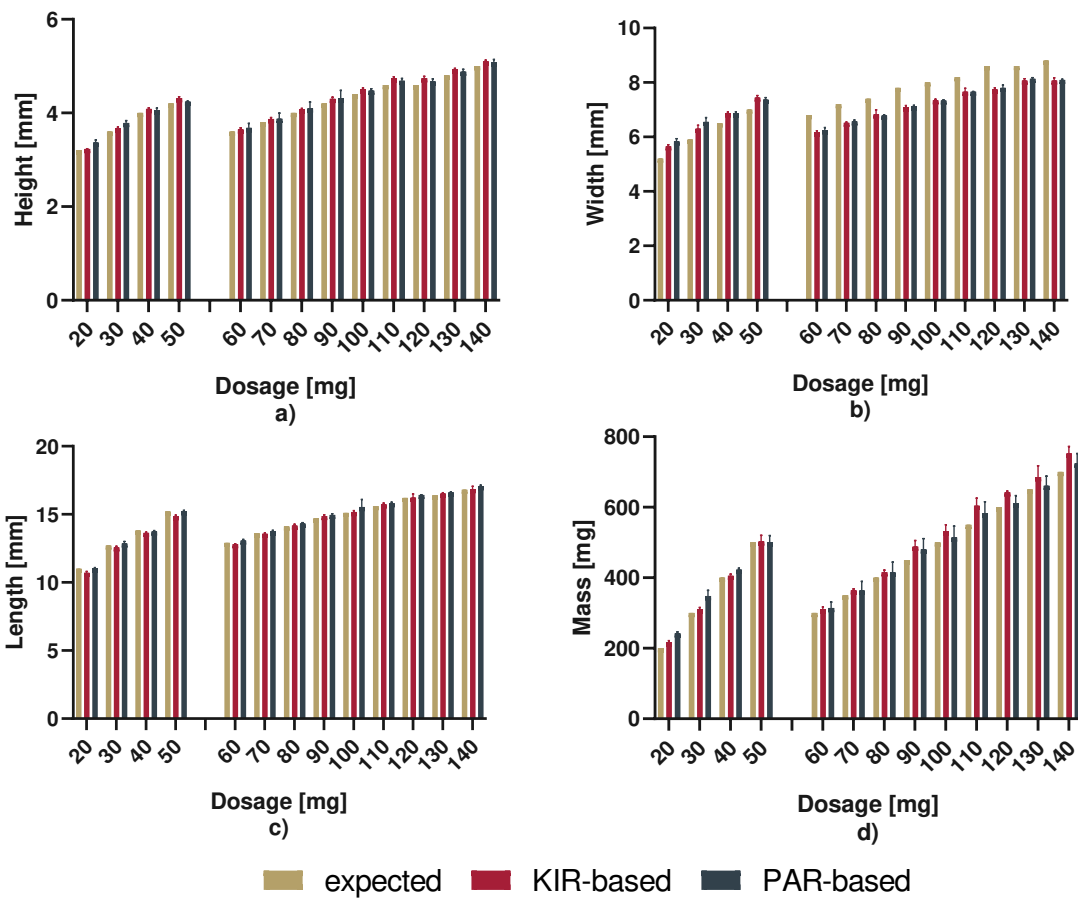
Figure S 12 Visual representation of correctness of height (a), width (b), length (c), and mass (d) of printed tablets (golden bars: expected value, red bars: PAR-based, black bars: KIR-based) (n=3 ± SD)

Figure S 13 detailed picture of the side of a printed tablet and the measured area overlay (KIR-SOR60%-CCS20%E_CAB20%_AER0.2%); right-hand is the scale bar used for coloration of the measured area-based on cabozantinib occurrence

6. Experimental section – part 3
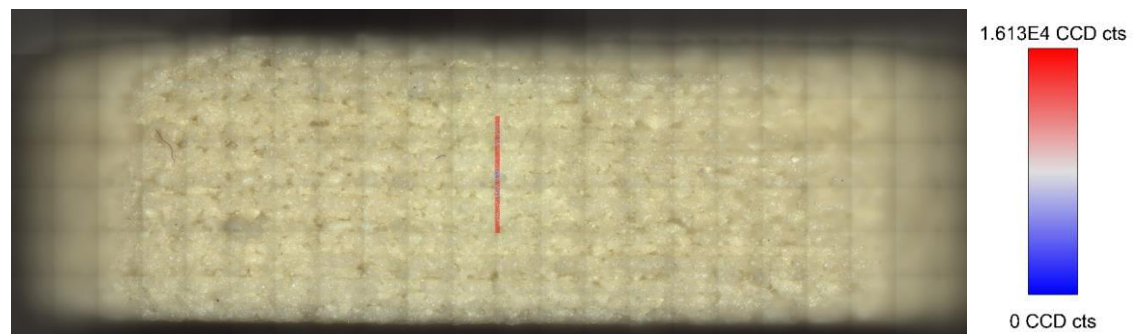
6.1.　　Evaluation of dissolution mechanism

Changes in the formulation's constitution, including modifications to the API and polymer, as well as the addition of disintegrants, suggest that the release mechanism for CAB in a formulation using 50% SOR may differ from the outcomes observed for LOP. Consequently, the identical experimental setup detailed in 4.1, with adjustments in sample times to accommodate accelerated dissolution, was employed for formulations based on KIR and PAR, incorporating 50% SOR and 10% CAB. Figure 8 illustrates the findings from both dissolution experiments.
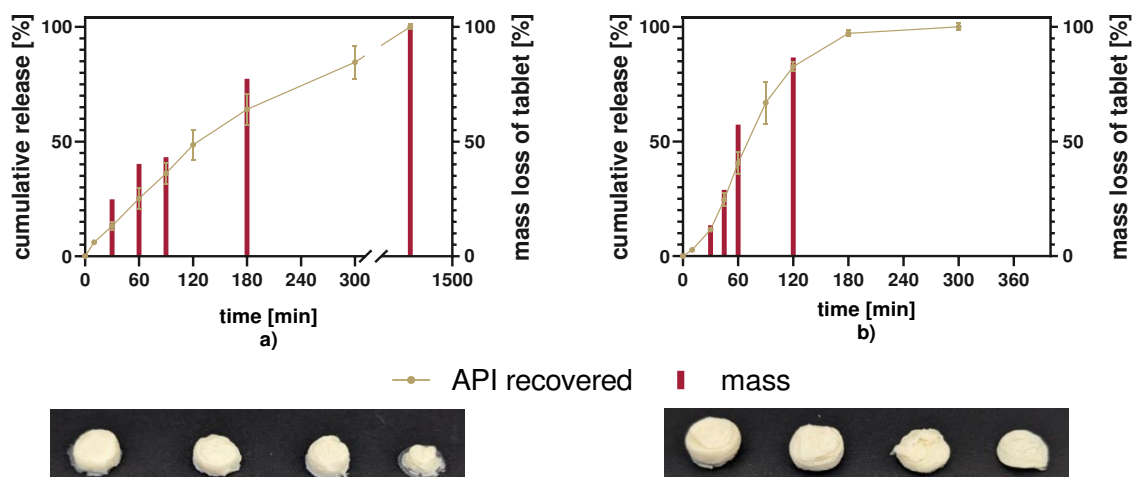
Figure 8 Experimental evaluation of the dissolution mechanism for CAB from tablets made from PAR (a) or KIR (b) with 50% SOR; below the graph: the remainder of the tablets removed at the 4 points in time

Neither the addition of sorbitol nor the exchange from PAR to KIR changed the release mechanism of CAB from the printed tablets. The change in mass fits the release of CAB well. While there is a slightly higher reduction of the total mass compared to the released CAB, this is most likely due to the dissolving of the much more water-soluble sorbitol from the outer layers of the tablet.

6.2.　　Transfer to other polymers

Changing from PAR to KIR was possible with few adaptations and resulted in a formulation with comparable or quicker dissolution times. This prompted an additional experiment involving changing the polymer. Aside from KIR and PAR, Kollidon VA64 (KVA) [161,162] and Eudragit E PO (EPO) [88,163] were considered as potential polymers, as existing literature

indicated the feasibility of producing tablets for immediate release. Attempting to print EPO with the M3dimaker proved unsuccessful, and there are no publications from other research groups suggesting otherwise. This outcome is likely a result of a combination of powder flow and melt rheological properties causing blockages in the nozzle. The small motor on the printhead may lack the necessary torque to extrude the material effectively compared to a larger-scale extruder. KVA was already printable as a standalone polymer. The combination of excipients used for the immediate release formulations with PAR and KIR was extruded and printed in two variations. Figure 9 depicts images of the printed tablets and dissolution data.
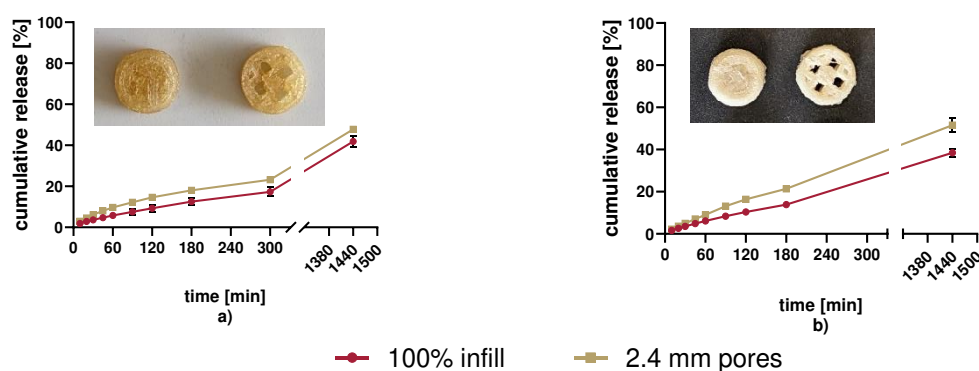
Figure 9 Dissolution pattern of KVA64-based printlets (a) KVA64-SOR30%-CCS10%E_CAB10%_AER0.2%; b) KVA64-SOR60%-CCS20%E_CAB20%_AER0.2%)

In the first step, KVA, with the addition of 30% SOR and 10% CCS, was printed with 10% CAB. The dissolution data showed a slow release of CAB. Thus, both fractions were increased to 60% SOR and 20% CCS and printed with 20% CAB. A slight improvement in the dissolution time was observed, but it was still much slower than expected using the same formulation with PAR and KIR as a reference. If a specific need exists to enable KVA for printing in future research and formulation development other plasticizers and their impact on extrusion temperature and dissolution rate should be tested.

7. Conclusion

This thesis demonstrated various techniques for processing APIs and excipients for 3D printing. The disadvantages of solvent-based processes, such as loading by soaking, were demonstrated experimentally, and the next step was to switch to extrusion. For cost and safety reasons, the necessary methods were evaluated using the model drug loperamide before the actual API, cabozantinib, was used. The methods include manufacturing processes (extrusion, 3D printing) as well as analytical (DSC, Raman, XRD, HPLC) and predictive (melt rheology) methods. These methods were used to develop and characterize a formulation that enables the production of patient-specific dosed cabozantinib tablets with immediate release.

The use of a model drug substance is a well-known technique used for several reasons (e.g., cost, availability, safety). This work demonstrates that considerations for selecting the model drug (in this case, solubility parameters) significantly contribute to the transferability of results from preliminary tests to the actual active substance. Limitations of this technique are evident in melt rheology. The results achieved with LOP could not be directly applied to formulations containing CAB. This indicates that predictability within a similar system is reliable, but it diminishes with significant changes in composition.

The topic of 3D printing in the pharmaceutical industry and clinical applications is attracting increasing attention. Both industry and academic research work on various fronts, such as modifying release, individual dosing, combining active ingredients, and ensuring high quality. The formulations developed here offer a wide range of release rates. They are suitable for formulation development for other active ingredients with accelerated and sustained release requirements. The approach of how tablets are designed based on the required dose could also prove to be a signpost for high-quality, on-demand production of individually dosed dosage forms. At the very least, however, the discourse is being driven forward by researching further ways of ensuring quality.

However, before 3D-printed medicines can be produced and administered as standard in Europe outside of clinical trials, some challenges related to quality assurance and regulatory requirements still need clarification. The relevant authorities must receive support from researchers in industry, the clinical environment, and academia. It should also be remembered that handling extruders and 3D printers requires careful training and experience, especially in the pharmaceutical environment. This is necessary to deliver consistently good results,

recognize sources of error, assess their risks, and ensure the longevity of the devices through careful handling and regular maintenance.

In summary, there is great potential in the research and application of 3D printing for the production of medicines, but there are still challenges to be overcome. This work aims to address some of the open questions or make progress towards the solution.

Literature

1. Lacy SA, Miles DR, Nguyen LT, Clinical Pharmacokinetics and Pharmacodynamics of Cabozantinib, Clin Pharmacokinet, 56, 2017, 477-491. DOI: 10.1007/s40262-016-0461-9.

2. Carmeliet P, Jain RK, Principles and mechanisms of vessel normalization for cancer and other angiogenic diseases, Nat Rev Drug Discov, 10, 2011, 417-427. DOI: 10.1038/nrd3455.

3. Trusolino L, Bertotti A, Comoglio PM, MET signalling: principles and functions in development, organ regeneration and cancer, Nat Rev Mol Cell Biol, 11, 2010, 834-848. DOI: 10.1038/nrm3012.

4. Comoglio PM, Giordano S, Trusolino L, Drug development of MET inhibitors: targeting oncogene addiction and expedience, Nat Rev Drug Discov, 7, 2008, 504-516. DOI: 10.1038/nrd2530.

5. Comoglio PM, Trusolino L, Invasive growth: from development to metastasis, J Clin Invest, 109, 2002, 857-862. DOI: 10.1172/JCI15392.

6. Nguyen L, Benrimoh N, Xie Y, Offman E, Lacy S, Pharmacokinetics of cabozantinib tablet and capsule formulations in healthy adults, Anticancer Drugs, 27, 2016, 669-678. DOI: 10.1097/CAD.0000000000000366.

7. Nguyen L, Holland J, Ramies D, Mamelok R, Benrimoh N, Ciric S, Marbury T, Preston RA, Heuman DM, Gavis E, Lacy S, Effect of Renal and Hepatic Impairment on the Pharmacokinetics of Cabozantinib, J Clin Pharmacol, 56, 2016, 1130-1140. DOI: 10.1002/jcph.714.

8. Lacy S, Hsu B, Miles D, Aftab D, Wang R, Nguyen L, Metabolism and Disposition of Cabozantinib in Healthy Male Volunteers and Pharmacologic Characterization of Its Major Metabolites, Drug Metab Dispos, 43, 2015, 1190-1207. DOI: 10.1124/dmd.115.063610.

9. Nguyen L, Holland J, Mamelok R, Laberge MK, Grenier J, Swearingen D, Armas D, Lacy S, Evaluation of the effect of food and gastric pH on the single-dose pharmacokinetics of cabozantinib in healthy adult subjects, J Clin Pharmacol, 55, 2015, 1293-1302. DOI: 10.1002/jcph.526.

10. Nguyen L, Holland J, Miles D, Engel C, Benrimoh N, O'Reilly T, Lacy S, Pharmacokinetic (PK) drug interaction studies of cabozantinib: Effect of CYP3A inducer rifampin and inhibitor ketoconazole on cabozantinib plasma PK and effect of cabozantinib on CYP2C8 probe substrate rosiglitazone plasma PK, J Clin Pharmacol, 55, 2015, 1012-1023. DOI: 10.1002/jcph.510.

11. Huang SM, Temple R, Throckmorton DC, Lesko LJ, Drug interaction studies: study design, data analysis, and implications for dosing and labeling, Clin Pharmacol Ther, 81, 2007, 298-304. DOI: 10.1038/sj.clpt.6100054.

12. Shakeel F, Haq N, Alsarra IA, Equilibrium solubility determination, Hansen solubility parameters and solution thermodynamics of cabozantinib malate in different monosolvents of pharmaceutical importance, Journal of Molecular Liquids, 324, 2021. DOI: 10.1016/j.molliq.2020.115146.

13. Cunha-Filho M, Araujo MR, Gelfuso GM, Gratieri T, FDM 3D printing of modified drug-delivery systems using hot melt extrusion: a new approach for individualized therapy, Ther Deliv, 8, 2017, 957-966. DOI: 10.4155/tde-2017-0067.

14. Melocchi A, Uboldi M, Parietti F, Cerea M, Foppoli A, Palugan L, Gazzaniga A, Maroni A, Zema L, Lego-Inspired Capsular Devices for the Development of Personalized Dietary Supplements: Proof of Concept With Multimodal Release of Caffeine, J Pharm Sci, 109, 2020, 1990-1999. DOI: 10.1016/j.xphs.2020.02.013.

15. Obeid S, Madžarević M, Ibrić S, Tailoring amlodipine release from 3D printed tablets: Influence of infill patterns and wall thickness, International Journal of Pharmaceutics, 610, 2021. DOI: 10.1016/j.ijpharm.2021.121261.

16. Okwuosa TC, Stefaniak D, Arafat B, Isreb A, Wan KW, Alhnan MA, A Lower Temperature FDM 3D Printing for the Manufacture of Patient-Specific Immediate Release Tablets, Pharm Res, 33, 2016, 2704-2712. DOI: 10.1007/s11095-016-1995-0.

17. Skowyra J, Pietrzak K, Alhnan MA, Fabrication of extended-release patient-tailored prednisolone tablets via fused deposition modelling (FDM) 3D printing, Eur J Pharm Sci, 68, 2015, 11-17. DOI: 10.1016/j.ejps.2014.11.009.

18. Zheng Z, Lv J, Yang W, Pi X, Lin W, Lin Z, Zhang W, Pang J, Zeng Y, Lv Z, Lao H, Chen Y, Yang F, Preparation and application of subdivided tablets using 3D printing for precise hospital dispensing, Eur J Pharm Sci, 149, 2020, 105293. DOI: 10.1016/j.ejps.2020.105293.

19. Amidon GL, Lennernas H, Shah VP, Crison JR, A theoretical basis for a biopharmaceutic drug classification: the correlation of in vitro drug product dissolution and in vivo bioavailability, Pharm Res, 12, 1995, 413-420. DOI: 10.1023/a:1016212804288.

20. Charalabidis A, Sfouni M, Bergstrom C, Macheras P, The Biopharmaceutics Classification System (BCS) and the Biopharmaceutics Drug Disposition Classification System (BDDCS): Beyond guidelines, Int J Pharm, 566, 2019, 264-281. DOI: 10.1016/j.ijpharm.2019.05.041.

21. Kumar S, Bhargava D, Thakkar A, Arora S, Drug carrier systems for solubility enhancement of BCS class II drugs: a critical review, Crit Rev Ther Drug Carrier Syst, 30, 2013, 217-256. DOI: 10.1615/critrevtherdrugcarriersyst.2013005964.

22. Uppoor VR, Regulatory perspectives on in vitro (dissolution)/in vivo (bioavailability) correlations, J Control Release, 72, 2001, 127-132. DOI: 10.1016/s0168-3659(01)00268-1.

23. Zaki NM, Artursson P, Bergstrom CA, A modified physiological BCS for prediction of intestinal absorption in drug discovery, Mol Pharm, 7, 2010, 1478-1487. DOI: 10.1021/mp100124f.

24. Beaumont K, Webster R, Gardner I, Dack K, Design of ester prodrugs to enhance oral absorption of poorly permeable compounds: challenges to the discovery scientist, Curr Drug Metab, 4, 2003, 461-485. DOI: 10.2174/1389200033489253.

25. Testa B, Prodrug research: futile or fertile?, Biochem Pharmacol, 68, 2004, 2097-2106. DOI: 10.1016/j.bcp.2004.07.005.

26. Najjar A, Najjar A, Karaman R, Newly Developed Prodrugs and Prodrugs in Development; an Insight of the Recent Years, Molecules, 25, 2020. DOI: 10.3390/molecules25040884.

27. Serajuddin AT, Salt formation to improve drug solubility, Adv Drug Deliv Rev, 59, 2007, 603-616. DOI: 10.1016/j.addr.2007.05.010.

28. Li S, Wong S, Sethia S, Almoazen H, Joshi YM, Serajuddin AT, Investigation of solubility and dissolution of a free base and two different salt forms as a function of pH, Pharm Res, 22, 2005, 628-635. DOI: 10.1007/s11095-005-2504-z.

29. Rasenack N, Muller BW, Micron-size drug particles: common and novel micronization techniques, Pharm Dev Technol, 9, 2004, 1-13. DOI: 10.1081/pdt-120027417.

30.   Martin A, Cocero MJ, Micronization processes with supercritical fluids: fundamentals and mechanisms, Adv Drug Deliv Rev, 60, 2008, 339-350. DOI: 10.1016/j.addr.2007.06.019.

31.   Boholm M, Arvidsson R, A Definition Framework for the Terms Nanomaterial and Nanoparticle, NanoEthics, 10, 2016, 25-40. DOI: 10.1007/s11569-015-0249-7.

32.   Doaa Hasan Alshora MAI, Fars Kaed Alanazi,, Nanotechnology from particle size reduction to enhancing aqueous solubility, Chapter 6 - Nanotechnology from particle size reduction to enhancing aqueous solubility,, 2016, 163-191. DOI: 10.1016/B978-0-323-42861-3.00006-6.

33.   D'Addio SM, Prud'homme RK, Controlling drug nanoparticle formation by rapid precipitation, Adv Drug Deliv Rev, 63, 2011, 417-426. DOI: 10.1016/j.addr.2011.04.005.

34.   Muller RH, Schmidt S, Buttle I, Akkar A, Schmitt J, Bromer S, SolEmuls-novel technology for the formulation of i.v. emulsions with poorly soluble drugs, Int J Pharm, 269, 2004, 293-302. DOI: 10.1016/j.ijpharm.2003.09.019.

35.   Singh A, Van den Mooter G, Spray drying formulation of amorphous solid dispersions, Adv Drug Deliv Rev, 100, 2016, 27-50. DOI: 10.1016/j.addr.2015.12.010.

36.   Jakubowska E, Lulek J, The application of freeze-drying as a production method of drug nanocrystals and solid dispersions – A review, Journal of Drug Delivery Science and Technology, 62, 2021. DOI: 10.1016/j.jddst.2021.102357.

37.   Alzahrani A, Nyavanandi D, Mandati P, Youssef AAA, Narala S, Bandari S, Repka M, A systematic and robust assessment of hot-melt extrusion-based amorphous solid dispersions: Theoretical prediction to practical implementation, Int J Pharm, 624, 2022, 121951. DOI: 10.1016/j.ijpharm.2022.121951.

38.   Karolewicz B, Gorniak A, Probst S, Owczarek A, Pluta J, Zurawska-Plaksej E, Solid dispersions in pharmaceutical technology. Part I. Classification and methods to obtain solid dispersions, Polim Med, 42, 2012, 17-27.

39.   Edueng K, Mahlin D, Bergstrom CAS, The Need for Restructuring the Disordered Science of Amorphous Drug Formulations, Pharm Res, 34, 2017, 1754-1772. DOI: 10.1007/s11095-017-2174-7.

40.   Pandi P, Bulusu R, Kommineni N, Khan W, Singh M, Amorphous solid dispersions: An update for preparation, characterization, mechanism on bioavailability, stability, regulatory considerations and marketed products, Int J Pharm, 586, 2020, 119560. DOI: 10.1016/j.ijpharm.2020.119560.

41.   Janssens S, Van den Mooter G, Review: physical chemistry of solid dispersions, J Pharm Pharmacol, 61, 2009, 1571-1586. DOI: 10.1211/jpp/61.12.0001.

42.   Qian F, Huang J, Hussain MA, Drug-polymer solubility and miscibility: Stability consideration and practical challenges in amorphous solid dispersion development, J Pharm Sci, 99, 2010, 2941-2947. DOI: 10.1002/jps.22074.

43.   Douroumis D, Fahr A, Drug Delivery Strategies for Poorly Water-Soluble Drugs, First edition, John Wiley & Sons, Ltd, 2013.

44.   Follonier N, Doelker E, Cole ET, Evaluation of hot-melt extrusion as a new technique for the production of polymer-based pellets for sustained release capsules containing high loadings of freely soluble drugs, Drug Development and Industrial Pharmacy, 20, 2008, 1323-1339. DOI: 10.3109/03639049409038373.

45.   Wilczyński KJ, Lewandowski A, Nastaj A, Wilczyński K, Modeling for Starve Fed/Flood Fed Mixing Single-Screw Extruders, International Polymer Processing, 31(1), 2016, 82-91. DOI: 10.3139/217.3154

46.   Lawal A, Kalyon DM, Mechanisms of mixing in single and co-rotating twin screw extruders, Polymer Engineering & Science, 35, 2004, 1325-1338. DOI: 10.1002/pen.760351702.

47.   Wilson M, Williams MA, Jones DS, Andrews GP, Hot-melt extrusion technology and pharmaceutical application, Ther Deliv, 3, 2012, 787-797. DOI: 10.4155/tde.12.26.

48.   Cogswell FN, Stretching flow instabilities at the exits of extrusion dies, Journal of Non-Newtonian Fluid Mechanics, 2, 1977, 37-47. DOI: 10.1016/0377-0257(77)80031-1.

49.   Lang B, McGinity JW, Williams RO, 3rd, Hot-melt extrusion--basic principles and pharmaceutical applications, Drug Dev Ind Pharm, 40, 2014, 1133-1155. DOI: 10.3109/03639045.2013.838577.

50.   Capone C, Di Landro L, Inzoli F, Penco M, Sartore L, Thermal and mechanical degradation during polymer extrusion processing, Polymer Engineering & Science, 47, 2007, 1813-1819. DOI: 10.1002/pen.20882.

51.   Maru SM, de Matas M, Kelly A, Paradkar A, Characterization of thermal and rheological properties of zidovudine, lamivudine and plasticizer blends with ethyl cellulose to assess their suitability for hot melt extrusion, Eur J Pharm Sci, 44, 2011, 471-478. DOI: 10.1016/j.ejps.2011.09.003.

52.   Bochmann ES, Gryczke A, Wagner KG, Validation of Model-Based Melt Viscosity in Hot-Melt Extrusion Numerical Simulation, Pharmaceutics, 10, 2018. DOI: 10.3390/pharmaceutics10030132.

53.   Bochmann ES, Ustuner EE, Gryczke A, Wagner KG, Predicting melt rheology for hot-melt extrusion by means of a simple T(g)-measurement, Eur J Pharm Biopharm, 119, 2017, 47-55. DOI: 10.1016/j.ejpb.2017.05.010.

54.   Williams ML, Landel, R. F., & Ferry, J. D., The temperature dependence of relaxation mechanisms in amorphous polymers and other glass-forming liquids, Journal of the American Chemical society, 77(14), 1955, 3701-3707.

55.   Bochmann ES, Neumann D, Gryczke A, Wagner KG, Micro-scale prediction method for API-solubility in polymeric matrices and process model for forming amorphous solid dispersion by hot-melt extrusion, Eur J Pharm Biopharm, 107, 2016, 40-48. DOI: 10.1016/j.ejpb.2016.06.015.

56.   Yu L, Amorphous pharmaceutical solids: preparation, characterization and stabilization, Adv Drug Deliv Rev, 48, 2001, 27-42. DOI: 10.1016/s0169-409x(01)00098-9.

57.   Breitenbach Jr, Melt Extrusion Can Bring New Benefits to HIV Therapy, American Journal of Drug Delivery, 4, 2006, 61-64. DOI: 10.2165/00137696-200604020-00001.

58.   Simoes MF, Pinto RMA, Simoes S, Hot-melt extrusion in the pharmaceutical industry: toward filing a new drug application, Drug Discov Today, 24, 2019, 1749-1768. DOI: 10.1016/j.drudis.2019.05.013.

59.   Alhijjaj M, Belton P, Qi S, An investigation into the use of polymer blends to improve the printability of and regulate drug release from pharmaceutical solid dispersions prepared via fused deposition modeling (FDM) 3D printing, Eur J Pharm Biopharm, 108, 2016, 111-125. DOI: 10.1016/j.ejpb.2016.08.016.

60.   Matijasic G, Gretic M, Kezeric K, Petanjek J, Vukelic E, Preparation of Filaments and the 3D Printing of Dronedarone HCl Tablets for Treating Cardiac Arrhythmias, AAPS PharmSciTech, 20, 2019, 310. DOI: 10.1208/s12249-019-1522-9.

61.   Tan DK, Maniruzzaman M, Nokhodchi A, Advanced Pharmaceutical Applications of Hot-Melt Extrusion Coupled with Fused Deposition Modelling (FDM) 3D Printing for

Personalised Drug Delivery, Pharmaceutics, 10, 2018. DOI: 10.3390/pharmaceutics10040203.

62. Lee J, Song C, Noh I, Song S, Rhee YS, Hot-Melt 3D Extrusion for the Fabrication of Customizable Modified-Release Solid Dosage Forms, Pharmaceutics, 12, 2020. DOI: 10.3390/pharmaceutics12080738.

63. Hollander J, Genina N, Jukarainen H, Khajeheian M, Rosling A, Makila E, Sandler N, Three-Dimensional Printed PCL-Based Implantable Prototypes of Medical Devices for Controlled Drug Delivery, J Pharm Sci, 105, 2016, 2665-2676. DOI: 10.1016/j.xphs.2015.12.012.

64. Korte C, Quodbach J, Formulation development and process analysis of drug-loaded filaments manufactured via hot-melt extrusion for 3D-printing of medicines, Pharm Dev Technol, 23, 2018, 1117-1127. DOI: 10.1080/10837450.2018.1433208.

65. Kristiawan RB, Imaduddin F, Ariawan D, Ubaidillah, Arifin Z, A review on the fused deposition modeling (FDM) 3D printing: Filament processing, materials, and printing parameters, Open Engineering, 11, 2021, 639-649. DOI: 10.1515/eng-2021-0063.

66. Xu P, Li J, Meda A, Osei-Yeboah F, Peterson ML, Repka M, Zhan X, Development of a quantitative method to evaluate the printability of filaments for fused deposition modeling 3D printing, Int J Pharm, 588, 2020, 119760. DOI: 10.1016/j.ijpharm.2020.119760.

67. Aho J, Botker JP, Genina N, Edinger M, Arnfast L, Rantanen J, Roadmap to 3D-Printed Oral Pharmaceutical Dosage Forms: Feedstock Filament Properties and Characterization for Fused Deposition Modeling, J Pharm Sci, 108, 2019, 26-35. DOI: 10.1016/j.xphs.2018.11.012.

68. Zhang J, Feng X, Patil H, Tiwari RV, Repka MA, Coupling 3D printing with hot-melt extrusion to produce controlled-release tablets, Int J Pharm, 519, 2017, 186-197. DOI: 10.1016/j.ijpharm.2016.12.049.

69. Nasereddin JM, Wellner N, Alhijjaj M, Belton P, Qi S, Development of a Simple Mechanical Screening Method for Predicting the Feedability of a Pharmaceutical FDM 3D Printing Filament, Pharm Res, 35, 2018, 151. DOI: 10.1007/s11095-018-2432-3.

70. Genina N, Hollander J, Jukarainen H, Makila E, Salonen J, Sandler N, Ethylene vinyl acetate (EVA) as a new drug carrier for 3D printed medical drug delivery devices, Eur J Pharm Sci, 90, 2016, 53-63. DOI: 10.1016/j.ejps.2015.11.005.

71. Korte C, Quodbach J, 3D-Printed Network Structures as Controlled-Release Drug Delivery Systems: Dose Adjustment, API Release Analysis and Prediction, AAPS PharmSciTech, 19, 2018, 3333-3342. DOI: 10.1208/s12249-018-1017-0.

72. Roulon S, Soulairol I, Lavastre V, Payre N, Cazes M, Delbreilh L, Alie J, Production of Reproducible Filament Batches for the Fabrication of 3D Printed Oral Forms, Pharmaceutics, 13, 2021. DOI: 10.3390/pharmaceutics13040472.

73. Crump SS. Apparatus and method for creating three-dimensional objects. In: Incorporated S, ed. Vol 51213291989.

74. Gioumouxouzis CI, Baklavaridis A, Katsamenis OL, Markopoulou CK, Bouropoulos N, Tzetzis D, Fatouros DG, A 3D printed bilayer oral solid dosage form combining metformin for prolonged and glimepiride for immediate drug delivery, Eur J Pharm Sci, 120, 2018, 40-52. DOI: 10.1016/j.ejps.2018.04.020.

75. Goyanes A, Scarpa M, Kamlow M, Gaisford S, Basit AW, Orlu M, Patient acceptability of 3D printed medicines, Int J Pharm, 530, 2017, 71-78. DOI: 10.1016/j.ijpharm.2017.07.064.

76.	Melocchi A, Briatico-Vangosa F, Uboldi M, Parietti F, Turchi M, von Zeppelin D, Maroni A, Zema L, Gazzaniga A, Zidan A, Quality considerations on the pharmaceutical applications of fused deposition modeling 3D printing, Int J Pharm, 592, 2021, 119901. DOI: 10.1016/j.ijpharm.2020.119901.

77.	Baumann F, Bugdayci H, Grunert J, Keller F, Roller D, Influence of slicing tools on quality of 3D printed parts, Computer-Aided Design and Applications, 13, 2015, 14-31. DOI: 10.1080/16864360.2015.1059184.

78.	Simpson M, Khoury S, Inexpensive Piezoelectric Elements for Nozzle Contact Detection and Build Platform Leveling in FFF 3D Printers, Inventions, 3, 2018. DOI: 10.3390/inventions3010008.

79.	Dizon JRC, Gache CCL, Cascolan HMS, Cancino LT, Advincula RC, Post-Processing of 3D-Printed Polymers, Technologies, 9, 2021. DOI: 10.3390/technologies9030061.

80.	Okwuosa TC, Sadia M, Isreb A, Habashy R, Peak M, Alhnan MA, Can filaments be stored as a shelf-item for on-demand manufacturing of oral 3D printed tablets? An initial stability assessment, Int J Pharm, 600, 2021, 120442. DOI: 10.1016/j.ijpharm.2021.120442.

81.	Pereira GG, Figueiredo S, Fernandes AI, Pinto JF, Polymer Selection for Hot-Melt Extrusion Coupled to Fused Deposition Modelling in Pharmaceutics, Pharmaceutics, 12, 2020. DOI: 10.3390/pharmaceutics12090795.

82.	Funk NL, Fantaus S, Beck RCR, Immediate release 3D printed oral dosage forms: How different polymers have been explored to reach suitable drug release behaviour, Int J Pharm, 625, 2022, 122066. DOI: 10.1016/j.ijpharm.2022.122066.

83.	Goyanes A, Buanz AB, Basit AW, Gaisford S, Fused-filament 3D printing (3DP) for fabrication of tablets, Int J Pharm, 476, 2014, 88-92. DOI: 10.1016/j.ijpharm.2014.09.044.

84.	Goyanes A, Buanz AB, Hatton GB, Gaisford S, Basit AW, 3D printing of modified-release aminosalicylate (4-ASA and 5-ASA) tablets, Eur J Pharm Biopharm, 89, 2015, 157-162. DOI: 10.1016/j.ejpb.2014.12.003.

85.	Cerda JR, Arifi T, Ayyoubi S, Knief P, Ballesteros MP, Keeble W, Barbu E, Healy AM, Lalatsa A, Serrano DR, Personalised 3D Printed Medicines: Optimising Material Properties for Successful Passive Diffusion Loading of Filaments for Fused Deposition Modelling of Solid Dosage Forms, Pharmaceutics, 12, 2020. DOI: 10.3390/pharmaceutics12040345.

86.	Arafat B, Wojsz M, Isreb A, Forbes RT, Isreb M, Ahmed W, Arafat T, Alhnan MA, Tablet fragmentation without a disintegrant: A novel design approach for accelerating disintegration and drug release from 3D printed cellulosic tablets, Eur J Pharm Sci, 118, 2018, 191-199. DOI: 10.1016/j.ejps.2018.03.019.

87.	Hussain A, Mahmood F, Arshad MS, Abbas N, Qamar N, Mudassir J, Farhaj S, Nirwan JS, Ghori MU, Personalised 3D Printed Fast-Dissolving Tablets for Managing Hypertensive Crisis: In-Vitro/In-Vivo Studies, Polymers (Basel), 12, 2020. DOI: 10.3390/polym12123057.

88.	Fanous M, Bitar M, Gold S, Sobczuk A, Hirsch S, Ogorka J, Imanidis G, Development of immediate release 3D-printed dosage forms for a poorly water-soluble drug by fused deposition modeling: Study of morphology, solid state and dissolution, Int J Pharm, 599, 2021, 120417. DOI: 10.1016/j.ijpharm.2021.120417.

89.	Crisan AG, Porfire A, Ambrus R, Katona G, Rus LM, Porav AS, Ilyes K, Tomuta I, Polyvinyl Alcohol-Based 3D Printed Tablets: Novel Insight into the Influence of Polymer Particle Size on Filament Preparation and Drug Release Performance, Pharmaceuticals (Basel), 14, 2021. DOI: 10.3390/ph14050418.

90.   Boyle BM, Xiong PT, Mensch TE, Werder TJ, Miyake GM, 3D printing using powder melt extrusion, Addit Manuf, 29, 2019. DOI: 10.1016/j.addma.2019.100811.

91.   Khaled SA, Burley JC, Alexander MR, Roberts CJ, Desktop 3D printing of controlled release pharmaceutical bilayer tablets, Int J Pharm, 461, 2014, 105-111. DOI: 10.1016/j.ijpharm.2013.11.021.

92.   Goyanes A, Allahham N, Trenfield SJ, Stoyanov E, Gaisford S, Basit AW, Direct powder extrusion 3D printing: Fabrication of drug products using a novel single-step process, Int J Pharm, 567, 2019, 118471. DOI: 10.1016/j.ijpharm.2019.118471.

93.   Zheng Y, Deng F, Wang B, Wu Y, Luo Q, Zuo X, Liu X, Cao L, Li M, Lu H, Cheng S, Li X, Melt extrusion deposition (MED) 3D printing technology - A paradigm shift in design and development of modified release drug products, Int J Pharm, 602, 2021, 120639. DOI: 10.1016/j.ijpharm.2021.120639.

94.   Pflieger T, Venkatesh R, Dachtler M, Eggenreich K, Laufer S, Lunter D, Novel Approach to Pharmaceutical 3D-Printing Omitting the Need for Filament-Investigation of Materials, Process, and Product Characteristics, Pharmaceutics, 14, 2022. DOI: 10.3390/pharmaceutics14112488.

95.   Goyanes A, Wang J, Buanz A, Martinez-Pacheco R, Telford R, Gaisford S, Basit AW, 3D Printing of Medicines: Engineering Novel Oral Devices with Unique Design and Drug Release Characteristics, Mol Pharm, 12, 2015, 4077-4084. DOI: 10.1021/acs.molpharmaceut.5b00510.

96.   Gioumouxouzis CI, Tzimtzimis E, Katsamenis OL, Dourou A, Markopoulou C, Bouropoulos N, Tzetzis D, Fatouros DG, Fabrication of an osmotic 3D printed solid dosage form for controlled release of active pharmaceutical ingredients, Eur J Pharm Sci, 143, 2020, 105176. DOI: 10.1016/j.ejps.2019.105176.

97.   Tidau M, Finke JH, Modified release kinetics in dual filament 3D printed individualized oral dosage forms, Eur J Pharm Sci, 175, 2022, 106221. DOI: 10.1016/j.ejps.2022.106221.

98.   Gorkem Buyukgoz G, Kossor CG, Ji S, Guvendiren M, Dave RN, Dose Titration of Solid Dosage Forms via FDM 3D-Printed Mini-Tablets, Pharmaceutics, 14, 2022. DOI: 10.3390/pharmaceutics14112305.

99.   Pietrzak K, Isreb A, Alhnan MA, A flexible-dose dispenser for immediate and extended release 3D printed tablets, Eur J Pharm Biopharm, 96, 2015, 380-387. DOI: 10.1016/j.ejpb.2015.07.027.

100.   Noyes AA, Whitney WR, The Rate of Solution of Solid Substances in Their Own Solutions, Journal of the American Chemical Society, 19, 1897, 930-934. DOI: 10.1021/ja02086a003.

101.   Goyanes A, Robles Martinez P, Buanz A, Basit AW, Gaisford S, Effect of geometry on drug release from 3D printed tablets, Int J Pharm, 494, 2015, 657-663. DOI: 10.1016/j.ijpharm.2015.04.069.

102.   Solanki NG, Tahsin M, Shah AV, Serajuddin ATM, Formulation of 3D Printed Tablet for Rapid Drug Release by Fused Deposition Modeling: Screening Polymers for Drug Release, Drug-Polymer Miscibility and Printability, J Pharm Sci, 107, 2018, 390-401. DOI: 10.1016/j.xphs.2017.10.021.

103.   Kempin W, Domsta V, Grathoff G, Brecht I, Semmling B, Tillmann S, Weitschies W, Seidlitz A, Immediate Release 3D-Printed Tablets Produced Via Fused Deposition Modeling of a Thermo-Sensitive Drug, Pharm Res, 35, 2018, 124. DOI: 10.1007/s11095-018-2405-6.

104. Windolf H, Chamberlain R, Quodbach J, Predicting Drug Release from 3D Printed Oral Medicines Based on the Surface Area to Volume Ratio of Tablet Geometry, Pharmaceutics, 13, 2021. DOI: 10.3390/pharmaceutics13091453.

105. Malik T, Razzaq H, Razzaque S, Nawaz H, Siddiqa A, Siddiq M, Qaisar S, Design and synthesis of polymeric membranes using water-soluble pore formers: an overview, Polymer Bulletin, 76, 2018, 4879-4901. DOI: 10.1007/s00289-018-2616-3.

106. Sadia M, Arafat B, Ahmed W, Forbes RT, Alhnan MA, Channelled tablets: An innovative approach to accelerating drug release from 3D printed tablets, J Control Release, 269, 2018, 355-363. DOI: 10.1016/j.jconrel.2017.11.022.

107. Melocchi A, Parietti F, Maroni A, Foppoli A, Gazzaniga A, Zema L, Hot-melt extruded filaments based on pharmaceutical grade polymers for 3D printing by fused deposition modeling, Int J Pharm, 509, 2016, 255-263. DOI: 10.1016/j.ijpharm.2016.05.036.

108. Giron D, Thermal Analysis, Microcalorimetry and Combined Techniques for the Study of Pharmaceuticals, Journal of Thermal Analysis and Calorimetry, 56, 1999, 1285-1304. DOI: 10.1023/a:1010194020563.

109. Bevis J, Bottom R, Duncan J, Farhat I, Forrest M, Saunders M, Furniss D, Gabott P, MacNaughtan B, Nazhat S, Seddon A, Principles and Applications of Thermal Analysis, Wiley Online Library, 2008.

110. Baird JA, Taylor LS, Evaluation of amorphous solid dispersion properties using thermal analysis techniques, Adv Drug Deliv Rev, 64, 2012, 396-421. DOI: 10.1016/j.addr.2011.07.009.

111. Duan P, Lamm MS, Yang F, Xu W, Skomski D, Su Y, Schmidt-Rohr K, Quantifying Molecular Mixing and Heterogeneity in Pharmaceutical Dispersions at Sub-100 nm Resolution by Spin Diffusion NMR, Mol Pharm, 17, 2020, 3567-3580. DOI: 10.1021/acs.molpharmaceut.0c00592.

112. Krause S, Iskandar M, Phase Separation in Styrene-Alpha-Methyl Styrene Block Copolymers, Abstracts of Papers of the American Chemical Society, 173, 1977, 130-130.

113. Lin D, Huang Y, A thermal analysis method to predict the complete phase diagram of drug-polymer solid dispersions, Int J Pharm, 399, 2010, 109-115. DOI: 10.1016/j.ijpharm.2010.08.013.

114. Röntgen WC, Über eine neue Art von Strahlen, Sitzungsbericht der Würzburg Physik und Medicin Gesellschaft, 1895.

115. Friedrich W, Knipping P, Laue M, Interferenzerscheinungen bei Roentgenstrahlen, Annalen der Physik, 346, 1913, 971-988.

116. Spieß L, Behnken H, Genzel C, Schwarzer R, Teichert G, Moderne Röntgenbeugung, Wiesbaden, Vieweg+ Teubner, 2009.

117. Nakel W, The elementary process of bremsstrahlung, Physics Reports, 243, 1994, 317-353. DOI: 10.1016/0370-1573(94)00068-9.

118. Epp J. X-ray diffraction (XRD) techniques for materials characterization. In. *Materials Characterization Using Nondestructive Evaluation (NDE) Methods* 2016:81-124.

119. Bragg WL, The diffraction of short electromagnetic waves by a crystal, Proceedings of the Cambridge Philosophical Society, 17, 1913.

120. Shah B, Kakumanu VK, Bansal AK, Analytical techniques for quantification of amorphous/crystalline phases in pharmaceutical solids, J Pharm Sci, 95, 2006, 1641-1665. DOI: 10.1002/jps.20644.

121. Dedroog S, Pas T, Vergauwen B, Huygens C, Van den Mooter G, Solid-state analysis of amorphous solid dispersions: Why DSC and XRPD may not be regarded as stand-alone techniques, J Pharm Biomed Anal, 178, 2020, 112937. DOI: 10.1016/j.jpba.2019.112937.

122. Raman CV, A Change of Wave-length in Light Scattering, Nature, 121, 1928, 619-619. DOI: 10.1038/121619b0.

123. Singh R, Riess F, Sir CV Raman and the story of the Nobel prize, Current Science, 75, 1998, 965-971.

124. McGoverin CM, Rades T, Gordon KC, Recent pharmaceutical applications of Raman and terahertz spectroscopies, J Pharm Sci, 97, 2008, 4598-4621. DOI: 10.1002/jps.21340.

125. Prochazka M, Basics of Raman scattering (RS) spectroscopy, Surface-Enhanced Raman Spectroscopy: Bioanalytical, Biomolecular and Medical Applications, 2016, 7-19. DOI: 10.1007/978-3-319-23992-7_2.

126. Giridhar G, Manepalli RRKN, Apparao G. confocal Raman spectroscopy. In. *Spectroscopic methods for nanomaterials characterization*: Elsevier; 2017:141-161.

127. Everall N, Depth profiling with confocal Raman microscopy, part I, Spectroscopy, 19(10), 2004, 22-27.

128. Juang C-B, Finzi L, Bustamante CJ, Design and application of a computer-controlled confocal scanning differential polarization microscope, Review of Scientific Instruments, 59, 1988, 2399-2408. DOI: 10.1063/1.1139918.

129. Aldalawi AA, Suardi N, Ahmed NM, Al-Farawn MAS, Dheyab MA, Jebur WI, Kadhim FJ, Comparison of Wavelength-Dependent Penetration Depth of 532 nm and 660 nm Lasers in Different Tissue Types, J Lasers Med Sci, 14, 2023, e28. DOI: 10.34172/jlms.2023.28.

130. Everall N, Depth Profiling with Confocal Raman Microscopy, Part II, Spectroscopy, 19(11), 2004.

131. Wilkes GL, An overview of the basic rheological behavior of polymer fluids with an emphasis on polymer melts, Journal of Chemical Education, 58, 1981. DOI: 10.1021/ed058p880.

132. Schramm G, A practical approach to rheology and rheometry, Karlsruhe, Gebrueder Haake GmbH, 1994.

133. Wypych G. Effect of plasticizers on properties of plasticized materials. In. *Handbook of plastizisers*: Handbook of plasticizers; 2004.

134. Bogdan C, Hales D, Cornila A, Casian T, Iovanov R, Tomuta I, Iurian S, Texture analysis - A versatile tool for pharmaceutical evaluation of solid oral dosage forms, Int J Pharm, 638, 2023, 122916. DOI: 10.1016/j.ijpharm.2023.122916.

135. Verstraete G, Samaro A, Grymonpre W, Vanhoorne V, Van Snick B, Boone MN, Hellemans T, Van Hoorebeke L, Remon JP, Vervaet C, 3D printing of high drug loaded dosage forms using thermoplastic polyurethanes, Int J Pharm, 536, 2018, 318-325. DOI: 10.1016/j.ijpharm.2017.12.002.

136. Viidik L, Vesala J, Laitinen R, Korhonen O, Ketolainen J, Aruvali J, Kirsimae K, Kogermann K, Heinamaki J, Laidmae I, Ervasti T, Preparation and characterization of hot-melt extruded polycaprolactone-based filaments intended for 3D-printing of tablets, Eur J Pharm Sci, 158, 2021, 105619. DOI: 10.1016/j.ejps.2020.105619.

137. Samiei N, Recent trends on applications of 3D printing technology on the design and manufacture of pharmaceutical oral formulation: a mini review, Beni-Suef University Journal of Basic and Applied Sciences, 9, 2020. DOI: 10.1186/s43088-020-00040-4.

138. EMA, ICH guideline for good clinical practice E6(R2) - Step 5, 2016.

139. Khairuzzaman A. Regulatory perspectives on 3D printing in pharmaceuticals. In. *3D Printing of Pharmaceuticals* 2018:218-236.

140. EMA. Regulatory Science to 2025 - Strategic reflection. In:2020.

141. EMA. Analysis and summaries of public consultation results - EMA Regulatory Science to 2025. In:2020.

142. EMA. New Quality Innovation Expert Group (QIG) supports medicine innovation. In:2022.

143. Pharma3DPI. International Pharmaceutical 3D Printing Initiative - Pharma3DPI. In:2023.

144. Krueger L, Awad A, Basit AW, Goyanes A, Miles JA, Popat A, Clinical translation of 3D printed pharmaceuticals, Nature Reviews Bioengineering, 2024. DOI: 10.1038/s44222-024-00217-x.

145. Carl AK, Hochmann D, Regulatory framework for 3D printed custom-made devices in Europe, Transactions on Additive Manufacturing Meets Medicine, 3, 2021, 542-542. DOI: 10.18416/AMMM.2021.2109542.

146. Union TEUatCotE. REGULATION (EU) 2017/745. In:2017.

147. FDA, Technical considerations for additive manufactured medical devices: guidance for industry and Food and Drug Administration staff, 2017.

148. Horst A, McDonald F, Uncertain But Not Unregulated: Medical Product Regulation in the Light of Three-Dimensional Printed Medical Products, 2020. DOI: 10.1089/3dp.2020.0076.

149. Minghetti P, Musazzi UM, Rocco P. Regulatory Aspects and Barriers in Using Groundbreaking Technologies. In. *Nano- and Microfabrication Techniques in Drug Delivery*: Springer International Publishing; 2023:467-491.

150. Seoane-Viano I, Xu X, Ong JJ, Teyeb A, Gaisford S, Campos-Alvarez A, Stulz A, Marcuta C, Kraschew L, Mohr W, Basit AW, Goyanes A, A case study on decentralized manufacturing of 3D printed medicines, Int J Pharm X, 5, 2023, 100184. DOI: 10.1016/j.ijpx.2023.100184.

151. Elbadawi M, McCoubrey LE, Gavins FKH, Ong JJ, Goyanes A, Gaisford S, Basit AW, Harnessing artificial intelligence for the next generation of 3D printed medicines, Adv Drug Deliv Rev, 175, 2021, 113805. DOI: 10.1016/j.addr.2021.05.015.

152. Triastek. Triastek 3DP Intelligent Pharmaceuticals. In. Vol 20242024.

153. Bustamante P, Pena MA, Barra J, The modified extended Hansen method to determine partial solubility parameters of drugs containing a single hydrogen bonding group and their sodium derivatives: benzoic acid/Na and ibuprofen/Na, Int J Pharm, 194, 2000, 117-124. DOI: 10.1016/s0378-5173(99)00374-9.

154. Tagami T, Kuwata E, Sakai N, Ozeki T, Drug Incorporation into Polymer Filament Using Simple Soaking Method for Tablet Preparation Using Fused Deposition Modeling, Biol Pharm Bull, 42, 2019, 1753-1760. DOI: 10.1248/bpb.b19-00482.

155. Grodowska K, Parczewski A, Organic solvents in the pharmaceutical industry, Acta Pol Pharm, 67, 2010, 3-12.

156. ICH. ICH Q3C (R9) Guideline on impurities guideline for residual solvents - Step 5. In:2024.

157. Lenhart J, Pöstges F, Wagner KG, Lunter DJ, Evaluation of Printability of PVA-Based Tablets from Powder and Assessment of Critical Rheological Parameters, Pharmaceutics, 16, 2024. DOI: 10.3390/pharmaceutics16040553.

158. Gomes-Filho MS, Oliveira FA, Barbosa MAA, Modeling the diffusion-erosion crossover dynamics in drug release, Phys Rev E, 105, 2022, 044110. DOI: 10.1103/PhysRevE.105.044110.

159. Lenhart J, Lunter DJ, Dosage by design - 3D printing individualized cabozantinib tablets with immediate release, Eur J Pharm Biopharm, 2024, 114501. DOI: 10.1016/j.ejpb.2024.114501.

160. Duranovic M, Madzarevic M, Ivkovic B, Ibric S, Cvijic S, The evaluation of the effect of different superdisintegrants on the drug release from FDM 3D printed tablets through different applied strategies: In vitro-in silico assessment, Int J Pharm, 610, 2021, 121194. DOI: 10.1016/j.ijpharm.2021.121194.

161. Fanous M, Gold S, Muller S, Hirsch S, Ogorka J, Imanidis G, Simplification of fused deposition modeling 3D-printing paradigm: Feasibility of 1-step direct powder printing for immediate release dosage form production, Int J Pharm, 578, 2020, 119124. DOI: 10.1016/j.ijpharm.2020.119124.

162. Kollamaram G, Croker DM, Walker GM, Goyanes A, Basit AW, Gaisford S, Low temperature fused deposition modeling (FDM) 3D printing of thermolabile drugs, Int J Pharm, 545, 2018, 144-152. DOI: 10.1016/j.ijpharm.2018.04.055.

163. Shadambikar G, Kipping T, Di-Gallo N, Elia AG, Knuttel AN, Treffer D, Repka MA, Vacuum Compression Molding as a Screening Tool to Investigate Carrier Suitability for Hot-Melt Extrusion Formulations, Pharmaceutics, 12, 2020. DOI: 10.3390/pharmaceutics12111019.